2014

# Insight into the universally conserved NTPases HflX and YchF

## Coatham, Mackenzie Leigh

Lethbridge, Alta. : University of Lethbridge, Dept. of Chemistry and Biochemistry

**Insight into the Universally Conserved NTPases HflX and YchF**

**MACKENZIE LEIGH COATHAM**
**Bachelor of Science, University of Lethbridge, 2012**

A Thesis
Submitted to the School of Graduate Studies
of the University of Lethbridge
in Partial Fulfillment of the
Requirements for the Degree

**MASTER OF SCIENCE**

Department of Chemistry and Biochemistry
University of Lethbridge
LETHBRIDGE, ALBERTA, CANADA

© Mackenzie Leigh Coatham, 2014

INSIGHT INTO THE UNIVERSALLY CONSERVED NTPASES HFLX AND YCHF

MACKENZIE LEIGH COATHAM

Date of Defence: May 16, 2014

| (Name) | (Rank) | (Highest Degree) |
|---|---|---|
| Dr. Hans-Joachim Wieden<br>Supervisor | Professor | Ph.D |
| Dr. Michael Gerken<br>Thesis Examination<br>Committee Member | Professor | Ph.D |
| Dr. Ute Kothe<br>Thesis Examination<br>Committee Member | Professor | Ph.D |
| Dr. Peter Dibble<br>Thesis Examination<br>Committee Chair | Professor | Ph.D |

**Abstract**

The functional roles of the two universally conserved bacterial GTPases, HflX and YchF, are poorly understood. Both proteins associate with 70S ribosomes as well as 30S and 50S ribosomal subunits. Understanding exactly how HflX and YchF interact with the ribosome and nucleotides will be important for the discovery of the *in vivo* relevant ribosomal complex. Presented in this thesis, is the development of a fluorescence-based system that can be used to monitor the association of HflX to 70S, 50S and 30S. Additionally, as HflX lacks the canonical glutamine that is required for the hydrolysis of GTP and ATP, an examination into how HflX hydrolyzes purine nucleotides was conducted. Furthermore, nucleotide association and dissociation rate constants were determined in the presence of ribosomes for YchF and in the presence and absence of antibiotics for HflX. The results presented here provide additional insight into the enzymatic properties of HflX and YchF.

## Acknowledgements

**Table of Contents**

Content                                                              Page

**List of Tables**

**List of Figures**

## List of Abbreviations

| | |
|---|---|
| β-ME | β-mercaptoethanol |
| 30S | Prokaryotic small ribosomal subunit (S=Svedberg) |
| 50S | Prokaryotic large ribosomal subunit (S=Svedberg) |
| 5-IAF | 5-iodoacetamidofluorescein |
| 70S | Prokaryotic ribosome (30S & 50S) |
| A-site | Aminoacyl-tRNA binding site |
| ADPNP | Adenosine-5'-(β,γ-imido)-triphosphate |
| ATP | Adenosine triphosphate |
| ATPase | Adenosine triphosphatase |
| DMSO | Dimethyl sulfoxide |
| DNA | Deoxyribonucleic acid |
| dNTPs | Deoxyribonucleotide triphosphates |
| E-site | tRNA exit site |
| EF | Elongation factor (Tu,Ts and G) |
| EMSA | Electrophoretic mobility shift assays |
| FRET | Fluorescence resonance energy transfer |
| G-domain | GTPase domain |
| GAP | GTPase activating protein |
| GEF | Guanine nucleotide exchange factor |
| GDPNP | Guanosine-5'-(β, γ-imido)-triphosphate |
| GST tag | Glutathione S-transferase |
| GTP | Guanosine triphosphate |
| GTPase | Guanosine triphosphatase |
| HAS | Hydrophobic amino acid substituted GTPase |
| HflX | High frequency of lysogeny factor X |
| hOLA1 | Human Obg-like ATPase 1 |
| IF | Initiation factor |
| IPTG | Isopropyl-β-D-galactopyranoside |
| K loop | Potassium loop |
| LB | Luria-Bertani |
| Mant | 2'(or 3')-O-(N-methylantraniloyl) |
| MBP | Maltose binding protein |
| mRNA | Messenger RNA |
| MWCO | Molecular weight cut-off |
| NTPase | Nucleoside triphosphatase |
| Obg | *spo-0B*-associated GTP-binding protein |
| OD | Optical density |
| PDB ID | Protein data bank identification |
| PEP | Phosphoenolpyruvate |
| PET | Peptide exit tunnel |
| $P_i$ | Inorganic phosphate |
| PK | Pyruvate kinase |
| P-loop | Phosphate-binding loop |
| PMSF | Phenylmethylsulfonyfluoride |

| | |
|---|---|
| P-site | Peptidyl-tRNA binding site |
| PTC | Peptidyl transferase centre |
| RNA | Ribonucleic acid |
| rRNA | Ribosomal RNA |
| SDS-PAGE | Sodium dodecyl sulfate polyacrylamide electrophoresis |
| SIMIBI | Signal recognition particle, MinD, BioD |
| TGS | Threonyl-tRNA synthetase, GTPase, SpoT domain |
| TLC | Thin layer chromatography |
| $T_M$ | Melting temperature |
| TRAFAC | Translation factor class |
| tRNA | Transfer RNA |

**Introduction**

*1.1 Translation*

   Protein biosynthesis is a highly conserved, complex process, and as such the target of numerous clinically relevant antibiotics. Although protein synthesis in prokaryotes and eukaryotes is very similar, the proteins and nucleic acids involved in the process in both domains of life differ significantly between them, which allow antibiotics to target bacteria specifically (1). Even though the chemical reaction linking two amino acid residues together to form a peptide bond is relatively simple, over a hundred different proteins and ribonucleic acids (RNA) participate in this highly accurate translational process (2,3). Ribosomes are the site of protein synthesis and have an extensive functional life cycle starting from their formation in a cell to their degradation upon completing their role in translation (4).  Initially, the two subunits comprising the ribosome must be assembled from proteins and RNA and matured via modification to their amino acids and bases, respectively (3). During ribosome biogenesis in prokaryotes, ribosomal RNA (rRNA) is processed and modified, ribosomal proteins and metal ions bind in a particular manner and conformational changes of regions of the complex take place to accommodate the final formation of a 70S ribosome (3). RNA chaperones catalyze the ribosome assembly process primarily by interacting with ribosomal RNA to assist it in adopting its correct fold (5). Initiation factors (IF1, IF2 and IF3) form a functional 70S bacterial ribosome from the 30S and 50S ribosomal subunits allowing for the genetic information encoded in

messenger RNA (mRNA) molecules to be translated in the presence of initiator transfer RNA (tRNA) (Figure 1.1.1) (6).  The prokaryotic ribosome is comprised of three tRNA binding sites: the A-site which can accommodate aminoacylated tRNA molecules, the P-site which holds the peptidyl-tRNA and the E-site which is the final location of accommodation on the ribosome for deacylated-tRNA prior to their release back into the cell (Figure 1.1.1) (7).  The growing polypeptide is formed within the ribosome in conjunction with the actions of elongation factors (EF-Tu and EF-G) (Figure 1.1.1) (8).  EF-Tu catalyzes the delivery of aminoacyl-tRNA to the A-site of the ribosome while the subsequent translocation of peptidyl-tRNA from the A-site to the P-site and deacylated tRNA from the P-site to the E-site is accelerated by EF-G (Figure 1.1.1) (8).  Once a completed polypeptide has been released from the peptidyl-tRNA in the P-site, EF-G and ribosome recycling factor (RRF) can rapidly dissociate the bacterial ribosome into its ribosomal subunits allowing for their recycling and use in the synthesis of another protein or their degradation (Figure 1.1.1) (9,10).
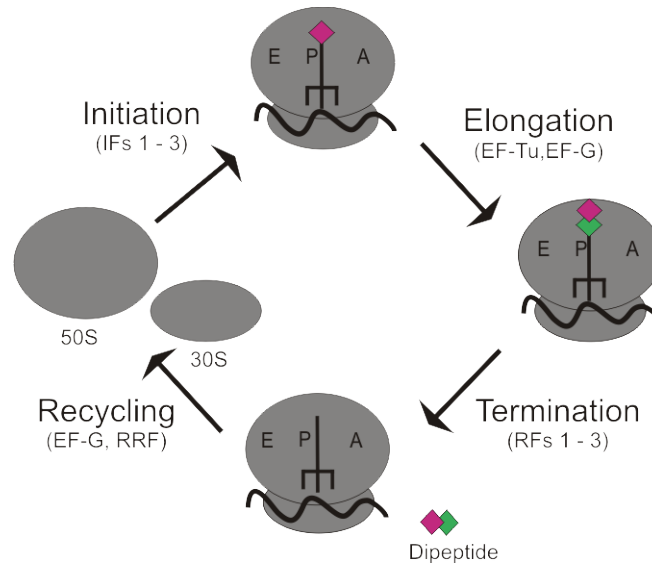
Figure 1.1.1 **Schematic overview of the translation cycle in prokaryotes.** Initiation factors bring the two ribosomal subunits together with initiator tRNA (pink) and mRNA to form a 70S initiation complex. Formation of a polypeptide takes place during successive elongation steps. Elongation factors bearing aminoacyl-tRNA add to a growing peptidyl-tRNA (pink and green). Termination of translation results in the release of the nascent polypeptide and eventual recycling of the 50S and 30S.

Although a minimal set of factors that participate in protein synthesis under ideal conditions is known, the question remains as to whether additional factors are necessary for the function of protein synthesis machinery during periods of cellular stress (i.e, heat, pH, nutrient and antibiotics). Universally conserved yet uncharacterized guanosine triphosphatases (GTPases) from the same superfamily as the canonical translation factors (EF-Tu, EF-G and IF2) such as HflX and YchF have been hypothesized to aid in efficient protein biosynthesis during these conditions.

*1.2 Antibiotics*

Antibiotics target almost every stage during protein synthesis. Visualization of the majority of the classes of antibiotics on the ribosome has been achieved by X-ray crystallography and NMR spectroscopy revealing that most of them target the functional centers predominantly consisting of ribosomal RNA (11,12). Highly conserved regions across all domains of life, the decoding centre on the small ribosomal subunit, the peptidyl-transferase centre (PTC) and the peptide exit tunnel (PET) on the large ribosomal subunit are common binding sites for drugs (11,12). Bacterial resistance to translation-inhibiting antibiotics can be accomplished through a variety of mechanisms. Modification of drugs, export of antibiotics from the cell, antibiotic degradation and/or mutations to nucleotides or ribosomal proteins are all successful mechanisms of resistance (13). Inhibitors of bacterial protein synthesis inhibit bacterial growth, and therefore are characterized as bacteriostatic not bacteriocidal (14). The antibiotics of interest in this thesis primarily target the elongation cycle of translation. Aminoglycosides possess the ability to stimulate misreading, or in other words, increase the chance of misincorporation of incorrect amino acids into the growing polypeptide chain. Paromomycin, a representative antibiotic of this class, promotes the binding and even accommodation of near-cognate aminoacyl-tRNA whereas streptomycin causes the rate at which cognate and near-cognate aminoacyl-tRNAs bind to the ribosome to become similar increasing the frequency of misincorporation (15-17). Regardless of their exact impact on amino acid

incorporation, all aminoglycosides interact with helix 44 of the 30S ribosomal subunit, which constitutes the decoding center (Figure 1.2.1) (18).
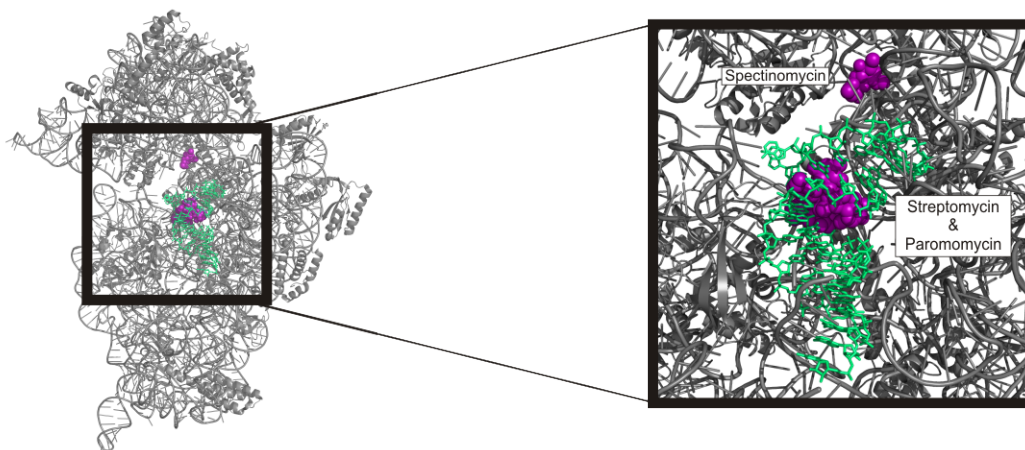


Figure 1.2.1 **Cartoon representation of the *Thermus Thermophilus* 30S ribosomal subunit (PDB ID: 1IBK, 1FJG) highlighting the binding sites of aminoglycoside antibiotics.** Spectinomycin, streptomycin and paromomycin (purple spheres) are shown bound to the decoding centre of the ribosome in relation to helix 44 (green sticks).

The main function of the ribosome is to catalyze peptide-bond formation at the peptidyl-transferase centre. The transfer of the growing polypeptide chain on peptidyl-tRNA in the P-site of the ribosome to the amino acid on the tRNA in the A-site is an irreversible reaction. If misincorporation occurs, the growing chain should be aborted and translation of that particular mRNA restarted (19,20). During the elongation cycle, the nascent polypeptide emerges from a tunnel within the large ribosomal subunit (21). The walls of this tunnel can make contact with the growing polypeptide chain and in turn, regulate the translation process and assist in the initial folding process (22). A number of antibiotics target the A-site of the PTC or the tunnel region adjacent to the PTC. The mode of action of these antibiotics can differ significantly. Puromycin, for example acts as a mimic of the 3'-end of aminoacyl-tRNA accepting the growing polypeptide

resulting in premature termination, as the structural differences between puromycin and peptidyl-tRNA make the antibiotic incapable of reacting with the incoming aminoacyl-tRNA (13). Chloramphenicol is a broad-spectrum antibiotic that achieves its widespread inhibition of bacterial translation by binding to the ribosome in a location where the aminoacyl moiety of aminoacyl-tRNA would be positioned, thereby interfering with peptide-bond formation in an aminoacyl-tRNA specific manner (Figure 1.2.2) (11). Amino acid residues that are bulky and contain aromatic side chains appear to be capable of displacing chloramphenicol from its binding site (23). Interestingly, additional binding sites for chloramphenicol have been reported and overlap with the ribosome exit tunnel (Figure 1.2.2) (24). A class of antibiotics that has an overlapping binding site with chloramphenicol are the lincosamides, which include lincomycin and its derivative, clindamycin (Figure 1.2.2). Lincosamides are capable of blocking aminoacyl-tRNA from the ribosome while simultaneously blocking the ribosomal exit tunnel (11). Macrolide antibiotics primarily target the tunnel region adjacent to the PTC (Figure 1.2.2) (25). The macrolides in clinical use include erythromycin and azithromycin (25). Obstruction of the ribosomal exit tunnel only allows for the synthesis of short oligopeptides, ultimately resulting in the release of peptidyl-tRNA from the ribosome (26). Finally, there are a few antibiotics that block the translocation of tRNA through the ribosome by either blocking the association of translation factors to the ribosome such as thiostrepton (27) or stabilizing ratcheted conformations of the ribosome in which tRNA exists in a hybrid state, spanning both the P and E sites, like viomycin (13). The binding

6

site of viomycin has been hypothesized to closely overlap the binding sites of aminoglycoside antibiotics.
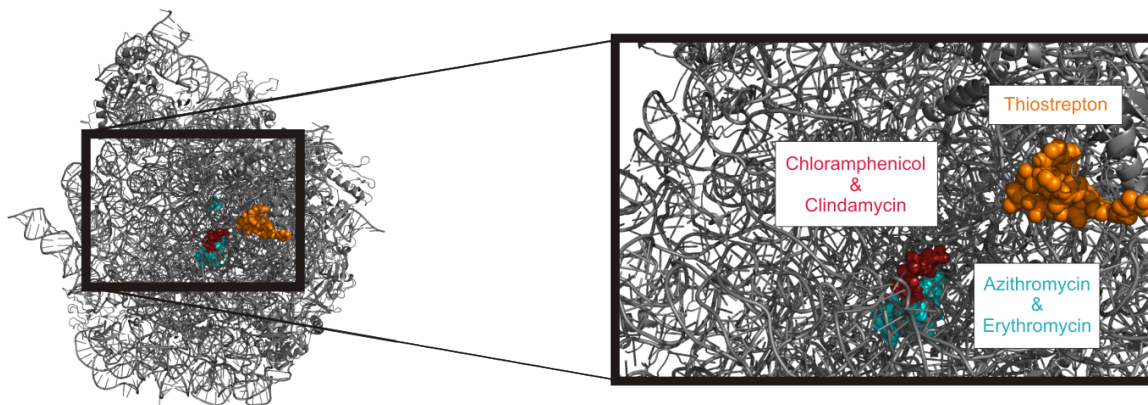


Figure 1.2.2 **Cartoon representation of the *Deinococcus radiodurans* 50S ribosomal subunit (PDB ID: 3CF5, 1JZY, 1JZX, 1KO1, 1NWY) highlighting the binding sites of antibiotics targeting the PTC, tunnel adjacent to the PTC or translation factors.** Chloramphenicol and clindamycin (red spheres) along with azithromycin and erythromycin (cyan spheres) are shown bound to the PTC and peptide exit tunnel (PET) region of the ribosome. Thiostrepton is represented as orange spheres.

Although the binding sites of inhibitors of protein synthesis have been elucidated on the prokaryotic ribosome, a complete understanding of all the modes of action for most of these antibiotics remains to be discovered. Questions as to how these antibiotics influence protein synthesis during cellular stress conditions, affect protein factors such as HflX or YchF whose functions have yet to be discovered, or interfere with communicating conformational changes to the ribosome as a whole have yet to be fully answered. Increasing evidence that antibiotics can have multiple binding sites on the 70S ribosome suggest as bacteria develop resistance to currently available drugs, a detailed knowledge of the mechanisms of antibiotic action *in vivo* will be key to use preexisting antibiotics in novel ways and to design new antibiotics with new targets.

*1.3 GTPases*

The GTPase superfamily of proteins exists in all three domains of life: prokaryotes, eukaryotes and archaea (28,29). The functions of these enzymes are to regulate a range of cellular processes such as protein synthesis, cell cycling and differentiation, and the sorting and amplification of cellular signals (28,29). The proliferation of cancers can be directly related to the action or mutation of GTPases and the downstream effects on their respective cellular roles (28,30). Interestingly, it has been proposed that all GTPases emerged from a single common ancestor despite their diversity in function (28,29). A striking similarity of sequence motifs, overall structure and general mechanism of action has been maintained throughout all domains of life. Simplified, GTPases can be considered as molecular switches that exist in two states, active and inactive (29). When a GTPase is not bound to any nucleotides it is inactive until it binds guanosine triphosphate (GTP) and undergoes a conformational change to become active (Figure 1.3.1) (28,29). The cellular effect of the enzyme can often be linked to the hydrolysis of GTP to guanosine diphosphate (GDP), resulting in the GTPase to return to its inactive, empty or *apo* state (Figure 1.3.1) (28,29). In this way, the GTPases act as timed switches that can be fine-tuned to regulate downstream cellular processes. However, external factors can influence the functional cycle of GTPases by either accelerating the hydrolysis step as GTPase activating proteins (GAPs) or behaving as guanine nucleotide exchange factors (GEFs) facilitating the exchange of GDP for GTP (Figure 1.3.1) (28,29).
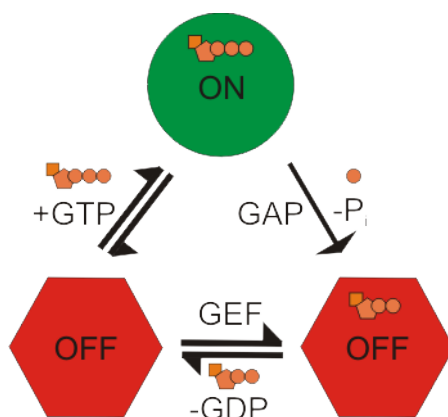
Figure 1.3.1 **Schematic representation of the GTPase cycle.** A GTPase is considered active (green circle) when bound to the triphosphate form of guanosine. Upon hydrolysis, GTPases are inactive (red hexagons) when bound to no substrate or guanosine diphosphate (28,29).

The specificity of these enzymes for guanine nucleotides is due to a defined fold that is invariant among all living organisms (31,32). All GTPases are comprised of a G-domain, but often these proteins contain extensions to the amino and/or carboxy termini that result in their differentiated cellular roles (33). Although the particular sequence of the G-domain can greatly vary among the GTPase superfamily, several motifs of highly conserved amino acids exist that are responsible for the interaction of the factor with guanine nucleotides and mediate the association of any effectors that can modulate the GTPase cycle. Five sequence motifs have been identified to define the G-domain of GTPases: G1, G2, G3, G4 and G5 (28,29). The G1 or Walker A (GXXXXGK(S/T)) motif, provides several residues that interact with the phosphates and stabilize the interaction of the GTPase with bound nucleotide (29). This structural element termed the phosphate binding loop (P-loop) is one of the most common protein folds and can be found in almost 20% of all cellular gene products, making the GTPase superfamily part of the P-loop NTPase class (34). Immediately following

the P-loop is the G2 region also termed Switch I for its changes in conformation depending on the presence of GTP or GDP. Although it is difficult to predict Switch I at the sequence level, what is known is that the orientation of a critical threonine residue within this motif is sensitive to the binding of GTP, coordinating the positioning of a magnesium ion that is essential for hydrolysis (28,35). The G3 or Walker B (DXXG) motif contains aspartate and glycine residues that are required for the coordination of the magnesium via a water molecule and the formation of a hydrogen bond with the γ-phosphate of GTP, respectively (35). The G3 motif is also referred to as Switch II as it can undergo extensive conformational changes whether it is in its GDP or GTP-bound forms. The last two motifs, G4 and G5, are primarily responsible for further stabilizing the nucleotide by the GTPase. G4 in particular, consists of four hydrophobic or nonpolar residues followed by the conserved sequence motif, (N/T)(K/Q)XD, which is capable of forming hydrogen bonds with groups on the guanine ring of the nucleotide (28). G5, providing only one additional contact with the guanosine nucleotide, cannot be easily identified in all GTPases yet like G4 greatly enhances the specificity of the protein for guanine nucleotides (28). Motifs G1 through G4 are the most general characteristics of the GTPase superfamily with further classification of this group resulting in two separate classes based on overall cellular function and conservation of G4: the translation factor (TRAFAC) and signal recognition particle MinD and BioD (SIMIBI) GTPases (34). The translation factor related class (TRAFAC) of GTPases not only includes classical translation factors such as EF-Tu and EF-G but also the closely related and

mostly eukaryotic Ras-like superfamily of proteins (34). The smaller SIMIBI class on the other hand, is constituted primarily by the signal recognition particle GTPases, MinD/Mrp and BioD-related superfamilies (34). There are many ATPases in the SIMIBI class of GTPases as one of the differentiating factors between the SIMIBI and the TRAFAC class is less conservation in the G4 motif (34).

The number and variety of eukaryotic GTPases is astounding, ranging from the Ras family of small GTPases (Ras, Rho, ARF, Rab and Ran) playing a role in growth, differentiation and vesicular transport, to the cell signaling heterotrimeric G-proteins (36). In bacteria, the number of GTPases is considerably smaller, with only eight proteins being universally conserved. These factors include EF-G, EF-Tu and IF2, which are involved in protein synthesis; FtsY and Ffh, which are signaling proteins and finally the enzymes with poorly understood functions, HflX, YchF and YihA (29). The three translation factors are the most comprehensively studied GTPases and as described previously have been shown to act on the ribosome during its functional cycle. Belonging to the Era group, YihA has not been well studied but other related GTPases of this cluster have shown roles requiring an interaction with RNA (29). Homologs of YihA in yeast have been implicated to be essential for large ribosomal subunit maturation and stability (37). Similarly for the FtsY/Ffh subfamily, either an interaction with the ribosome or RNA is necessary for the delivery of proteins to the bacterial plasma membrane (29). Not surprisingly, an interaction with the ribosome and ribosomal RNA has been observed with HflX and YchF (members of the Obg

group), making it even more imperative to understand the cellular roles of these remaining universally conserved GTPases.

For Ras and Rho, their associated GAPs have a major role in the GTP hydrolysis reaction, introducing a catalytic residue, most often an arginine into the active site of GTPases stimulating GTP hydrolysis by stabilizing the transition state of the reaction (38). However, for the translation factors EF-G and EF-Tu, the ribosome does not contribute an arginine residue in particular, to enhance the rate of GTP hydrolysis (38). Instead, a glutamine residue in the GTPase positions a water molecule for a nucleophilic attack on the $\gamma$-phosphate of GTP speeding up the hydrolysis reaction (39). Recently, variations to this mode of stimulation of intrinsic GTP hydrolysis have been discovered (39). In these GTPases of which HflX and YchF are included, the catalytic glutamine is substituted with a hydrophobic amino acid underlining the importance of elucidating how these unique universally conserved GTPases interact with guanine nucleotides and the role of the ribosome as an effector molecule. The similarities and differences between the molecular mechanisms and downstream cellular effects of these prokaryotic GTPases, HflX and YchF will not only allow scientists to marvel at the natural design of enzymes but can eventually lead scientists to rationally designing proteins and perhaps even novel targets for antibiotics.

*1.4 HflX*

Protein products from the *hflA* and *hflB* loci with roles in the lytic and lysogeny cycle of bacteriophage lambda were discovered upon examination of the *Escherichia coli* genome (40,41). Three genes make up the *hflA* locus: *hflX, hflK* and *hflC.* The *hflB* locus gives rise to the ATP-dependent metalloprotease HflB, which has been shown to push *E. coli* towards the lytic pathway (40,41). Although HflB along with the membrane proteins HflK and HflC form a protease complex, an associated role of HflX in the lambda lysogeny cycle has not been discovered (40,41). Present in most prokaryotes, archaea and eukaryotes, the *hflX* gene has been identified to possess a GTP-binding motif (41). The *hflA* loci is located on a superoperon wherein seven genes are alternatively cotranscribed from two heat shock promoters $E\sigma^{70}$ and $E\sigma^{32}$ (42). Interestingly, the *hflA* region appears to only be transcribed with the promoters that are upstream of the *hfq* gene, whose corresponding protein regulates the levels of mRNA under stress conditions (42). Under optimal growth conditions, the expression of *hflX* is low, but expression levels have been shown to increase upon subjection to heat shock (43). Deletion of *hflX* in many bacterial species has no distinctive phenotype, suggesting that although HflX is universally conserved, it is not essential under optimal conditions. As a role of HflX in the lysogenic frequency of bacteriophage lambda has been dismissed (44), the cellular function of the protein remains unknown.

*1.4.1 Structure of HflX*

Crystal structures of HflX in its nucleotide free and GDP bound states have been obtained from the hypothermophilic archaeon *Sulfolobus solfataricus* (*S. solfataricus*) (45). HflX is a two-domain protein consisting of a canonical C-terminal GTPase domain (G-domain) preceded by a unique N-terminal HflX domain (Figure 1.4.1.1) (45). Homologs of HflX from other organisms such as *E. coli* also contain a poorly conserved C-terminal extension of approximately 50 amino acids. Characteristic for the TRAFAC related class of P-loop GTPases, HflX possesses the five-nucleotide binding motifs, G1 through G5 (Figure 1.4.1.1). The G domain forms a four-stranded parallel β-sheet that is surrounded by two α-helices (Figure 1.4.1.1). Another two α-helices comprise an anti-parallel coiled coil structure that connects the two domains (Figure 1.4.1.1). These helices contain numerous positively charged residues contributing to a patch of positive charge on the surface of HflX that has been speculated to bind nucleic acids (45). An extensive interaction surface between the HflX and G-domains can be observed within the archael crystal structures. One of the helices in the HflX domain interacts with the P-loop and Switch II of the G-domain through hydrogen bond and salt bridge interactions (Figure 1.4.1.1) (45). Residues involved in these domain interactions are conserved within the HflX family of proteins suggesting that contact between domains is an important feature of HflX function (46).
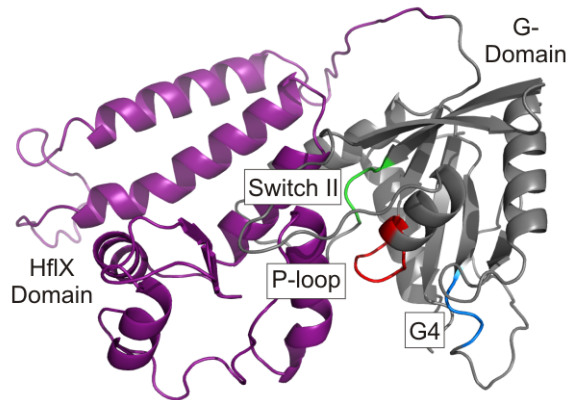
Figure 1.4.1.1 **Homology model of *E. coli* HflX based on the crystal structure from *S. solfataricus* (PDB 2QTF).** The G1 motif is visible in red, G3 is featured in green and G4 is shown in blue.

*1.4.2. The Nucleotide Hydrolysis Activity of HflX*

HflX from *Escherichia coli* has been shown to exhibit both GTPase and ATPase activity (42,47). Out of the core group of eight universally conserved GTPases, only YchF, another member of the Obg-HflX superfamily, which possesses an altered G4 motif, displays a high affinity for adenine nucleotides. Interestingly, the G4 motif of HflX corresponds well to the consensus sequence derived from other P-loop GTPases. HflX can bind and hydrolyze both purine nucleotides but based on the determined nucleotide affinities, HflX prefers guanine nucleotides under cellular purine nucleotide concentrations (47). The guanosine-bound form of the protein will constitute 80% of all cellular HflX (47). Another feature of HflX is that it is a member of the hydrophobic amino acid substituted HAS-GTPase class wherein the catalytic glutamine residue found adjacent to the G3 motif is substituted with a phenylalanine (48,49). This raises the question as to the mechanism of both GTP and ATP hydrolysis by HflX. HflX does contain two asparagine residues in its G1 motif that recently have been linked to the coordination of a potassium ion by other GTPases (48,49). The

presence of potassium will force Switch I to adopt a conformation in which it sits directly on top of the nucleotide binding site, acting as a GTPase activating element similar to the arginine finger found in canonical GTPases (48,49). However, a GTPase or ATPase activity that is dependent on potassium has not been observed for HflX so far (44). It is therefore still unclear what further requirements beyond the conservation of these elements are necessary to regulate and accomplish efficient purine nucleotide hydrolysis by HflX alone and in the presence of ribosomes.

*1.4.3 Hypotheses as to the Functional Role of HflX*

Mounting evidence suggests a role for HflX during protein synthesis (44,47,50,51). In *Chlamydophila pneumonia, S. solfataricus* and *E. coli,* HflX has been shown to associate with 50S ribosomal subunits, in both the guanosine diphosphate and guanosine triphosphate states (44,51,52). The GTPase activity of HflX is not only stimulated by 50S ribosomal subunits but also by 70S ribosomes (47,53). Furthermore, electrophoretic mobility shift assays (EMSA) have revealed an interaction between ribosomal RNA, both the 23S and 16S, and HflX in different nucleotide bound states (51). Most recently, the ribosomes and ribosomal subunits from *E. coli* were shown to interact with HflX but only the 50S and 70S stabilize the binding of GTP and induce a structurally distinct form of HflX that is hypothesized to be the protein's "GTPase activated" state (50). Based on these findings, the functionally relevant state of HflX *in vivo* is in complex with the ribosome and tightly bound to GTP (50). A minimal mechanistic model for the interaction of the ribosome with HflX has been

proposed (Figure 1.4.3.1) (50). It is proposed that in its GDP-bound state HflX binds to the ribosome, exchanges the diphosphate form of guanosine for GTP, and hydrolyzes the triphosphate form (Figure 1.4.3.1).



Figure 1.4.3.1 **Minimal mechanistic model of HflX.** HflX (purple and black) in its GDP-bound form will be found bound to 70S ribosomes (grey). Upon dissociation of GDP, HflX will bind GTP and adopt a closed, GTPase-activated conformation on the 70S ribosome, allowing GTP hydrolysis to take place.

HflX remains bound to ribosomal particles during its entire functional cycle therefore some signal, unknown at this time, must exist within the cell or originating from the ribosome to regulate not only the release of HflX but also to regulate the hydrolysis of GTP. It has not yet been determined whether this signal originates from the ribosome itself or from an additional factor. However, the fact that antibiotics such as chloramphenicol can affect ribosome stimulated GTP hydrolysis hints at ribosomal regulation (47,50). Increasing evidence supports a role of HflX during translation, however the stage during protein synthesis remains to be discovered.

*1.5 YchF*

In the genomes of many bacterial species the *ychF* gene is located next to the gene encoding for peptidyl-tRNA hydrolase, *pth* (54). The role of peptidyl-tRNA hydrolase in the cell is to cleave the ester bond between the growing polypeptide and tRNA to recycle peptidyl-tRNAs from stalled ribosomes and ensure the continuation of translation (55). Northern-blot experiments have demonstrated that *pth* and *ychF* are cotranscribed in a bicistronic transcript and further evidence of related functions can be inferred from their similar phylogenetic patterns (54). In *Escherichia coli,* downregulation of *ychF* has been observed as a response to DNA damage (56). Treatment of *E. coli* cells with the potent DNA crosslinker mitomycin C produced an expression profile for *ychF* that closely correlated with genes related to protein biosynthesis, in particular ribosomal protein genes (56). Down regulation of both ribosomal proteins and YchF might serve as an indicator that these important molecules elicit similar responses to conditions of stress. YchF has been shown to be essential in *Staphylococcus aureus* (57) whereas in *E. coli,* deletion of the *ychF* gene results in growth retardation and at elevated temperatures, filamentation (58). The human homolog (hOLA1) has been found to be overexpressed in a variety of cancers ranging from colon to ovary, lung and stomach (59). hOLA1 has also been implicated in centrosome regulation with the breast and ovarian cancer specific tumor suppressor, BRCA1 (60). In *E. coli,* overexpression of YchF has been associated with hydrogen peroxide hypersensitivity (61). YchF is capable of inhibiting the catalase activity of KatG through a direct interaction. Furthermore

the transcription levels of YchF are repressed by the transcription factor OxyR (61). When the cellular concentration of hOLA1 is reduced, resistance to peroxides and thiols is increased therefore drawing a correlation between YchF and its human homolog would suggest that both enzymes function as a negative regulators of the oxidative stress response (62). Due to its high level of conservation and functional similarity with hOLA1, determining and understanding the cellular function YchF will provide key information necessary for unraveling the cellular role of hOLA1.

### 1.5.1 Structure of YchF

Crystal structures of YchF have been determined from several organisms including *Thermus thermophilus, Haemophilus influenza (H. influenza)* and *Homo sapiens* (59,63). All structures revealed that YchF folds into three well-defined domains. Apart from the typical P-loop NTPase G-domain located at the N-terminus, YchF possesses a $\alpha$-helical domain and a C-terminal TGS (Threonyl-tRNA synthetases, GTPases, SpoT) domain (Figure 1.5.1.1) (59,63). Present in YchF and characteristic of the common structure formed by canonical G-domains is a parallel $\beta$-sheet surrounded by $\alpha$-helices on each side (Figure 1.5.1.1) (63). YchF also contains the two conserved sequence motifs, the Walker A (G1) and Walker B (G2) that play a major role in coordinating the phosphates of bound nucleotides (Figure 1.5.1.1) (63). The differentiating feature of YchF within the TRAFAC class of P-loop GTPases is the guanine nucleotide-binding site. The G4 (N/TKXD) motif of YchF and the Obg-like ATPase subfamily is variable, with bacterial proteins containing the consensus sequence NVNE, whereas human

proteins contain the sequence NLSE (59,63). The crystal structure from *H. influenza* revealed that the missing lysine residue in this motif was replaced by a conserved phenylalanine residue from an adjacent G-domain loop, $\beta$5 (63). Stacking of the guanine base is accomplished through a pi-pi stacking interaction with the phenylalanine residue (63). The asparagine residue together with the glutamate residue further position the nucleotide by contacting the amino groups of the guanine base (63). This alteration in the G4 motif of the G-domain results in an altered specificity of YchF, preferring adenine nucleotides over guanine nucleotides. This altered specificity has been confirmed experimentally in *Trypanosoma cruzi* (*T. cruzi*)*, H. influenza, E. coli, Saccharomyces cerevisiae* and with hOLA1 (59,64-66). The two domains flanking the N-terminal G-domain, the $\alpha$-helical domain and TGS domain form what could be considered a binding site for a double-stranded nucleic acid as the inner helices of both these regions of the protein consist of clusters of positively-charged residues (Figure 1.5.1.1) (63). Both domains resemble proteins known to bind RNAs, suggesting a similar function for YchF. Proteins such as seryl-tRNA synthetase and threonyl-tRNA synthetase in particular make contact with tRNA, and topologically match the $\alpha$-helical domain and TGS domain, respectively (63). The potential of YchF to interact with a structured RNA needs to be further explored and considered in light of its interaction with ribonucleoprotein complexes, such as the ribosome.
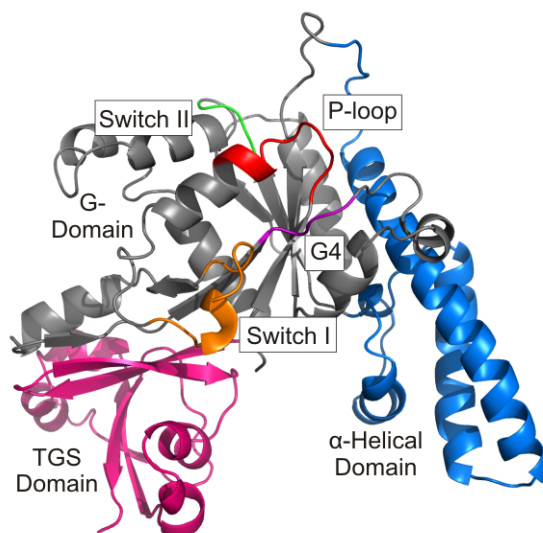
Figure 1.5.1.1 **Homology model of *E. coli* YchF based on the crystal structure from *H. influenzae* (1JAL).** The G1 motif is shown in red, G2 in orange, and G3 in green and G4 in purple.

*1.5.2. The Nucleotide Hydrolysis Activity of YchF*

Within the GTPase superfamily, YchF belongs to the subfamily of HAS-GTPases wherein the catalytic glutamine residue is replaced with a hydrophobic leucine (64). YchF contains all the conserved elements to be considered a potassium-dependent GTPase, which includes a K-loop element inserted into switch I and an asparagine in the P-loop (64). The slow intrinsic hydrolysis of ATP can be stimulated by potassium ions, with the asparagine residue demonstrated to be critical for coordinating it (64). Other HAS-GTPases such as MnmE and YqeH have catalytic residues that are provided by α-helices adjacent to the G3 motif (67,68). Examination of YchF led to the discovery that a highly conserved lysine in position 78 in *E. coli* could potentially position a water molecule for a nucleophilic attack on the gamma phosphate of the adenine nucleotide (64). When mutated to alanine, the actual role for this lysine residue appears to be in influencing the extent of potassium-dependent activation of ATP

21

hydrolysis (64). The potassium dependence of YchF could serve as an effective mode of regulation. In *E. coli*, where the concentration of the monovalent cation is around 200 mM, its levels within the cell fluctuate in response to osmotic stress in order for bacterial growth to continue (69,70). However, before the context of regulation by potassium ions can be fully understood, the single or multiple residues required for catalysis in YchF in the presence or absence of ribosomes need to be elucidated.

*1.5.3 Hypotheses as to the Functional Role of YchF*

A role for YchF in protein synthesis has also been hypothesized much like HflX and several of the previously characterized, universally conserved GTPases. YchF from the protozoan, *Trypanosoma brucei,* has been found to associate with ribosomes (65). *T. cruzi* YchF immunoprecipitates with ribosomal subunits and a subunit of the proteasome (65). This data correlates well with the discovery that YchF in *S. cerevisiae* interacts with the multisubunit translation elongation factor eEF1 and the yeast proteasome (71). In *E. coli*, His-tagged YchF has been reported to associate with a megadalton complex containing 70S ribosomes (66). YchF in complex with both ribosomes and ribosomal subunits can be reconstituted *in vitro,* and this interaction has been shown to be dependent on the nucleotide bound state of the factor with tighter binding to 70S and 50S particles observed in the presence of ATP (66). Intact 70S ribosomes can stimulate the ATPase activity of YchF, but only 30% of this ribosome population is capable of interacting with the protein (66).
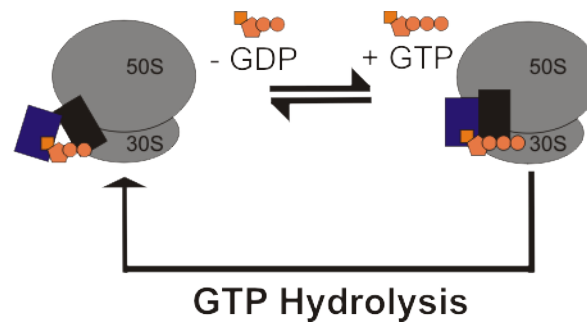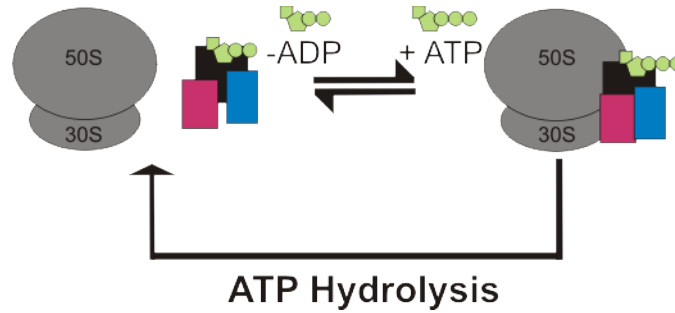
Figure 1.5.3.1 **Minimal mechanistic model of YchF.** YchF (pink, blue and black) in its ADP-bound form may not be found bound to 70S ribosomes (grey). Upon dissociation of ADP and binding of ATP, YchF will interact with the 70S ribosomes, stimulating the factor's ATPase activity.

This low occupancy of ribosomes with YchF is similar to other ribosome biogenesis factors like EngA and Era (66) and suggests that YchF most likely interacts with an intermediate in the ribosome assembly pathway. The exact nature of this intermediate remains to be identified, as well if the ribosome can modulate and stabilize various nucleotide bound states of YchF.

*1.6 Objectives*

The universally conserved GTPases, IF2, EF-Tu and EF-G are essential to the process of ribosome-dependent protein synthesis. HflX and YchF are universally conserved ribosome-associated GTPases but their cellular roles are poorly understood. Examining the structural and functional dynamics of these proteins' GTPase cycles is critical to understanding their functions in the cell. This thesis focuses on HflX and YchF in relation to their GTPase cycles and addresses the following questions:

1. What are the rates of the interactions of HflX and YchF in different nucleotide-bound states with ribosomal particles (70S, 30S and 50S)?

A fluorescence-based system was designed and used to study the interaction of HflX and YchF with 70S ribosomes and 50S and 30S ribosomal subunits. Both proteins naturally contain multiple cysteines, thus initial construction of modified HflX and YchF was undertaken to allow for the incorporation of fluorescent dyes in specific locations for future fluorescence experiments.

2. Does the nucleotide hydrolysis activity of HflX require monovalent cations, large-scale movement of protein domains or its poorly conserved C-terminal extension?

Variants of HflX were constructed to dissect whether the structural dynamics of HflX and the interactions between its structural elements influences its ribosome-associated catalytic activities.

3. To what extent can the ribosome regulate nucleotide association and dissociation from HflX and YchF?

Kinetic parameters associated with nucleotide binding and hydrolysis were obtained in both the presence and absence of antibiotics to induce various conformational states of the ribosome in order to gain insight into the "NTPase activated" states of HflX and YchF.

## Chapter 2 –

## *Development of a Fluorescence-Based System to Study the Interaction of HflX and YchF with the Ribosome*

## 2.1 Introduction

A variety of biochemical and biophysical methods have been developed to study protein-protein interactions. In order to identify novel cellular interaction partners, pull-down assays with affinity-tagged proteins or co-immunopreciptation techniques can be used (72). To understand how an interaction between two proteins is related to its specific activity and response *in vivo*, a method sensitive enough to detect interactions between molecules with affinities ranging from micro to picomolar levels is required (72). Fluorescence based assays can allow for particular interactions to be quantified and even reveal the dynamics of a molecular system. Fluorophores are able to provide such information by exhibiting changes in fluorescence upon perturbations in the local environment. The formation of a complex of proteins can lead to the reduction of interfaces with solvent molecules shifting fluorescence emission and providing researchers with temporal information about biomolecular interactions. Proteins contain two amino acids with either sulfhydryl or amino groups that allow for conjugation to chemically reactive groups attached to fluorophores (73). It is most informative to place these cysteine or lysine residues in specific locations of interest upon the removal of the naturally-occurring residues elsewhere in the protein. Once a protein has been shown to retain its activity following the substitution of naturally occurring reactive residues, the modified enzyme can then be used in fluorescent experiments. For many of the canonical translational GTPases, residues critical

26

to catalysis or that are required to mediate interactions with other biomolecules such as nucleotides, RNAs or other proteins have been discovered (74). Even residues that have been found to not directly participate in any molecular interactions may have lesser-defined functional roles in the protein or could participate in a communication network of residues that taken all together are responsible for the specific dynamics of that GTPase.  Alterations to residues in GTPases should only be undertaken if their contribution to regulating and fine-tuning the function of the protein is well understood. For *E. coli* EF-Tu, a GTPase containing three intrinsic cysteines, a fully functional Cys-less variant has been constructed by ensuring naturally occuring substitutions were made in the place of the respective cysteine residues (74).  A similar approach was used with *E. coli* HflX and YchF.  First, the requirements of the two factors for cysteine residues in their intrinsic positions will be assessed upon their respective removal.  For HflX and YchF, possessing three and six cysteines respectively, Cys-less variants of both factors will allow for the inclusion of site-specific fluorescent labels for single-molecule experiments. As a starting point, the susceptibility of the naturally-occuring cysteines within these proteins to react with a fluorophore was tested to ensure that the known activities of the factors are unchanged upon modification.  Additionally, preliminary kinetic information relating to the dynamics of fluorescently labeled HflX and YchF interacting with ribosomes will be elucidated.

## 2.2 Materials and Methods

DH5α cells were purchased from New England BioLabs and BL21-DE3 competent cells were purchased from Novagen. PCR primers were purchased from Invitrogen and Integrated DNA technologies. Restriction enzymes were obtained from New England BioLabs. Radiochemicals were purchased from Perkin-Elmer. Nucleotides and fluorescent nucleotide analogs were purchased from Sigma and Jena BioScience. All buffers were filtered through 0.45 µm Whatman nitrocellulose membranes.

### 2.2.1 Sequence Alignments

Protein sequences from the Entrez Gene database (www.ncbi.nlm.nih.gov/gene) were aligned using ClustalW2 from EBI (http://www.ebi.ac.uk/Tools/clustalw2). Images of the multiple sequence alignments were generated in GeneDoc and shaded based on percent identity. Amino acids highlighted in white are less than 60% identical, residues in light grey are 60-80% identical, dark grey coloring is indicative of greater than 80% identity and 100% identity is shown with black shading (75).

### 2.2.2 Site-directed Mutagenesis

A pET28a plasmid harboring the nucleotide sequence for N-terminal His$_6$-tagged *E. coli* HflX was subjected to the Quikchange® Site-Directed Mutagenesis method to introduce amino acid substitutions. At position 96 within the protein, a cysteine was substituted to a serine whereas cysteines at 98 and 415 were changed to leucine residues. Restriction sites were incorporated into the DNA

sequences to allow for the screening of variants prior to sequencing. In Table 2.2.2.1, the respective nucleotide changes are denoted in bold while restriction sites are underlined. Reactions with a final volume of 25 µL were composed as follows: 1000 ng of template DNA, 0.4 µM of each forward and reverse primer (Invitrogen), 400 µM of dNTPs and 3 units of *Pfu* DNA polymerase (Truin Science). A $T_{Gradient}$ thermocycler (Biometra) was used to initially heat the reactions to 95°C for 5 minutes, followed by 18 cycles of 95°C for 1 minute, a 1 minute annealing step at a temperature 10°C below the melting temperature of the primer ($T_M$), and extension at 68°C for 20 minutes. The reaction was subjected to a final extension at 68°C prior to treatment with the restriction enzyme *DpnI* (Fermentas). Overnight incubation at 37°C with the enzyme results in the complete cleavage of methylated template DNA. A dilution of 1:100 of the reaction products were transformed into 20 µL of *E. coli* DH5α competent cells (New England BioLabs) and subsequently grown on 50 mg/mL kanamycin-supplemented Luria-Bertani (LB) agar plates and LB media. To identify positive mutants, restriction digestion screening was performed on plasmids isolated from individual colonies using a miniprep purification kit (EZ-10 Spin Column Plasmid DNA Kit, BioBasic). Following further verification through Sanger sequencing (Genewiz), plasmids harboring the desired variants of HflX were transformed into 15 µL of *E. coli* BL21-DE3 competent cells (Invitrogen) for subsequent overexpression.

Table. 2.2.2.1  Primers for Site-Directed Mutagenesis of HflX

| | C96SC98L | C415L |
|---|---|---|
| Forward Primer | 5' AAC CTG GAG CGT TTG **TCC** <u>GAG</u> **CTC** CGT ATC GAC CGC ACC GG 3' | 5' CGC CTC **CTT** <u>AAG</u> CAA GAA CCG GCG 3' |
| Reverse Primer | 5' CCG GTG TCG ATA ACA CG<u>G</u> **AG**C TC**G GA**C AAA CGC TCC AGG TT 3' | 5' CGC CGG TTC TTG <u>CTT</u> **AAG** GAG GCG 3' |
| T$_M$ (°C) | 72.8 | 70.6 |
| Restriction Site | SacI | AflII |

## 2.2.3 Protein Expression and Purification

*HflX* - Transformed *E. coli* BL21-DE3 cells were grown at 37°C in LB media containing 50 mg/mL kanamycin until mid-log phase or an optical density of approximately 0.6 at 600 nm, followed by subsequent induction with 1 mM IPTG (isopropyl-β-D-galactopyranoside) (BioBasic).  The late logarithmic stage was reached following three additional hours of incubation at 37°C and cells were harvested by centrifugation at 5000xg in order to be flash frozen and stored at -80°C until purification.  Protein expression levels were monitored by obtaining 1 OD culture samples every hour upon induction and analyzing the cell pellets dissolved in 8 M urea by 12% sodium dodecyl sulfate polyacrylamide gel electrophoresis (SDS-PAGE) (BioRad Mini Protean 3 System).  SDS-PAGE were

performed at 80 V for 20 minutes followed by 60 minutes at 200 V. Gels were stained with Coomassie blue and all other SDS-PAGEs were completed in a similar fashion. All HflX overexpressing frozen cell pellets were first resuspended in 7 mL/g of cells of Buffer A (50 mM Tris-Cl pH 8.0 at 4°C, 60 mM $NH_4Cl$, 300 mM KCl, 7 mM $MgCl_2$, 7 mM β-mercaptoethanol, 10 mM imidazole, 15% v/v glycerol and 1 mM phenylmethylsulfonyl fluoride (PMSF)). Lysis was achieved by a 30 minute incubation at 4°C with 1 mg/mL of cells of lysozyme. Subsequently, sodium deoxycholate to a final concentration of 12.5 mg/g of cells was added and incubation at 4°C was carried out until the viscosity of the solution increased. The solution was then sonicated to shear genomic DNA prior to centrifugation at 3000xg to pellet cell debris. Cleared cell lysate was obtained by further centrifugation at 30000xg for 45 minutes (Beckman). To isolate HflX by affinity chromatography, the resulting cell lysate was applied to a 5 mL $Ni^{2+}$-Sepharose column (GE Healthcare) pre-equilibrated in Buffer A. The resin was first washed with 30 column volumes of Buffer A followed by 30 column volumes of Buffer B (Buffer A with 20 mM imidazole) to remove any nonspecifically bound protein. Elution of $His_6$-tagged HflX variants was done with 8 column volumes of Buffer E (Buffer A with 300 mM imidazole). Size exclusion chromatography using a pre-equilibrated Superdex 75 XK26/100 column (GE Healthcare) was utilized to further purify and rebuffer the pooled and concentrated elutions from affinity chromatography. Fractions in final storage buffer ($TAKM_7$: 50 mM Tris-Cl pH 7.5 at 4°C, 70 mM $NH_4Cl$, 300 mM KCl and 7 mM $MgCl_2$) were pooled and concentrated. The final concentration of the protein preparations were

determined photometrically at 280 nm using a molar extinction coefficient of 32555 $M^{-1}cm^{-1}$ and confirmed by SDS-PAGE analysis followed by quantification with ImageJ software (76). Aliquots of HflX protein were flash frozen and stored at -80°C until future use.

*Insoluble HflX Variants* - Expression of insoluble variants of HflX was achieved in a similar manner as above, but upon induction *E. coli* cells were grown at 18°C overnight instead of 37°C for three hours. Solubility tests were performed by opening cells as outlined previously but pellets from the two centrifugation runs were dissolved in 8 M urea to ascertain whether HflX variants were being sequestered in inclusion bodies within *E. coli.*

*YchF* - Expression and purification of wildtype and variants of YchF was carried out as described for HflX but with the addition of an anion exchange chromatography (Q-Sepharose XK26 Fast Flow – GE Healthcare) step prior to subjecting the protein preparations to size exclusion chromatography. Pooled and concentrated elutions from affinity chromatography were exchanged into Q-Sepharose Buffer A (50 mM Tris-Cl pH 7.5 at 4°C, 10 mM $MgCl_2$, 5 mM EDTA, 1 mM diothiothreitol (DTT)). To remove any bound RNA, a salt gradient from 0 to 100% Q-Sepharose Buffer B (Q-Sepharose Buffer A with 1 M KCl) was utilized resulting in protein free of nucleic acid. A molar extinction coefficient of 16305 $M^{-1}cm^{-1}$ was used to determine the final concentrations of YchF protein preparations photometrically at 280 nm.

*2.2.4 Preparation of Ribosomes*

Ribosomes were purified from *E. coli* MRE600 cells as described but with a Ti 45 rotor rather than a Ti 50.2 rotor (77).

*2.2.5 Fluorescent Labeling with 5-IAF*

In a total volume of 5 mL, 100 000 pmol of purified $His_6$-tagged HflX or YchF was incubated with 5 mM β-mercaptoethanol (β-ME) for 30 minutes in Labeling Buffer ($TAKM_7$ with 15% glycerol) to reduce the cysteines found within the proteins. To adequately space the protein in solution, protein was applied to a $Ni^{2+}$-Sepharose column pre-equilibrated in Labeling Buffer for 30 minutes at 4°C. Unbound protein was collected from the resin by centrifugation at 500xg for 2 minutes. 30 column volumes of Labeling Buffer were utilized to further remove any remaining β-ME or unbound protein. Treatment of the bound protein sample with a 40 molar excess of the cysteine-specific fluorescent dye, 5-iodoacetoamidofluorescein (5-IAF) (Sigma) dissolved in dimethylsulfoxide (DMSO), was carried out at room temperature for 2 hours initially, followed by overnight at 4°C in 20 mL of Labeling Buffer. Incubation of the resin coated in labeled factor with 40 column volumes of Labeling Buffer allowed for the removal of excess fluorescent dye in the supernatant. Elution of HflX or YchF labeled with 5-IAF was accomplished by 20 minute incubations with 8 column volumes of Buffer E (as described in 2.2.3). Three successive overnight dialysis steps into 1 L of Labeling Buffer, utilizing high retention seamless cellulose tubing (MWCO 11033 – Sigma), were required to reduce the concentration of imidazole in the final fluorescently labeled protein preparations. ImageJ (76) was used to

determine the concentration of fluorescently-labeled HflX or YchF from 12% SDS-PAGE gels.  HflX or YchF concentration upon labeling and the number of 5-IAF molecules per molecule of protein were also quantified from absorbance measurements at 280 and 490 nm ($A_{280}$ and $A_{490}$) using Equations 2.2.5.1, 2.2.5.2 and 2.2.5.3, where $\varepsilon$ are the molar extinction coefficients of 5-IAF or the protein factors in solution.

$$\frac{A_{490}}{\varepsilon_{5-IAF\ @\ 490\ nm}} \times \varepsilon_{5-IAF\ @\ 280\ nm} = A_{280\ of\ 5-IAF} \qquad (2.2.5.1)$$

$$\frac{A_{280} - A_{280\ of\ 5-IAF}}{\varepsilon_{Factor\ @\ 280\ nm}} = [Factor] \qquad (2.2.5.2)$$

$$\frac{A_{490}}{\varepsilon_{5-IAF\ @\ 490\ nm} \times [Factor]} = \#\ molecules\ of\ dye\ per\ factor\ molecule \qquad (2.2.5.3)$$

To avoid photobleaching, the labeling procedure was carried out under dark conditions.

*2.2.6 Steady State Fluorescence Measurements*

Fluorescence emission spectra of HflX or YchF labeled with 5-IAF were obtained using a QuantaMaster Fluorescence Spectrophotometer (Photon Technology International) with a 2 mm by 10 mm quartz cuvette (18F-Q-1MS – Starna Cells). The fluorescence emission of 0.25 µM of labeled protein was monitored from 500 to 600 nm upon excitation at 490 nm.  Slit widths were set to 1 and 5 nm for excitation and emission, respectively.

Since HflX and YchF contain tryptophan residues in their G and TGS domains, the intrinsic fluorescence of these residues can be monitored during nucleotide binding experiments.  In TAKM$_7$ buffer, 1 µM of protein was incubated with

increasing amounts of purine nucleotides. Following excitation at 280 nm with a slit width of 1 nm, fluorescence emission was recorded from 300 to 500 nm at a step size of 1 nm and a slit width of 5 nm. The overall fluorescence intensity detected for each nucleotide binding experiment was calculated by subtracting the fluorescence intensity observed for the addition of nucleotide into buffer and the change in fluorescence was also corrected for dilution. From the concentration dependence of the fluorescence change at 337 nm, equilibrium dissociation constants for HflX and YchF and nucleotides were determined. Using Table Curve (Jandel) and Prism (GraphPad) software the data was fit with a hyperbolic function (Equation 2.2.6.1), where $Fl$ is the final fluorescence, $Fl_0$ is the initial fluorescence value, $\Delta F_{max}$ is the overall change in fluorescence and $K_D$ is the characteristic equilibrium dissociation constant.

$$Fl = Fl_0 + \frac{\Delta F_{max} \times [nt]}{K_D + [nt]}$$ 
(2.2.6.1)

*2.2.7 Nucleotide Hydrolysis Assays*

*HflX* - The release of $^{32}$P-labeled inorganic phosphate (P$_i$) from [γ-$^{32}$P] GTP (Perkin-Elmer) was monitored to determine the rate of GTP hydrolysis by HflX (47). To ensure that nucleotides were in their triphosphate form and multiple turnover experiments would not be inhibited by nucleotide diphosphates, [γ-$^{32}$P] GTP (approximately 100 dpm/pmol) was incubated with 0.25 µg/µL pyruvate kinase (PK), and 3 mM phosphenolpyruvate (PEP) for 15 minutes at 37°C (47). Similarly, 15 µM HflX was also incubated with PK and PEP (47). Reactions were composed of 1 µM HflX, 125 µM radiolabeled nucleotide solution, 1 µM ribosomes or ribosomal subunits and carried out in TAKM$_{30}$ buffer (50 mM Tris-Cl

pH 7.5 at room temperature, 70 mM NH$_4$Cl, 30 mM KCl, 30 mM MgCl$_2$). At different time points, 5 µL of reactions were removed and quenched in 50 µL of 1 M HClO$_4$ with 3 mM K$_2$HPO$_4$ (47). Inorganic phosphate was extracted as a phosphate-molybdate complex following the addition of 300 µL of 20 mM Na$_2$MoO$_4$ and 400 µL of isopropyl acetate, mixing for 30 seconds and centrifugation at 17000xg for 5 minutes (47). The organic phase containing the radiolabeled inorganic phosphate was added to 2 mL of scintillation cocktail (MP EcoLite) and counted in a Perkin-Elmer Tri-Carb 2800TR liquid scintillation counter. To determine the concentration of $^{32}$P$_i$ released as a function of time the concentration of NTPs hydrolyzed by buffer or ribosomes alone was subtracted from the concentration of NTPs hydrolyzed by enzyme in the presence or absence of ribosomes. The rates of purine nucleotide hydrolysis by HflX in the presence of ribosomes was found by fitting the multiple turnover experiments with a linear equation, where the slope is equal to the apparent rate of nucleotide hydrolysis.

*YchF* – The methodology to monitor the ATP hydrolysis by YchF was identical to the methods previously described for HflX except that the final concentration of YchF in the reaction was 5 µM.

*2.2.8 Pre-Steady State Fluorescence Stopped-Flow Experiments*

Fluorescently labled HflX was excited at 490 nm and the emission of the fluorophore detected upon passing through LG-500F cutoff filters (NewPort Filters). Changes in fluorescence were monitored and recorded upon rapidly mixing 1 µM 5-IAF labeled HflX in the apo, GDP or GDPNP bound state (250 µM

of guanine nucleotides) against 0.30 µM ribosomal subunits (50S or 30S) or ribosomes (70S) in a KinTek SF-2004 Stopped-flow apparatus. The fluorescence changes observed were best fit with a two exponential function using TableCurve software. To ascertain whether any of the fluorescence changes were dependent on concentration, 50S ribosomal subunits (0.40 µM to 1.2 µM) were titrated against preformed complexes of 1 µM 5-IAF HflX and 250 µM GDP. Normalized traces were averaged and refit with a three exponential function where $k_{app}$ is the characteristic apparent rate constant, $A$ is the signal amplitude, $Fl$ is the fluorescence at time $t$, and $Fl_\infty$ is the final value of fluorescence (Equation 2.2.8.1).

$$Fl = Fl_\infty + A_1 \exp(-k_{app1}t) + A_2 \exp(-k_{app2}t) + A_3 \exp(-k_{app3}t) \qquad (2.2.8.1)$$

*2.2.9 Microfiltration Binding Assays*

*HflX* - In $TAKM_{30}$ buffer, complexes of HflX with the ribosome were formed by incubating 5 µM of wild-type or variant HflX with 1 µM of 70S in the presence of 1 mM GDP or GDPNP for 15 minutes at 37°C. Incubation on ice for 5 minutes preceded the addition of the samples to 480 µL of $TAKM_{30}$ buffer and centrifugation for 5 minutes at 10000xg in Vivaspin-500 columns with a MWCO of 100 kDa (GE Healthcare). Once a final volume of 20 µL was reached, the samples were diluted a second time to 500 µL and refiltered. The binding of HflX to ribosomes or ribosomal subunits was analyzed using 12% SDS-PAGE gels. *YchF* - Microfiltration assays with various YchF preparations were performed identically to those carried out with HflX with the exception of the buffer system

being TAKM$_7$ buffer and the concentration of the components being 4 µM YchF variant, 0.68 µM 70S ribosomes and 500 µM ADP or ADPNP.

*2.2.10 Circular Dichroism Spectroscopy Experiments*

Using a Jasco J815 CD Spectrometer, the spectra of variant HflX and YchF proteins was compared to the spectra of wild-type HflX and YchF. Prior to analysis, protein samples were dialyzed overnight into water or 50 mM Na$_3$PO$_4$ to avoid any chemicals that would absorb light of lower wavelengths. Higher yields of HflX were found when dialyzed into 50 mM Na$_3$PO$_4$ whereas a greater yield of YchF protein was obtained following dialysis in water. At 20°C, 1 µM of protein in 150 µL of appropriate buffer is scanned from 250 nm to 350 nm to obtain ellipticity values.

## 2.3 Results

*2.3.1 Initial Characterization of Fluorescently Labeled YchF*

The susceptibility of the intrinsic cysteines within HflX and YchF to react with the fluorescent dye, 5-iodoacetoamidofluorescein and an initial assessment of whether once labeled the two proteins retained wildtype behavior, had not been studied until recently. In our laboratory, HflX labeled with the 5-IAF, was shown to function comparably to unlabeled wildtype HflX, being capable of hydrolyzing GTP and binding to 70S ribosomes (Mackenzie Coatham, Undergraduate Thesis 2012). An analogous approach of labeling wildtype YchF, containing six cysteine residues, was attempted to initially characterize the factor. Fluorescence emission for fluorescently labeled YchF (Fl-YchF) was observed upon exciting the fluorophore at 490 nm. A maximal increase in fluorescence was observed at 520 nm, the fluorescence emission for the fluorophore (Figure 2.3.1.1 Panel A). Having confirmed that YchF was fluorescently labeled with one molecule of 5-IAF, the factor's ability to bind adenine nucleotides, hydrolyze ATP and bind ribosomes was examined. Interestingly, following modification of YchF by the introduction of a fluorescent dye, the 70S ribosome stimulated ATPase activity of YchF was slower by approximately 20-fold from $0.53\pm0.04$ pmol min$^{-1}$ for wildtype to $0.03\pm0.02$ pmol min$^{-1}$ with labeled YchF (Figure 2.3.1.1 Panel B).
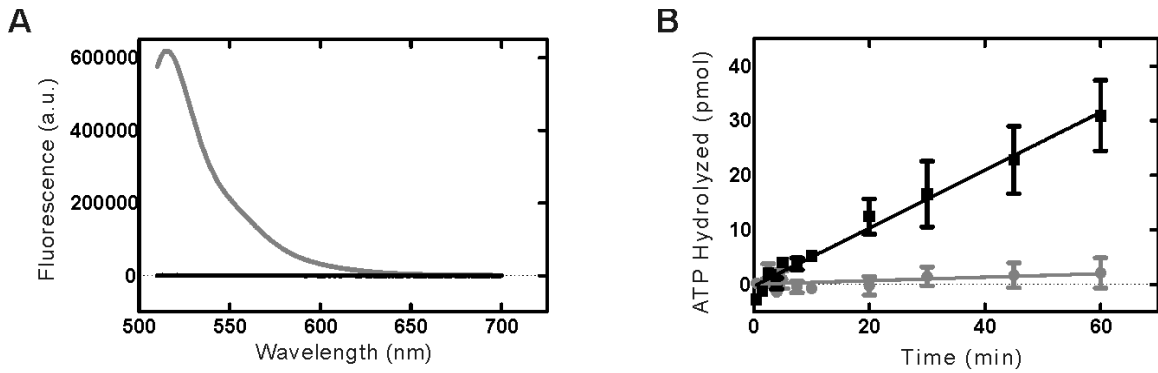
Figure 2.3.1.1. **Fluorescently labeled YchF is inactive compared to unlabeled wildtype YchF.** (A) Fluorescence emission spectra upon exciting YchF labeled with 5-IAF at 490 nm. A fluorescence maximum for Fl-YchF (dark grey) at 520 nm was not observed with wild-type YchF (black). (B) Time course of ATP hydrolysis by Fl-YchF (dark grey) and wild-type YchF (black) stimulated by 1 µM 70S ribosomes.

To determine whether this effect on ATP hydrolysis is due to YchF having a lower affinity for adenosine nucleotides or 70S ribosomes, the ability of Fl-YchF to perform both of these functions was tested. The amount of YchF bound to 70S ribosomes has been reported to be sub-stochiometric but stronger binding can be observed in the presence of ADPNP over ADP (66). A similar interaction with 70S ribosomes modulated by the adenine nucleotide present in solution was observed for Fl-YchF, with more YchF present after microfiltration in the ADPNP rather than the ADP bound states (Figure 2.3.1.2).
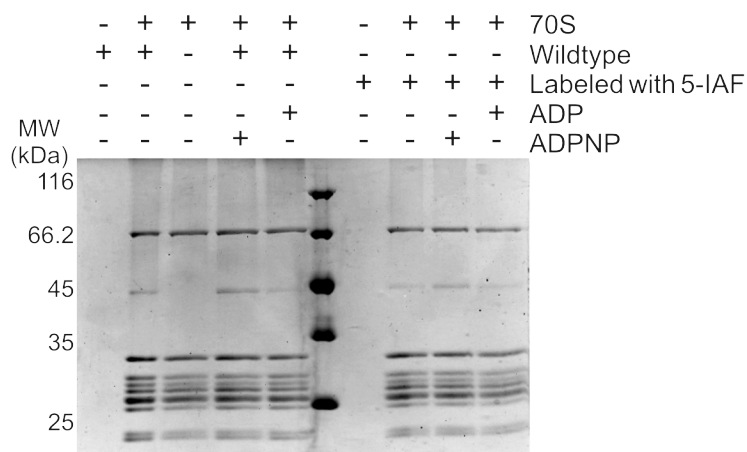
Figure 2.3.1.2 **YchF labeled with 5-IAF binds 70S ribosomes in its ADP and ADPNP bound states like wildtype YchF.** Fl-YchF (45 kDa) is found with 70S in the presence of adenine nucleotides similar to wildtype YchF when subjected to microfiltration centrifugation in 100 kDa molecular weight cut off filters.

As binding to 70S ribosomes was not significantly affected and could not provide an explanation for the inability of Fl-YchF to hydrolyze ATP in the presence of 70S, an examination of the ADP and ATP binding to fluorescently labeled YchF was carried out. As the phosphorylation state of the nucleotide bound can be critical to the function of an ATPase, equilibrium fluorescence titrations allow for the determination of affinities that in turn provide information related to the nucleotide specificity of the factor. By plotting the decrease in tryptophan fluorescence at 337 nm as a function of adenine nucleotide concentration, preliminary dissociation constants can be determined for Fl-YchF. For ADP and ATP, affinities of 106±34 µM and 247±265 µM, respectively were determined for Fl-YchF (Figure 2.3.1.3). The above mentioned affinities differ significantly when compared to the affinities of wild-type YchF for adenosine nucleotides reported in Becker *et al.* (66). This could be attributed to the affect fluorescently labeling has on the protein. Furthermore, these affinities of Fl-YchF for the di- and

41

triphosphate forms of adenosine, could be resulting in the slower rate of multiple-turnover ATP hydrolysis in the presence of ribosomes.
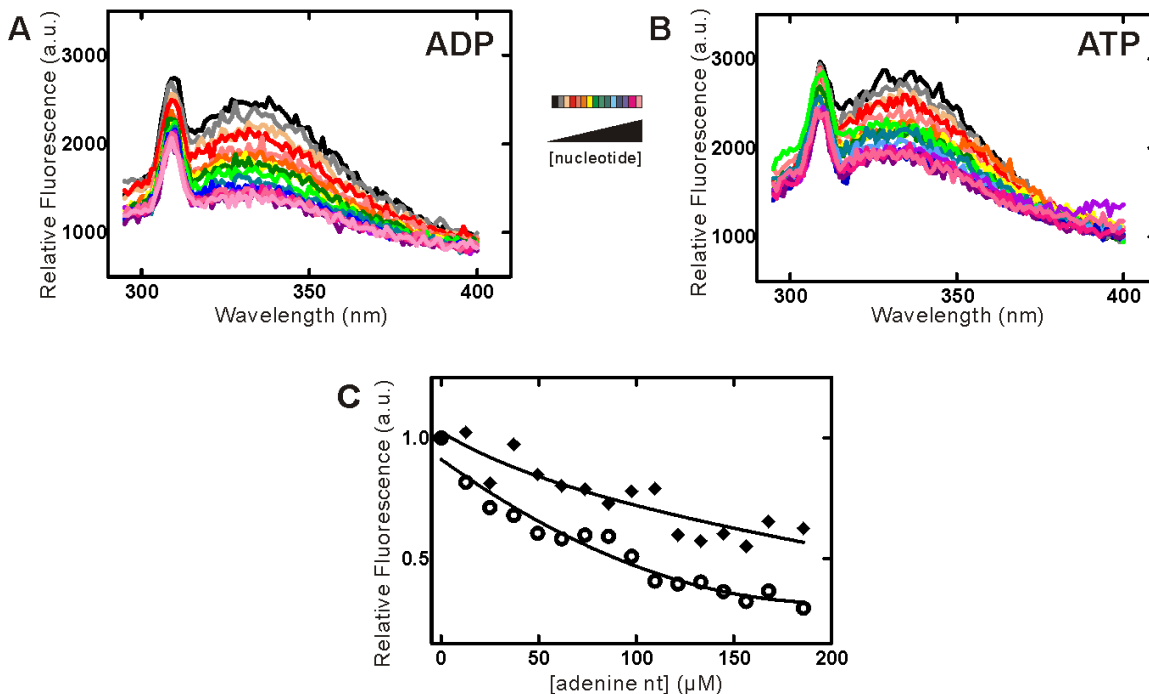


Figure 2.3.1.3 **YchF labeled with 5-IAF binds both ADP and ATP.** (A) Fluorescence emission spectra from 300 to 500 nm upon exciting the intrinsic tryptophan of 1 μM Fl-YchF at 280 nm in the presence of increasing concentrations of ADP. (B) Fluorescence emission spectra from 300 to 500 nm upon exciting the intrinsic tryptophan of 1 μM Fl-YchF at 280 nm in the presence of increasing concentrations of ATP. (C) Plot of the decrease in fluorescence signals at 337 nm as a function of the concentration of ADP (black diamonds) and ATP (clear circles).

*2.3.2 Characterization of a YchF Variant Lacking Cysteine Residues*

As YchF labeled with the fluorescent dye, 5-IAF, at naturally occurring cysteines was severely affected in its ability to bind adenine nucleotides and hydrolyze ATP, further probing of the structural and functional contributions of the cysteine residues within wildtype YchF was pursued. A previously constructed but otherwise uncharacterized variant of YchF in which three of its 6 intrinsic

cysteines were substituted for alanine residues, YchF$_{C5AC35AC106A}$, served as a starting point for the assessment of whether modifying YchF in order to achieve a Cys-less state effects its functions. Having half of the cysteines in its G-domain substituted, YchF$_{C5AC35AC106A}$ was a variant that could assist in answering the question if these residues play a critical role in the activity of the factor.
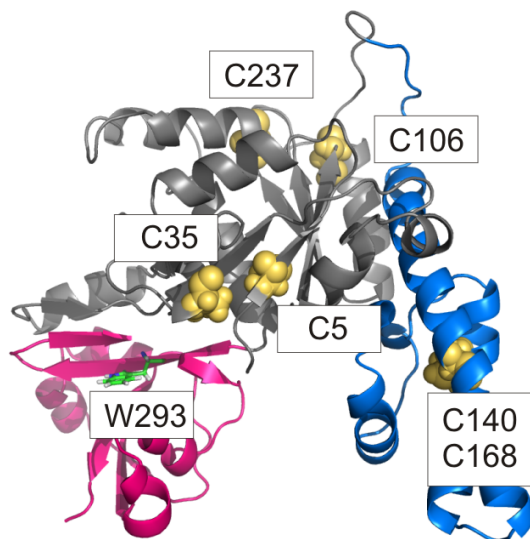


Figure 2.3.2.1 **Homology model of YchF from *E. coli*.** The G-domain (grey) harbors four of the six cysteines in YchF depicted in yellow. The remaining two cysteines are found within the alpha-helical domain (blue). The tryptophan (green sticks) is located in the TGS domain of YchF (pink).

Firstly, the structure of the YchF variant was compared to wildtype using circular-dichroism spectroscopy, but subsequently also its ability to bind adenine nucleotides, hydrolyze ATP and associate with 70S ribosomes were examined. Similar to Fl-YchF, the 70S ribosome-stimulated ATPase activity of YchF$_{C5AC35AC106A}$ was significantly lower than that of wildtype YchF (Figure 2.3.2.2 Panel B). The initial rate of ribosome-stimulated ATP hydrolysis of labeled YchF was ten-fold slower at 0.030±0.009 pmol min$^{-1}$ than that observed for wildtype YchF (0.74±0.04 pmol min$^{-1}$).
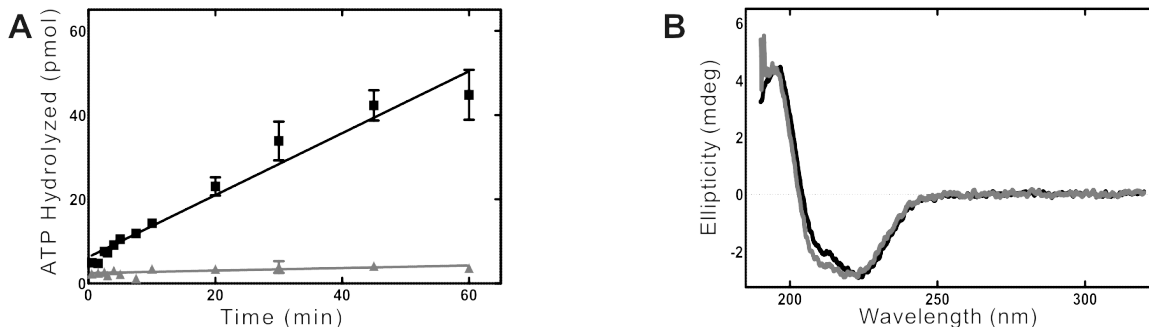
Figure 2.3.2.2 **YchF$_{C5AC35AC106A}$ differs from wild-type YchF in both its structure and ability to hydrolyze ATP.** (A) Time course of ATP hydrolysis by YchF$_{C5AC35AC106A}$ (dark grey) and wildtype YchF (black) in the presence of 1 μM 70S ribosomes. (B) Overlaid CD spectra of YchF$_{C5AC35AC106A}$ (dark grey) and wildtype YchF (black).

Several differences between wildtype YchF and YchF$_{C5AC35AC106A}$ became evident upon further analysis. Firstly, discrepancy between the CD spectra obtained for wildtype YchF and YchF$_{C5AC35AC106A}$ indicates a deviation in protein secondary structure (Figure 2.3.2.2 Panel A). The spectra obtained for both the variant and wildtype YchF are most indicative of proteins containing multiple alpha-helices (78). The shift in the spectrum for YchF$_{C5AC35AC106A}$ below 225 nm hints at some disorder of the alpha-helices comprising the G-domain of the protein upon removal of the cysteines located in the vicinity (Figure 2.3.2.2 Panel A). Equilibrium fluorescence titrations revealed that the affinities governing the interaction of YchF$_{C5AC35AC106A}$ with ADP and ATP were indistinguishable. Wildtype YchF can bind tightly to both the di- and tri-phosphate forms of adenosine but a smaller $K_D$ for ATP at 16±1 μM than ADP at 22±3 μM has been discovered (Figure 2.3.2.3). The $K_D$s for ADP and ATP determined for YchF$_{C5AC35AC106A}$ were both 11±2 μM compared to the equilibrium dissociation constants of 9±8 μM for ADPNP and 14±5 μM for ADP determined in (66) (Figure

2.3.2.3). Thus, along with structural differences, YchF$_{C5AC35AC106A}$ is unable to differentiate between the different forms of adenine nucleotides, all providing probable explanations for the inactivity of the factor.
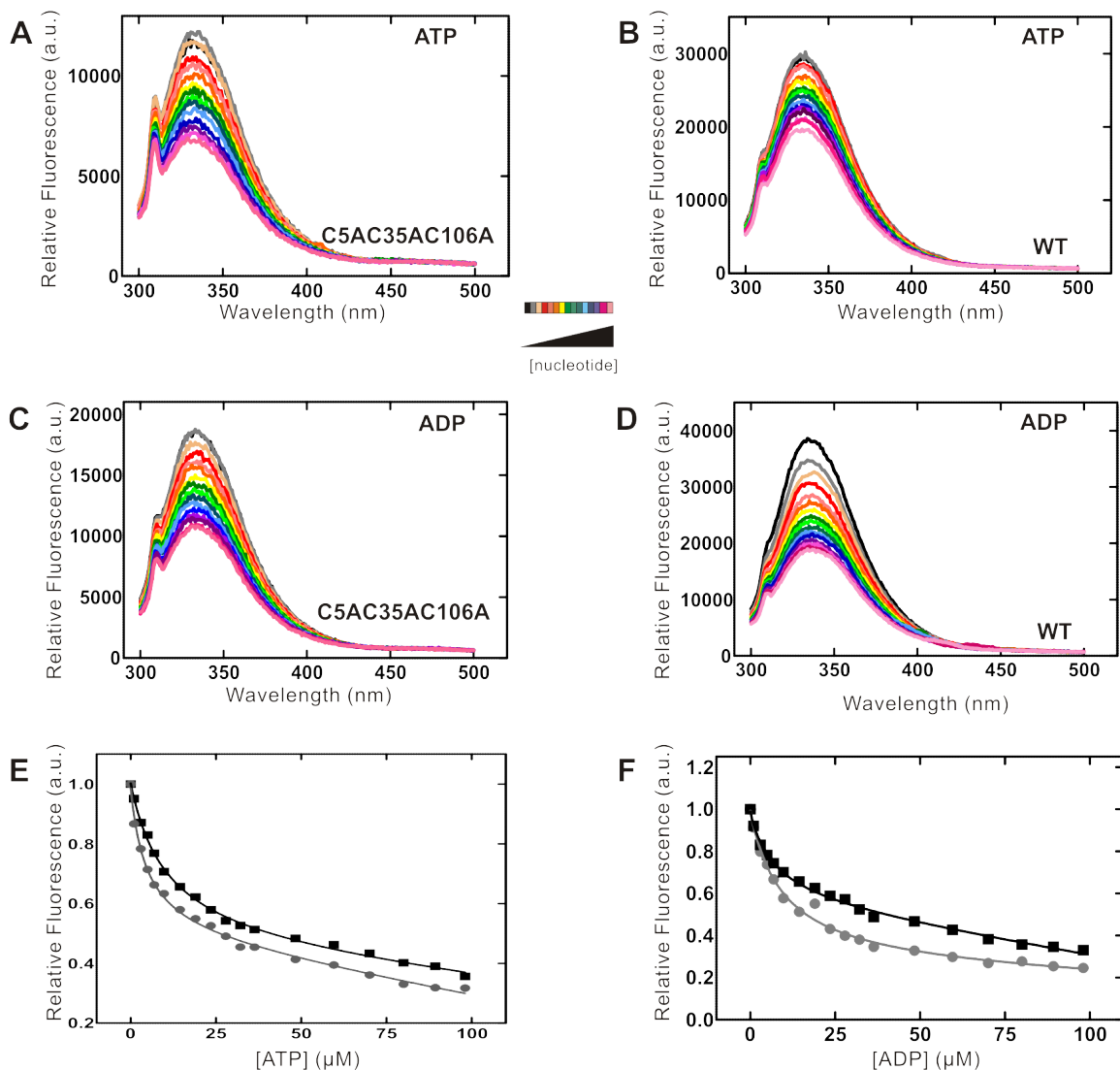
Figure 2.3.2.3 **YchF_{C5AC35AC106A} binds ADP and ATP with the similar affinities.**
(A) Fluorescence emission spectra from 300 to 500 nm upon exciting the intrinsic tryptophan of 1 μM YchF_{C5AC35AC106A} at 280 nm in the presence of increasing concentrations of ATP.  (B) Fluorescence emission spectra of 1 μM YchF as performed in (A). (C) Fluorescence emission spectra of 1 μM YchF_{C5AC35AC106A} as performed in (A) but in the presence of increasing concentrations of ADP.  (D) Fluorescence emission spectra of 1 μM YchF as performed in (C). (E) Plot of the decrease in fluorescence signals for wildtype YchF (black squares) and YchF_{C5AC35AC106A} (grey circles) at 337 nm as a function of the concentration of ATP. (F) A plot of the decrease in fluorescence signals for wildtype YchF (black squares) and YchF_{C5AC35AC106A} (grey circles) at 337 nm as a function of the concentration of ADP.

46

Microfiltration assays revealed that the binding of YchF$_{C5AC35AC106A}$ to 70S was completely abolished, which contrasts with the 30% binding of factor to ribosomes that is normally exhibited by wildtype YchF (Figure 2.3.2.4). Therefore, it seems that on their own or in consort, Cys 5, Cys 35 or Cys 106 are critical to the structure and adenine nucleotide associated activities of YchF.
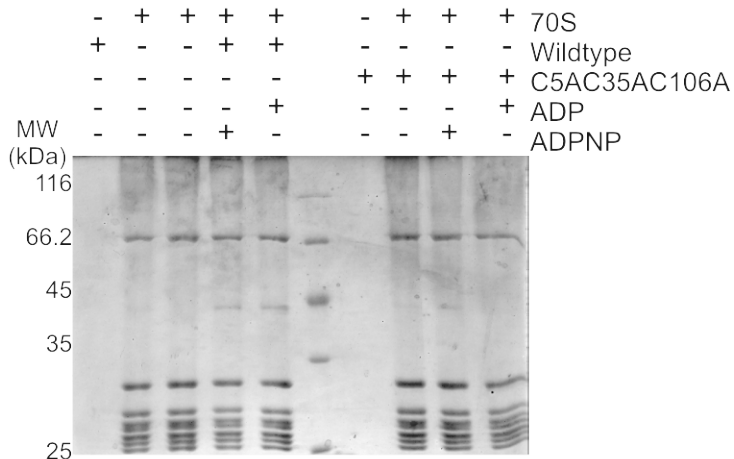


Figure 2.3.2.4 **YchF$_{C5AC35AC106A}$ cannot bind 70S ribosomes in its ADP and ADPNP bound states.** YchF$_{C5AC35AC106A}$ (45 kDa) is not found with 70S in the presence of adenine nucleotides when subjected to centrifugation in 100 kDa molecular weight cut off filters unlike wildtype YchF.

*2.3.3 Preliminary Kinetic Studies with Fluorescently Labeled HflX*

It has been reported previously that HflX is capable of binding to the 70S ribosome and 50S and 30S ribosomal subunits (50). In order to determine the most probable functional interaction partner of HflX in the cell and to further characterize wild-type HflX labeled with 5-IAF, the rate of fluorescently labeled HflX binding to ribosomal particles was assessed using rapid kinetics. Using a stopped-flow apparatus, fluorescently labeled HflX (0.50 µM final) was rapidly mixed with 70S, 50S or 30S to a final concentration of 0.15 µM respectively. Experiments were performed with HflX in the *apo* state or in the presence of

47

GDP and GDPNP (125 µM final respectively). Increases in fluorescence over time were observed when Fl-HflX was rapidly mixed with 30S, 50S and 70S ribosomal particles (Figure 2.3.3.1). The multiphasic increases in fluorescence were best fit with two or three exponential functions (Figure 2.3.3.1). The largest overall change in amplitude of the fluorescence signal was observed when the Fl-HflX interacted with 50S ribosomal subunits in all nucleotide bound states (Figure 2.3.3.1 Panel A-C). Significantly smaller differences between final and initial fluorescence were observed when Fl-HflX associated with 30S ribosomal subunits or empty 70S ribosomes (Figure 2.3.3.1 Panel A-C). Interestingly, the final fluorescence levels for the guanine nucleotide bound states of Fl-HflX were considerably higher than that detected for Fl-HflX in its *apo* form (Figure 2.3.3.1). This might suggest that in solution, the conformation of the protein and therefore the attached fluorophore in the presence of nucleotides differs from the *apo* state of the fluorescently labeled protein.
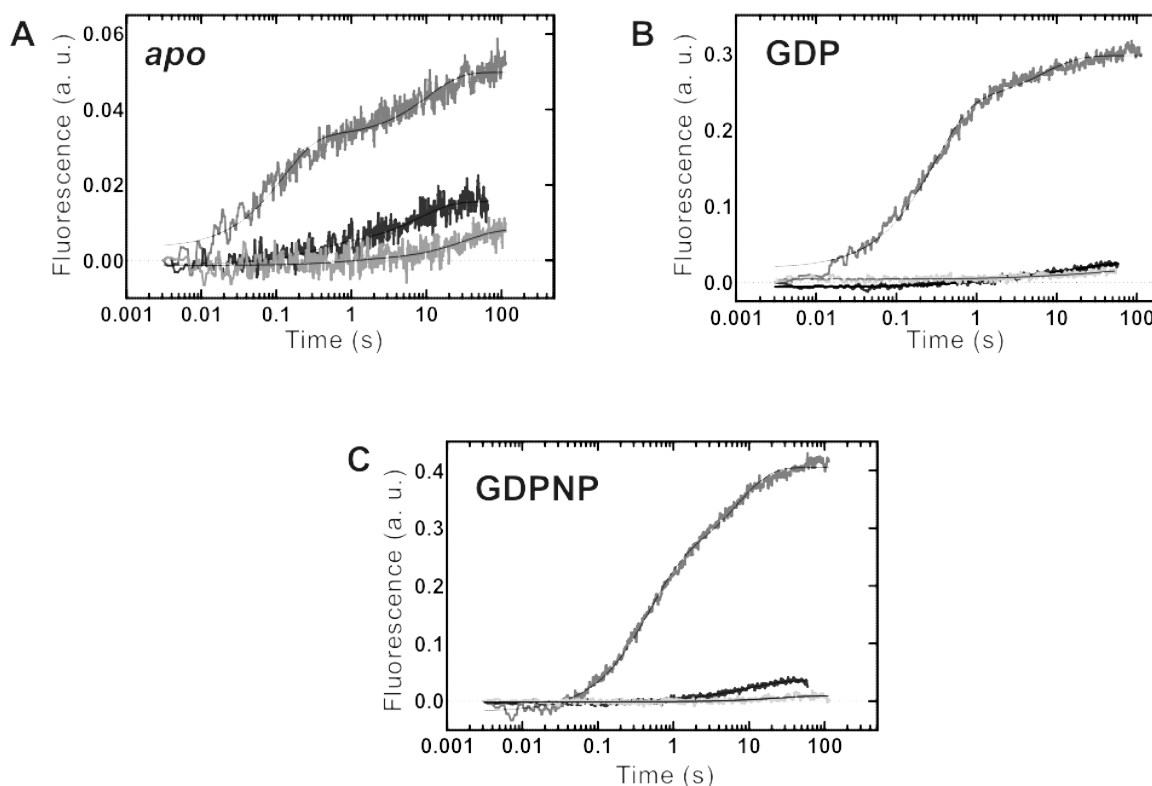
Figure 2.3.3.1 **Changes in fluorescence observed upon Fl-HflX in various nucleotide bound states interacting with 30S, 50S and 70S.** (A) Fluorescence increase over time as 0.50 µM HflX was rapidly mixed with 0.15 µM 50S (dark grey), 70S (black) and 30S (light grey). (B) Fluorescence increase over time as 0.50 µM HflX in the presence of 125 µM GDP was rapidly mixed with 0.15 µM 50S (dark grey), 70S (black) and 30S (light grey). (C) Fluorescence increase over time as 0.50 µM HflX in the presence of 125 µM GDPNP was rapidly mixed with 0.15 µM 50S (dark grey), 70S (black) and 30S (light grey).

To obtain affinities for fluorescently labeled HflX for 50S ribosomal subunits, pre-steady state experiments in which increasing concentrations of 50S ribosomal subunits were added into a final concentration of 0.15 µM HflX in the presence of 125 µM GDP was undertaken in the stopped-flow. 50S ribosomal subunits were examined first due to the fact that the signal change was substantial compared to 30S and 70S. Upon increasing the 50S concentration, no concentration dependence of the rates or amplitudes associated with the interaction of HflX

49

labeled with 5-IAF with ribosomal subunits was observed (Figure 2.3.3.2).  These results indicate that either the utilization of 5-IAF as a fluorophore or its placement at the intrinsic cysteines within HflX only results in concentration-independent conformational changes being detected.  Being able to obtain kinetic parameters associated with conformational changes can provide valuable information though with regard to the structural dynamics of the HflX-ribosome complex.
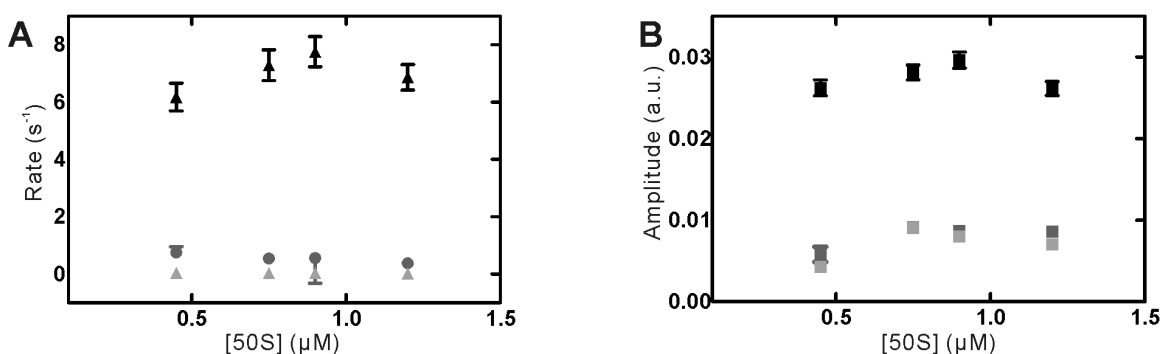


Figure 2.3.3.2 **Concentration independent rates and amplitudes associated with rapidly mixing an increasing concentration of 50S ribosomal subunits with GDP-bound Fl-HflX.** (A) The rates obtained from fitting fluorescence changes upon rapidly mixing 0.15 µM fluorescently labeled HflX in its GDP-bound state with increasing concentrations of 50S to three-exponential functions. (B) The amplitudes associated with the fluorescence changes observed upon rapidly mixing 0.15 µM fluorescently labeled HflX with increasing concentrations of 50S.

*2.3.4 Characterization of HflX Variants Lacking Cysteine Residues*

Work towards the construction of a Cys-less HflX variant was undertaken, to be able to control the future placement of fluorophores with the end result being garnering kinetic information related to the interaction of HflX with ribosomal particles.  Two of the three cysteines, Cys 96 and Cys 98 in *E. coli* HflX are found

in the N-terminal HflX domain.  The third cysteine Cys 415 is located in the poorly conserved C-terminal extension, immediately following the G-domain.
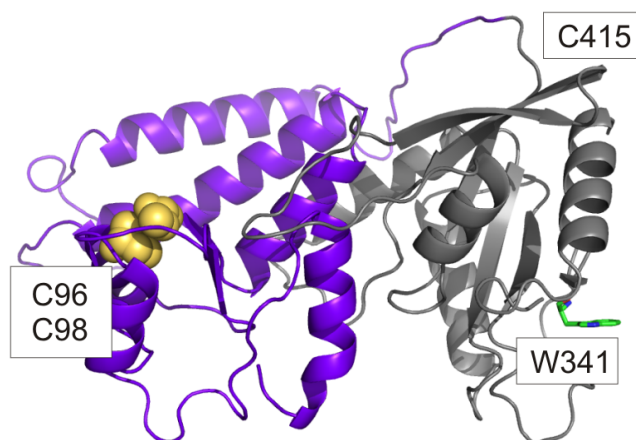


Figure 2.3.4.1 **Homology model of *E. coli* HflX.**  Within the N-terminal HflX domain (purple) are two cysteines 96 and 98 (yellow).  The G-domain (black) harbors the protein's single tryptophan residue at position 341 shown in sticks.

Cys 98 and 415 were replaced with leucine residues while a serine was substituted in position 96.  In a sequence alignment of various bacterial species, the amino acid cysteine is most often replaced with the unreactive, nonpolar residue, leucine.  Serine closely resembles cysteine in size and structure and additionally, cysteine can be synthesized from serine.   Upon expression and purification of the single and fully Cys-less variants, their overall structure and activity with regards to binding of GTP, GTP hydrolysis and binding of ribosomes was compared to wild-type HflX.  At 37°C, *E. coli* BL21-DE3 cells upon induction of the expression of $HflX_{C96SC98L}$ and $HflX_{C96SC98LC415L}$ displayed typical bacterial growth. An initial lag phase was followed by exponential growth and eventually the growth of the *E. coli* cells reached an $OD_{600}$ of greater than 2 (Figure 2.3.4.2 Panel A).  However, protein bands indicative of the HflX variants were not visible

by SDS-PAGE analysis when cells were opened under non-denaturing conditions in the absence of 8 M urea. The expression of proteins that are not naturally occurring within *E. coli* can often be detrimental to the growth of cells and may result in the seclusion of the expressed protein in inclusion bodies (79). In an attempt to obtain soluble $HflX_{C96SC98L}$ and $HflX_{C96SC98LC415L}$, BL21-DE3 *E. coli* cells were grown overnight at 18°C. Expression of HflX variants was also induced by 0.1 mM rather than 1 mM IPTG. Lowering the concentration of IPTG was undertaken to promote lower levels of expression within *E. coli*, while the colder temperature ensures the correct folding of variants by temperature-induced chaperone activity to prevent formation of insoluble inclusion bodies containing $HflX_{C96SC98L}$ and $HflX_{C96SC98LC415L}$ (80). Under these conditions, production of soluble $HflX_{C96SC98L}$ and $HflX_{C96SC98LC415L}$ was still unsuccessful (Figure 2.3.4.2 Panel B).
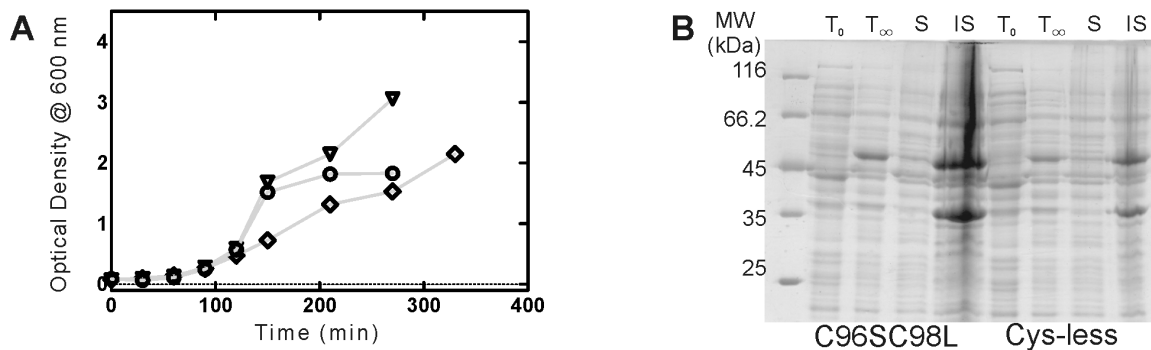


Figure 2.3.4.2 **$HflX_{C96SC98L}$ and $HflX_{C96SC98LC415L}$ do not alter *E. coli* cell growth but are found in inclusion bodies.** (A) Growth curves of *E. coli* BL21-DE3 cells producing $HflX_{C96SC98L}$ (open triangles), $HflX_{C96SC98LC415L}$ (open diamonds) and $HflX_{C415L}$ (open circles). (B) 12% SDS-PAGE analysis of *E. coli* cell lysates before ($T_0$) and 16 hours after induction ($T_\infty$). Overexpression of HflX is visible for both $HflX_{C96SC98L}$ and $HflX_{C96SC98LC415L}$ (Cys-less) at 50.5 kDa at $T_\infty$. Soluble (S) and insoluble fractions (IS) were obtained after *E. coli* cells were opened with lysozyme and centrifuged at 30000*g*. Pellets from the centrifugation step were resuspended in 8 M urea and contain HflX as confirmed by SDS-PAGE.

Reagents such as urea or guanidinium chloride can break apart inclusion bodies, releasing insoluble and unfolded proteins into solution that can later be refolded and their functionality tested (80). In order to obtain $HflX_{C96SC98L}$ and $HflX_{C96SC98LC415L}$ using a similar approach, purification of wildtype HflX under denaturing conditions followed by refolding, resulted in a protein that was unable to hydrolyze GTP in the presence of ribosomes (Figure 2.3.4.3 Panel A). $HflX_{C415L}$ was successfully purified from *E. coli* cell lysate by affinity and size exclusion chromatography under non-denaturing conditions. The $HflX_{C415L}$ variant displayed a nearly superimposable CD spectrum as the wildtype protein, indicating that introduction of a different amino acid in the variable C-terminus of the protein does not significantly alter the structure of HflX (Figure 2.3.4.3 Panel B). The spectrum obtained for both variant and wildtype HflX were characteristic of proteins comprised of multiple alpha-helices (78).
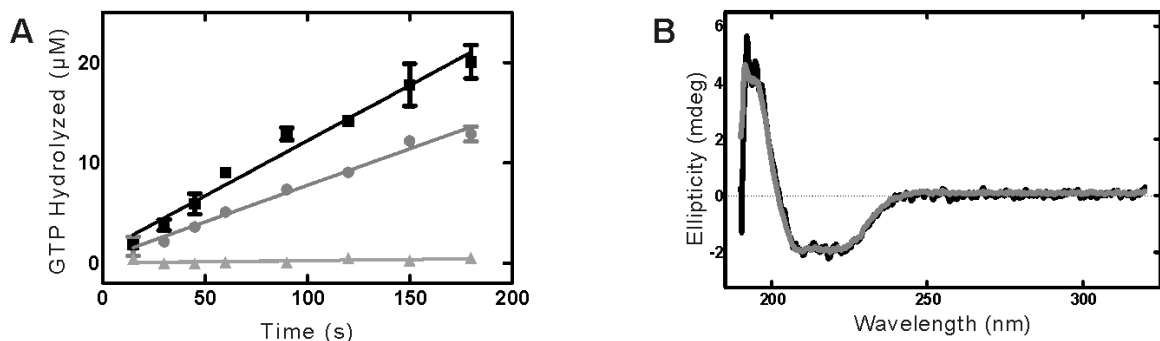


Figure 2.3.4.3 **$HflX_{C415L}$ is similar to wildtype HflX in both its structure and its ability to hydrolyze GTP in the presence of 70S ribosomes.** (A) Time course of GTP hydrolysis by HflX WT (black squares), $HflX_{C415L}$ (dark grey circles) and refolded wild-type HflX purified in 8 M urea (light grey triangles) in the presence of 1 µM 70S ribosomes. (B) Superimposed CD spectra of HflX WT (black) and $HflX_{C415L}$ (dark grey).

Table 2.3.4.1 Specific GTPase activity of different HflX preparations stimulated by 70S ribosomes.

| | Rate ($\mu M \ s^{-1}$) |
|---|---|
| Wildtype HflX | 0.11 ± 0.01 |
| HflX$_{C415L}$ | 0.072 ± 0.003 |
| Refolded Wildtype HflX | 0.002 ±0.001 |

Having established that the structure of HflX$_{C415L}$ is in agreement with wildtype HflX, equilibrium fluorescence titrations were performed to characterize whether the HflX$_{C415L}$ variant had similar nucleotide binding properties to wildtype as well. The change in the fluorescence of the intrinsic tryptophan residues in HflX was monitored in the presence of guanosine nucleotides. The addition of increasing concentrations of GTP resulted in a decrease in fluorescence at 337 nm that was plotted in order to obtain an K$_D$ for GTP of 124±12 µM for HflX$_{C415L}$ and a dissociation constant of 103±19 µM for wildtype HflX (Figure 2.3.4.4). Thus, a similar K$_D$ within error for the triphosphate form of guanine nucleotides was determined for the single Cys-less variant, HflX$_{C415L}$ and wildtype HflX.
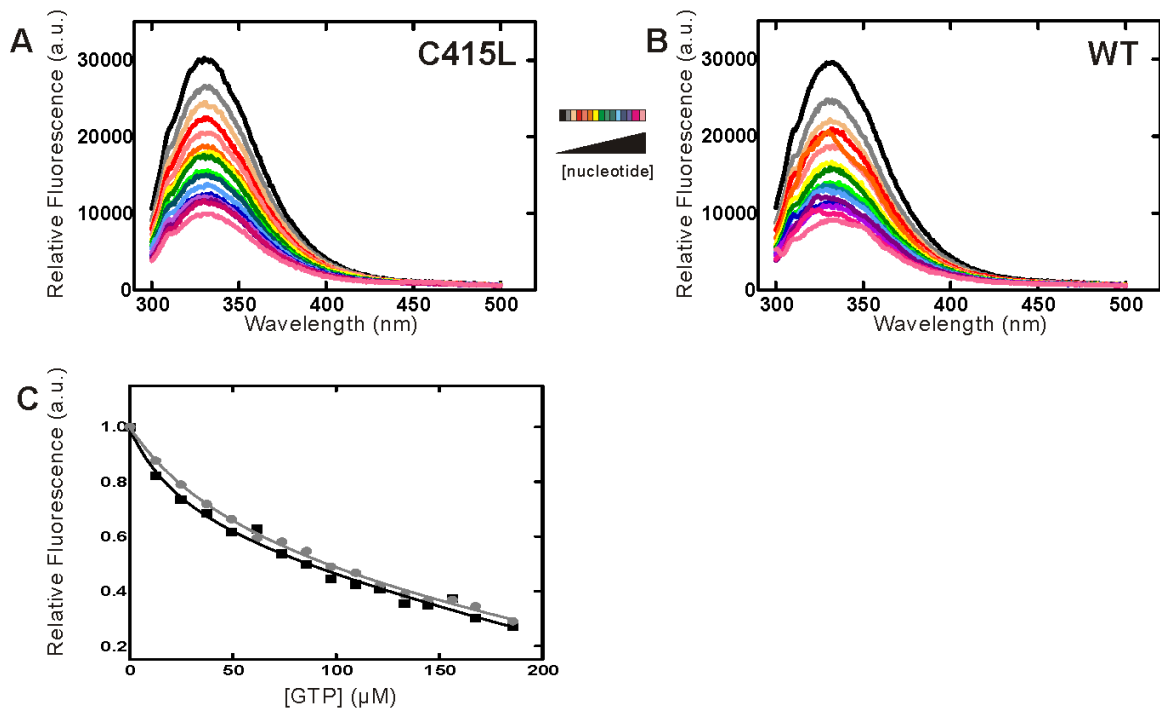
Figure 2.3.4.4 **HflX$_{C415L}$ and wildtype HflX bind GTP with a similar affinity.**
(A) Fluorescence emission spectra from 300 to 500 nm upon exciting the intrinsic
tryptophan of 1 µM HflX$_{C415L}$ at 280 nm in the presence of increasing
concentrations of GTP.  (B) Fluorescence emission spectra from 300 to 500 nm
upon exciting the intrinsic tryptophan of 1 µM HflX at 280 nm in the presence of
increasing concentrations of GTP.  (C) Plot of the decrease in fluorescence
signals for wildtype HflX (black squares) and HflX$_{C415L}$ (grey circles) at 337 nm as
a function of the concentration of GTP.

The next activity assessed was the ability of HflX$_{C415L}$ to bind ribosomes and
hydrolyze GTP in the presence of 70S ribosomes. HflX$_{C415L}$ was retained above
the filter with 70S ribosome in microfiltration assays (Figure 2.3.4.5). Only a two-
fold decrease in 70S ribosome stimulated GTPase activity was observed for
HflX$_{C415L}$ when compared to the wildtype enzyme (Figure 2.3.4.3 Panel A). Taken
together these results suggest that HflX$_{C415L}$ is capable of performing ribosome-
associated activities like wildtype factor.

55
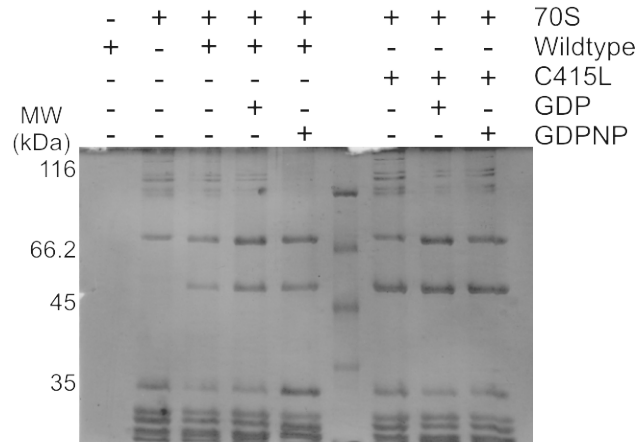
Figure 2.3.4.5 **HflX$_{C415L}$ binds 70S ribosomes regardless of the guanine nucleotide present.** HflX$_{C415L}$ (50.5 kDa) in its apo, GDP and GDPNP bound states remained above the filter with 70S in when subjected to centrifugation in 100 kDa molecular weight cut off filters.

## 2.4 Discussion and Future Directions

To gain kinetic information relating to the association and dissociation of HflX and YchF from ribosomes, a fluorescence-based system was developed. The affinities that could be generated by this system could eventually lead to elucidation of the functional complexes that these factors interact with in the cell. To reach this goal, wildtype HflX and YchF have been labeled with the cysteine-specific fluorescent dye, 5-IAF and their published functions compared to wildtype. HflX with its intrinsic cysteines labeled with 5-IAF, hydrolyzes GTP and binds 70S ribosomes. Pre-steady state stopped-flow analysis did not reveal any concentration dependence on the changes in fluorescence or associated rates when 50S ribosomal subunits were titrated against HflX-GDP. The fact that only concentration-independent conformational changes, not concentration-dependent binding events between labeled HflX and 50S ribosomal subunits, can

be detected suggests that the choice of fluorophore and its placement within the wild-type protein may need to be addressed.

To combat the issue of the positioning of the fluorophores within HflX, a Cys-less background is required in which new locations for cysteine residues to be placed can be assigned. Sequence alignments have revealed that in HflX, the cysteine residues are highly conserved, besides 415. In HflX, Cys 96 is 88% identical while the cysteine at position 98 possesses 99% identity among 501 bacterial species.  Construction of an active Cys-less variant of HflX was necessary to obtain variants in the future, in which the specific locations of fluorophores could be known.  In this way, control over the *in vitro* system that is unattainable when labeling intrinsic cysteine residues would be possible. At the very least, the contributions of the intrinsic cysteines to the structure and function of HflX would be revealed.  Interestingly, HflX$_{C415L}$ interacted with ribosomal particles and nucleotides much like wild-type protein. Removal of cysteines 96 and 98 simultaneously led to the production of insoluble protein. The proximity of the amino acids to one another in space suggested that perhaps the two cysteines could be forming a disulfide bond, stabilizing the structure of the protein, but measurement of the distance between the residues was much farther (6 Å) than the 2 Å normally associated with such an interaction (81).  Cysteine is a residue of relatively low abundance within proteins yet a propensity for cysteines to be found two amino acids apart has been observed among bacterial organisms such as *E. coli* (82).  Although the two cysteines in HflX are located only one amino acid apart, the importance of these residues to stabilizing long-

range intramolecular or interpolypeptide interactions should not be overlooked. Cys 96 and 98 link together an alpha-helix and beta-sheet made up of a number of positively-charged amino acids and, as a consequence, may be critical for the structure of the regions constituting the N-terminus of HflX, thought to be required to interact with RNA.   In order to be able to work with variants of HflX lacking cysteines at 96 and 98 or 415 as well, a different tagging system to purify the mutated recombinant protein will likely be required.  Potentially, using GST or MBP tags which have been shown to improve the solubility and stability of proteins in solution over histidine tags will have to be considered (83).  If the proteins fused to HflX variants have enhanced solubility in solution, it is more likely that these GST and MBP tags will facilitate protein folding and reduce protein aggregation, increasing the expression and purification yield of HflX (83).

Table 2.4.1 Summary of the Characterization of HflX Variants Lacking Cysteines

| Variant | HflX$_{C96SC98L}$ | HflX$_{C415L}$ |
|---|---|---|
| Amino Acid Conservation of Mutated Cysteines | 88, 99% | <60% |
| Expression | At 18°C with 0.1 M IPTG | At 37°C with 1 M IPTG |
| Purification | Not Possible with Denaturing Conditions | Non-Denaturing Conditions |
| Structure | N/A | Identical CD Spectra to WT |
| Nucleotide Binding | N/A | K$_D$ For GTP Within Error of WT |
| Ribosome Binding | N/A | 1:1 Binding of Variant to 70S |
| Nucleotide Hydrolysis | N/A | 2-Fold Slower GTPase Activity with 70S |

The variant of YchF lacking cysteines at positions 5, 35 and 106 could be purified, but upon analysis of its structure by circular dichroism studies and assessment of its ribosome-associated functions, the protein was found to be significantly different from wild-type YchF. YchF$_{C5AC35AC106A}$ had all but one of the cysteines that are found within the G-domain replaced. The cysteine residue at position 5 is 98% identical, which contrasts with the 100% conservation found for Cys 35 and 106 among 291 bacterial organisms. As with HflX, the distance between the cysteines close in space was examined to infer whether disulfide bonds were capable of forming between the reactive residues. Cys 5 and 35 and Cys 106 and 236 were all much farther apart than would be required to form a disulfide bond, with measurements of 13 and 11 Å, respectively. Interestingly, the

cysteine at position 35 is located within Switch I of YchF and cysteine 106 serves as an attachment point for the flexible linker containing one of the proposed catalytic residues for YchF, histidine 114.  From the results presented in this thesis from equilibrium fluorescence titrations, the ability of Fl-YchF to differentiate between the di-and tri-phosphate forms of adenosine appeared to be negatively affected. Switch I is critical for sensing the presence of GTP or GDP by numerous translational GTPases.  In direct relation then, the alteration to cysteine residue 35 upon the addition of a fluorescent dye within this motif of YchF leads directly to the hypothesis that it interferes with the specificity of the factor for adenosine nucleotides. An explanation for the very slow hydrolysis rate of ATP by YchF$_{C5AC35AC106A}$ observed in the presence of 70S ribosomes can be linked to the substitution of cysteine 106.  This residue in conjunction with the ribosome could be responsible for orientating the catalytic machinery of YchF to position a water molecule for a nucleophilic attack on ATP.  In addition to roles in regulating the concerted movements of the G-domain and sensing of the number of phosphate groups present on nucleotides, the cysteines within YchF have also been proposed to be indispensible for its role in the oxidative stress response (61).  This same group hypothesized that the intrinsic cysteines of YchF could be influencing its ATPase activity. For the first time, using fluorescence emission spectra and nucleotide hydrolysis assays to study a variant of YchF lacking three naturally occurring cysteine residues and fluorescently labeled YchF preparation, a connection between the absence of cysteines and the disruption of the interaction of YchF with ribosomes and nucleotides can be drawn. A detailed

examination of the structure and function of YchF variants bearing single cysteine substitutions within the G domain will be of upmost interest to study in order to validate the influence of the individual cysteine residues on the ATPase activity and cellular function of YchF.

Table 2.4.2 Summary of the Characterization of Modified YchF Preparations

| Variant | Fl-YchF | YchF$_{C5AC35AC106A}$ |
|---|---|---|
| Amino Acid Conservation of Mutated Cysteines | N/A | 98, 100, 100% |
| Expression | At 37°C with 1 M IPTG | At 37°C with 1 M IPTG |
| Purification | Non-Denaturing Conditions | Non-Denaturing Conditions |
| Structure | N/A | Deviation from WT CD Spectra |
| Nucleotide Binding | Similar K$_D$s for ATP and ADP Unlike WT | Similar K$_D$s for ATP and ADP and Similar to WT |
| Ribosome Binding | 30% Binding of Variant to 70S | No Binding of Variant to 70S |
| Nucleotide Hydrolysis | > 20-fold reduction in ATPase Activity with 70S | > 20-fold reduction in ATPase Activity with 70S |

## 2.5 Conclusion

Classical biochemical methods and state-of-the-art biophysical techniques have revealed that the naturally-occurring cysteine residues within HflX and YchF can accept fluorescent dye.  In the case of HflX, although increases in fluorescence over time can be observed when the labeled wild-type protein is

rapidly mixed with ribosomal particles, the placement of the fluorescent dye did not result in the determination of equilibrium dissociation constants between HflX and 30S, 50S and 70S. Fluorescent labeling of YchF's intrinsic cysteines resulted in protein unable to differentiate between adenosine nucleotides consistent with the fact that highly conserved cysteines can play important roles in the function of a factor. It has also been shown that work towards Cys-less variants of both HflX and YchF resulted in insoluble protein and inactive protein, respectively. Thus, structurally and functionally relevant roles for cysteines within HflX and YchF showing a high percentage of identity among bacterial species can be proposed.

## Chapter 3 –

### *Toward Understanding the Catalytic Mechanism and Structural Dynamics of HflX*

### 3.1 Introduction

Guanine triphosphatases, grouped together based on the possession of a G-domain containing common sequence and structural motifs, have evolved unique differentiating factors that allow their specific roles in cells to be fine-tuned (28). The rate in which the switch is turned over *in vivo* can be dependent on its interactions with external GAPs or GEFs, but the intrinsic properties of the GTPase can also lead to catalysis of the hydrolysis or nucleotide exchange steps of the GTPase cycle (29). HflX is no exception to this observation acquiring what appear to be single amino acids or arrangements of residues that currently remain unclear as to how they directly influence catalysis and in turn the cellular function of the factor. To note about HflX though, is the fact that it does not possess the catalytic histidine that is present in other TRAFAC GTPases (84,85). Histidine 84 and 91 in EF-Tu and EF-G, respectively, are present to coordinate a water molecule for a nucleophilic attack of guanine nucleotides. In the place of the histidine in the G-domain, there is a phenylalanine present in the G-domain of HflX, characterizing the protein as a hydrophobic amino acid-substituted GTPase (HAS-GTPase) (39). This knowledge raises the question as to how GTP and ATP hydrolysis is carried out by HflX. Furthermore, several groups have also proposed that HflX along with other GTPases contain an element called the K loop and several conserved asparagines, which can coordinate potassium ions that are capable of stimulating the very slow intrinsic catalysis of some GTP

hydrolyzing proteins (48).  This ionic mode of stimulation of NTPase activity has not yet been proven for HflX or correlated with the fact that the ribosome can also provide stimulation of the protein's hydrolysis activity.

Multidomain proteins like HflX must also evolve ways to effectively communicate and correlate movements in one domain to the action of other areas in the protein.  Typically, the G-domain of GTPases does not act alone. Additional domains can influence the performance of a GTPase's cellular function by providing binding sites for nucleic acids or in some cases the presence of a tandem G-domain can aid in the regulation of the GTPase activity of its actively hydrolyzing G-domain (86,87).   HflX is novel in that its domain upstream of the G-domain is found only within its superfamily (33).  Recently, this N-terminal HflX domain has been proposed to possess nucleotide hydrolysis capabilities and interactions between the HflX- and G-domains have been proposed to modulate the purine nucleotide hydrolysis rates of HflX in the absence of ribosomes (46). Seeking an explanation as to the ability of HflX to hydrolyze ATP, structural bioinformatics analyses were carried out and weak structural homology between the first 120 amino acids of HflX to ATP/ADP binding domains in other proteins was found (46).   Confirmation of ATP hydrolysis activity was achieved by testing a truncation of the protein consisting of the first 120 residues of the HflX domain (46).   The group proceeded to demonstrate that salt-bridges fastening the HflX- and G-domains together can regulate the nucleotide hydrolysis activities of HflX (46). The C-terminal extension of HflX, present in HflX from *E. coli* but lacking among a small subset

of other organisms such as *S. solfataricus* was also examined but its regulatory effect on the functions of HflX still remains unclear (46). Many questions remain to be answered with regards to the regulation of purine nucleotide catalysis by HflX. Although the roles of the N and C-terminal domains on intrinsic nucleotide hydrolysis by HflX have been examined, their exact activity in the context of the cell is poorly understood. How the ribosome influences the dynamics of all the domains of HflX with regard to stimulated NTP hydrolysis is also a question that remains to be answered. As one of the most likely substrates for HflX in the cell is the ribosome, a better understanding of all the contributing factors to catalysis is required in order to elucidate the functional the cycle of HflX.

**3.2 Materials and Methods**

*3.2.1 Sequence Alignments*

Refer to Section 2.2.1.

*3.2.2 Site-directed Mutagenesis*

A glutamate residue at position 29 and an arginine at position 114 were both replaced with alanine residues using the Quikchange® Site-Directed Mutagenesis Method. The deletion of the C-terminal domain of HflX was achieved by introducing an amber stop codon at the position in the *hflx* gene coding for leucine 372.

Table. 3.2.2.1 Primers for Site-Directed Mutagenesis

| | E29A | R114A | ΔL372 |
|---|---|---|---|
| Forward Primer | 5' <u>GAT ATC</u> GAA GAC CTC CAG **GCG** TTT G 3' | 5' ATT TTC GCC CAA **GCG** GCG <u>CGT ACG</u> CAT 3' | 5' GCA TAC ATT GCG TCT **GTA ATA G**CC GGC AGG GCG TCT GAG A 3' |
| Reverse Primer | 5' CAA A**CG C**CT GGA GGT CTT <u>CGA TAT</u> C 3' | 5' ATG <u>CGT ACG</u> CGC **CGC** TTG GGC GAA AAT 3' | 5' TCT CAG ACG CCC TGC CGG **CTA TTA C**AG ACG CAA TGT ATG C 3' |
| T$_M$ (°C) | 67.4 | 68.6 | 69.2 |
| Restriction Site | EcoRV | BsiWI | N/A |

Refer to Section 2.2.2 for methodology.

*3.2.3. Protein Expression and Purification*

Refer to Section 2.2.3.

*3.2.4 Preparation of Ribosomes*

Refer to Section 2.2.4

*3.2.5 Nucleotide Hydrolysis Assays*

*HflX Variants* - The release of $^{32}$P-labeled inorganic phosphate (P$_i$) from [γ-$^{32}$P] GTP or [γ-$^{32}$P] ATP (Perkin-Elmer) was monitored to determine the rate of GTP or ATP hydrolysis by HflX. Reactions were composed of 1 µM HflX, 125 µM radiolabeled nucleotide solution, in the presence or absence of 1 µM 70S ribosomes or 50S ribosomal subunits and carried out in TAKM$_7$ or TAKM$_{30}$ buffer

66

(50 mM Tris-Cl pH 7.5 at room temperature, 70 mM $NH_4Cl$, 30 mM KCl, 30 mM $MgCl_2$). Refer to Section 2.2.7 for further procedural details.

*Wild-type HflX (Intrinsic)* - The rate of intrinsic GTP hydrolysis by HflX was determined following separation by thin layer chromatography rather than extraction. Reactions were composed as in 2.2.7 but with GTP concentration varying from 10 µM (approximately 20-fold lower than the $K_D$ of HflX for GTP) to 500 µM (about 3-fold higher than the $K_D$). Samples (5 µL) were removed from the reaction and subsequently quenched with 1 µL of 6 M formic acid. Following separation of $^{32}P_i$ from [γ-$^{32}$P] GTP by thin layer chromatography, plates (TLC PEI Cellulose F, EMD Millipore) were visualized using a Typhoon Trio Scanner (GE Healthcare) and the amount of $^{32}P_i$ formed calculated from ImageJ (76).

*Wild-type HflX (Potassium Ion Dependence)* - To assess the dependence of ribosome-stimulated wild-type HflX GTPase activity on potassium ions, 25 000 pmols of wild-type HflX were dialyzed either into 1 L final storage buffer or 1 L final storage buffer containing 300 mM NaCl rather than KCl. To be able to control the concentration of potassium ion present within the reaction, a new buffer system had to be utilized. A 10X buffer with the same composition as $TAKM_{30}$ but lacking any potassium ions (10X $TAM_{30}$) allowed for the ionic strength of the other buffer components present to remain constant. The desired concentration of potassium ions while maintaining the relative ionic strength of the other buffer components was achieved by using a 1X $TAKM_{30}$ buffer containing 600 mM of potassium ions (1X $TAK_{600}M_{30}$). In this way, a final concentration of potassium ions in the reaction of 30 and 300 mM could be

directly compared with reactions in $TAKM_{30}$ as performed in 2.2.7. A titration of potassium ions was achieved by maintaining an overall ionic strength of monovalent cations (sodium or potassium ions) in solution around 300 mM and using 1X $TAK_{600}M_{30}$ or 1X $TAN_{600}M_{30}$ buffers. Wild-type HflX dialyzed into sodium ion- or potassium ion- containing final storage buffers were subjected to GTP hydrolysis reactions as previously described in 2.2.7 using the new buffer system (10X $TAM_{30}$ and 1X $TAK_{600}M_{30}$ or 1X $TAN_{600}M_{30}$).

*3.2.6 Light Scattering*

To monitor the dissociation of 70S ribosomes into 50S and 30S ribosomal subunits, a KinTek SF-2004 Stopped-flow apparatus at 20°C was utilized. Samples were excited at 436 nm and scattering was detected at a 90° angle after passing through 400 nm filters. Reactions were performed in $TAKM_5$ buffer (similar to $TAKM_7$ but with 5 mM $MgCl_2$), by rapidly mixing 2 µM of wildtype or variant HflX in the presence of 250 µM GTP and 0.30 µM of 70S ribosomes. The resulting signals were normalized with respect to the initial light scattering of the solution, setting the first value as 100% of intact 70S ribosomes.

*3.2.7 Microfiltration Binding Assays*

Refer to Section 2.2.9.

**3.3 Results**

*3.3.1 Potassium ion dependence of ribosome-stimulated HflX GTPase activity*

To address whether HflX is indeed dependent on potassium ions for its nucleotide hydrolysis activity, the ability of the wild-type protein under different monovalent ion conditions to bind 70S ribosomes and hydrolyze GTP in the

presence or absence of 70S was assessed.  On the sequence and structural

level, HflX possesses features indicative of cation dependence, specifically a

requirement for potassium ions (Figure 3.3.1.1) that is shared by other GTPases

such as YihA, FeoB, and MnmE (49).  Two asparagines from the GTPase, the

oxygens from phosphate groups of the nucleotide and backbone carbon atoms

from Switch I can all contribute to the coordination of a potassium ion (49).

Switch I in these GTPases is also altered, adopting a distinct conformation that

places a so-called K loop over top of the bound nucleotide (49).  The conserved

asparagines in the G1 motif play a role in positioning Switch I in its K-loop

orientation by forming hydrogen bonds with its backbone atoms (49).
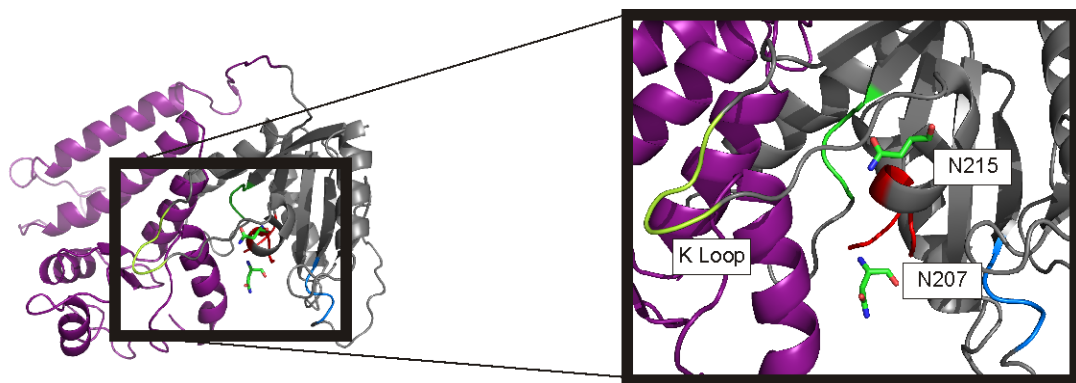


Figure 3.3.1.1 **Homology model of *E. coli* HflX showing the features that
have classified it as potassium-selective cation dependent GTPase.** N207
and N215 (green sticks) of the G-domain are shown in proximity to the K-loop
(yellow-green).

As a starting point, a Michaelis-Menten titration was performed to determine if

potassium ions had an effect on the GTP hydrolysis of HflX alone.   The

determination of initial rates of HflX GTPase activity using extraction followed by

scintillation counting as a detection method proved not to be a very sensitive

approach.  This is due to the fact that the amount of inorganic phosphate

released by wildtype HflX alone is within levels of the amount of GTP hydrolyzed

by buffer. Thus, the titration was repeated using a different detection method, thin

layer chromatography (TLC), which allows for the complete separation of

radiolabeled inorganic phosphate from GTP. Additionally, TLC had been used to

determine the catalytic parameters associated with the intrinsic GTPase activity

of the archael homolog of HflX from *S. solfataricus* (45). Comparison of the

kinetic parameters between those previously described for *S. solfataricus* HflX

and those found for *E. coli* using the extraction method utilized in our laboratory,

led to the discovery that the catalytic efficiency or $k_{cat}$/$K_M$ were similar within error.

Upon repetition of the same experiment but using TLC, to separate low levels of

liberated inorganic phosphate from di- and triphosphate forms of guanosine

nucleotides, no $k_{cat}$ or $K_M$ could be calculated from the rates of intrinsic GTP

hydrolysis when plotted against increasing concentrations of guanosine

triphosphates (Figure 3.3.1.2).
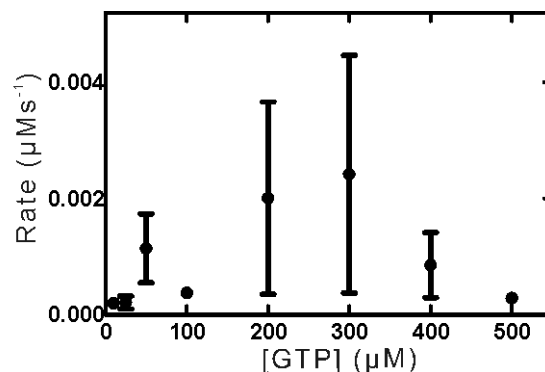


Figure 3.3.1.2 **Plot of initial rates of GTPase activity of wild-type HflX alone over increasing concentrations of GTP.** 1 µM HflX was incubated with increasing concentrations of radiolabeled GTP to obtain intrinsic rates of GTP hydrolysis for a range of nucleotide concentrations using thin layer chromatography as a detection method. No concentration dependence was observed for the GTPase activity of the enzyme alone.

Based on the fact that the amount of GTP hydrolyzed by wild-type HflX is intrinsically difficult to detect and a concentration dependence of the initial rates not observable, a study of the effect of potassium ions on the ribosome-stimulated GTPase activity of HflX was undertaken for the very first time. The GTPase activity of HflX stimulated by 70S was measured at increasing concentrations of potassium ions.  To exclude the effects of ionic strength on the interaction of HflX with the ribosome and ultimately on the observed multiple turnover GTPase activity, alteration to the buffer composition was required in order to maintain a constant ionic strength while varying the concentration of potassium ions.  The ability of HflX in complex with 70S ribosomes to hydrolyze GTP in $TAK_{600}M_{30}$, the adjusted buffer system, which can allow for potassium ion concentration to be manipulated, was compared to its activity using the established 1X $TAKM_{30}$ buffer system.  At a final potassium ion concentration of 30 mM in both reaction buffers, the 70S-stimulated GTPase activities of HflX were very similar at $0.089 \pm 0.006$ $\mu Ms^{-1}$ and $0.104 \pm 0.004$ $\mu Ms^{-1}$ (Figure 3.3.1.3 Panel A and Table 3.3.1.1).  Interestingly, increasing the potassium ion concentration 10-fold to 300 mM, reduced the GTPase rate about 5-fold to $0.020 \pm 0.002$ $\mu Ms^{-1}$ (Figure 3.3.1.3 Panel A and Table 3.3.1.1).  Dialysis of the protein into a buffer containing a different monovalent cation, sodium, was necessary to reduce the concentration of potassium ions that was present in the protein preparation due to the purification procedure.  HflX was dialyzed into the same potassium ion-containing buffer to take into account the effect the dialysis process alone has on the GTPase activity of the factor. To further validate a

71

potassium ion concentration dependence on the rate of ribosome-stimulated GTPase activity on HflX, the GTP hydrolysis capabilities of both dialyzed preparations were compared to that of wild-type undialyzed protein in $TAKM_{30}$. Treatment of wild-type HflX to dialysis led to a 2-fold decrease in GTPase activity in the presence of 70S (Figure 3.3.1.3. Panel B and Table 3.3.1.2). The inhibition of GTPase activity was even more pronounced (4-fold) when wild-type HflX was dialyzed into sodium ion-containing buffer not potassium ions, further suggesting that HflX does require potassium ions to some degree (Figure 3.3.1.3. Panel B and Table 3.3.1.2).
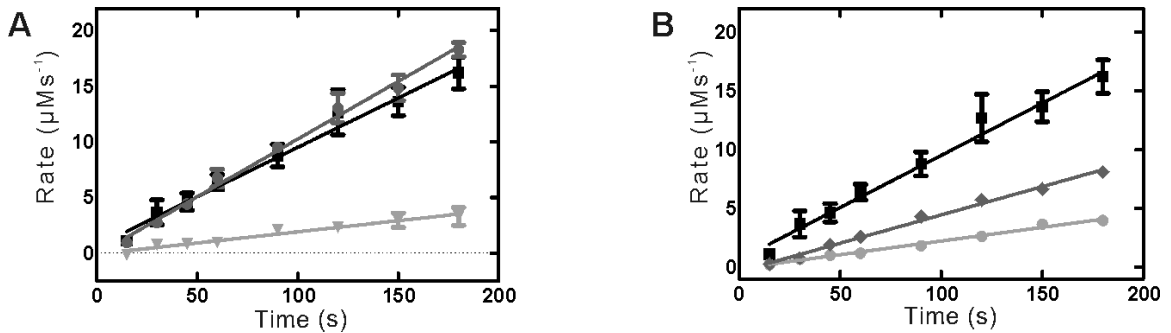


Figure 3.3.1.3 **Potassium ion concentration can affect the 70S ribosome stimulated GTPase activity of HflX to different extents.** (A) Time course of GTP hydrolysis by wildtype HflX stimulated by 1 µM 70S ribosomes in $TAKM_{30}$ (black squares), in $TAK_{600}M_{30}$ buffer with a final $[K^+]$ of 30 mM (dark grey circles) and in $TAK_{600}M_{30}$ buffers with a final $[K^+]$ of 300 mM (light grey inverted triangles). (B) Time course of wildtype HflX GTPase activity in the presence of 1 µM ribosomes in $TAKM_{30}$ (black squares), in $TAKM_{30}$ following dialysis into a KCl containing final storage buffer (dark grey diamonds), and in $TAKM_{30}$ after dialysis into a final storage buffer containing NaCl (light grey circles).

Table 3.3.1.1 Specific GTPase activity of wildtype HflX subjected to different potassium ion-containing buffer conditions.

| | Rate ($\mu M\ s^{-1}$) |
|---|---|
| $HflX_{WT}$ ($TAKM_{30}$) | $0.089 \pm 0.006$ |
| $HflX_{WT}$ (Final $[K^+]$ = 30 mM) ($TAK_{600}M_{30}$) | $0.104 \pm 0.004$ |
| $HflX_{WT}$ (Final $[K^+]$ = 300 mM) ($TAK_{600}M_{30}$) | $0.020 \pm 0.002$ |

Table 3.3.1.2 Specific GTPase activity of dialyzed preparations of HflX subjected to different potassium ion-containing buffer conditions.

| | Rate ($\mu M\ s^{-1}$) |
|---|---|
| $K^+$- dialyzed $HflX_{WT}$ ($TAKM_{30}$) | $0.048 \pm 0.002$ |
| $Na^+$- dialyzed $HflX_{WT}$ ($TAKM_{30}$) | $0.023 \pm 0.001$ |

To further investigate the dependence of the ribosome stimulated GTPase activity of HflX on the potassium ion concentration; the rates of GTP hydrolysis by HflX at increasing concentrations of the monovalent cation were determined. While no trend could be observed when the HflX preparation dialyzed into NaCl was subjected to increasing potassium concentration, the preparation of HflX dialyzed into KCl showed a 3-fold decrease in the rate of 70S ribosome-stimulated GTP hydrolysis once the KCl concentration in the reaction buffer exceeded 50 mM (Figure 3.3.1.4. Panel B). To ensure that the observed difference in the ribosome stimulated GTPase activity of the two wildtype HflX preparations was not due to altered binding affinities under these buffer conditions, microfiltration assays were carried out at 0 and 50 mM potassium ion concentrations to confirm binding of HflX to 70S ribosomes. At both monovalent cation concentrations and in the presence of GDPNP, HflX was retained above

the filter together with 70S ribosomes (Figure 3.3.1.4. Panel A). Finally, of interest to note is that the ribosome-stimulated GTPase activity of both the KCl and NaCl-dialyzed HflX were significantly faster in hydrolyzing GTP than the GTPase activity of wildtype HflX not stimulated by ribosomes (Figure 3.3.1.4. Panel B). Thus, the rates of GTP hydrolysis by these HflX preparations are most similar to ribosome-stimulated, non-dialyzed wildtype HflX GTPase activity (Figure 3.3.1.4. Panel B).
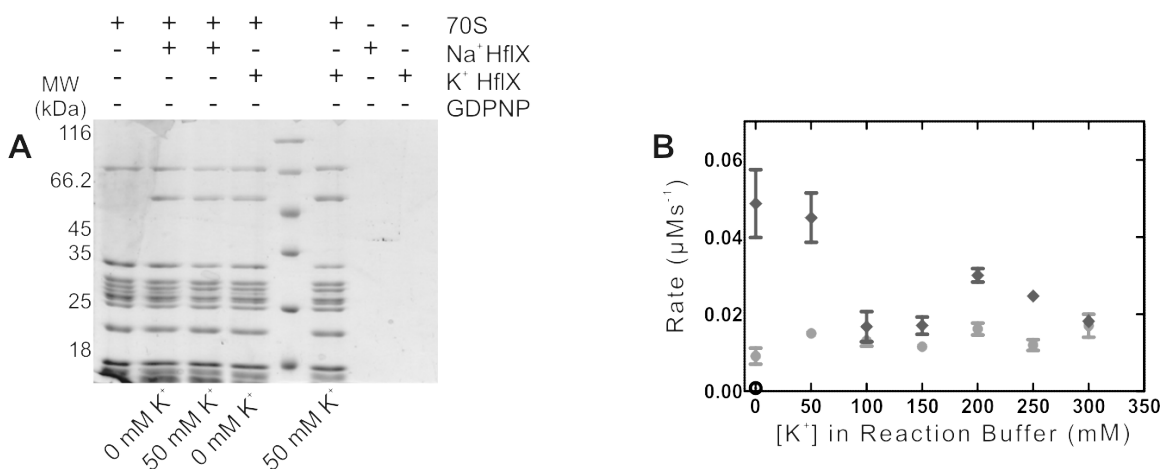


Figure 3.3.1.4. **At low K$^+$ concentrations Na$^+$ and K$^+$ dialyzed HflX can bind 70S ribosomes but only KCl dialyzed HflX can hydrolyze GTP near wild-type activity.** (A) In the presence of 70S, Na$^+$ and K$^+$ dialyzed HflX (50.5 kDa) in their GDPNP bound states, were retained above the 100 kDa molecular weight cut off filters following centrifugation in buffer containing 0 and 50 mM KCl. (B) Plot of the initial rates of GTP hydrolysis by 1 µM Na$^+$ HflX (light grey circles) and 1 µM K$^+$ HflX (dark grey diamonds) incubated with 1 µM 70S and radiolabeled GTP in TAK(600mM)M$_{30}$ buffer containing increasing concentrations of potassium ions. The GTPase rate of undialyzed, unstimulated wildtype HflX for comparison purposes is shown as a black circle.

The fact that the GTPase activity of dialyzed HflX in the presence of 70S is slower at concentrations of potassium ions higher than 50 mM correlates with the results observed with the non-dialyzed HflX. For the first time, the GTP hydrolysis activity of HflX has been shown to be regulated by potassium ions as its rate of

ribosome-stimulated GTPase activity is optimal at lower concentrations of the monovalent cation. Up to this point, this is a phenomenon that has only been observed with other GTPases in the absence of their GAPs (48).

### 3.3.2 Functional Role of the Interdomain Interactions and C-terminus of HflX

There are many residues located along the interface between the HflX- and G-domains that form salt-bridge and hydrogen bonding interactions. The role of these interdomain interactions in regulating the factor's ability to hydrolyze GTP in the presence of 70S remains unclear. In addition, the C-terminus of HflX not present in all organisms must have been retained by some homologs for some specific cellular purpose. As the function of HflX *in vivo* most likely involves the ribosome, an understanding of the effects of overall domain movements and the role of the C-terminus is vital. Two salt bridges, R114A-D251 and E29A-R257 were focused on primarily in this thesis. Both R114 and E29 are highly conserved with over 80% identity as revealed by a sequence alignment of 501 bacterial species. Glu 29 and Arg 114 were substituted with the non-reactive, nonpolar and smaller residue, alanine to generate the variants $HflX_{E29A}$ and $HflX_{R114A}$ (46). The introduction of a premature stop codon following a leucine residue at position 372 generated $HflX_{\Delta L372}$ and resulted in a truncation of the C-terminal extension that is normally found branching off the G-domain of HflX (46).
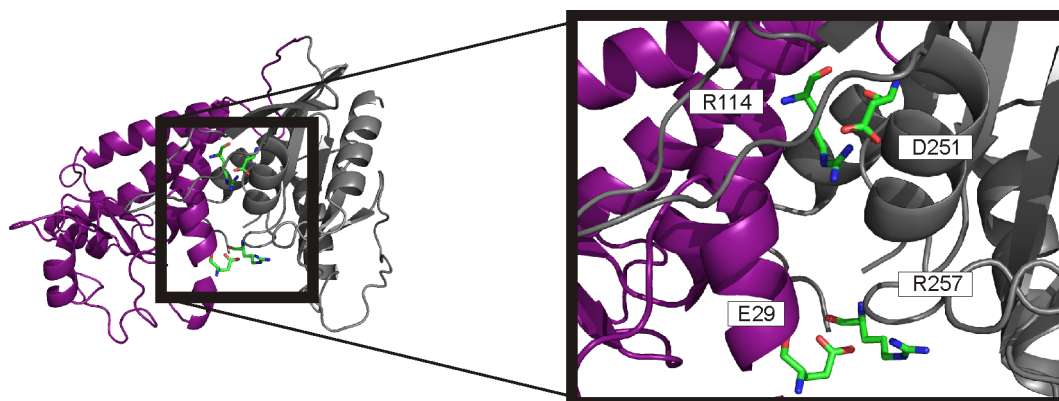
**Figure 3.3.2.1. Homology model of *E. coli* HflX featuring two of the salt bridge interactions between the N-terminal HflX domain and the C-terminal G-domain.** E29 and R114 of the HflX domain interact with R257 and D251 of the G-domain of HflX, respectively.

Due to the hypothesis that HflX will function primarily as a guanine nucleotide-dependent enzyme at cellular concentrations of purine nucleotides (47), the intrinsic and 70S ribosome-stimulated GTPase activity of these HflX variants was assessed first with nucleotide hydrolysis assays. The rate of GTPase activity for HflX$_{E29A,}$ HflX$_{R114A}$ and HflX$_{\Delta L372}$ in the presence of 70S ribosomes was slower than wildtype (0.103 ± 0.0008 µMs$^{-1}$) by a factor ranging from 2 to 3-fold (Figure 3.3.2.2 Panel A and Table 3.3.2.1). A similar behavior was observed for the 50S ribosomal subunit stimulated rates of GTP hydrolysis by HflX variants (Figure 3.3.2.2 Panel B and Table 3.3.2.1).
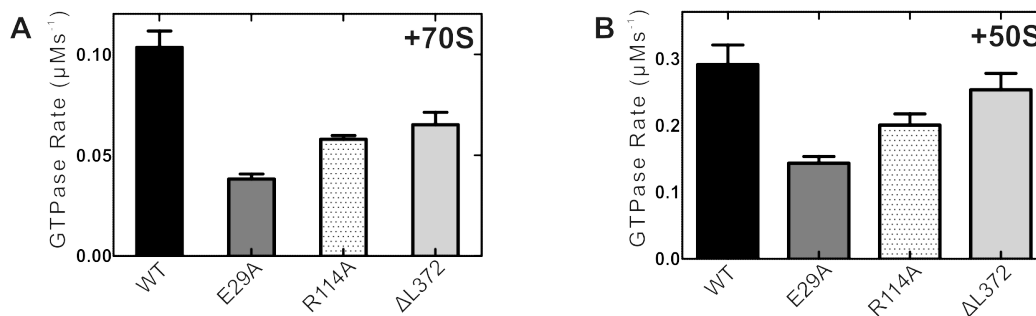
Figure 3.3.2.2 **Comparison of the rates of 70S and 50S stimulated GTPase activity for HflX variants, HflX$_{E29A}$, HflX$_{R114A}$ and HflX$_{\Delta L372}$.** (A) Comparison of the rates of GTP hydrolysis by indicated HflX variants in the presence of 70S ribosomes with wildtype HflX (black) exhibiting the fastest rate followed by HflX$_{\Delta L372}$ (light grey), HflX$_{R114A}$ (white with polka dots) and HflX$_{E29A}$ (dark grey). (B) Comparison of the rates of GTP hydrolysis by HflX variants in the presence of 50S ribosomal subunits with wildtype HflX (black) exhibiting the fastest rate followed by HflX$_{\Delta L372}$ (light grey), HflX$_{R114A}$ (white with polka dots) and HflX$_{E29A}$ (dark grey).

Table 3.3.2.1 Specific GTPase activitiy of HflX variants stimulated by 70S ribosomes and 50S ribosomal subunits.

| | 70S | 50S |
|---|---|---|
| **Variant** | **Rate ($\mu M\ s^{-1}$)** | **Rate ($\mu M\ s^{-1}$)** |
| HflX$_{WT}$ | 0.103 ± 0.0008 | 0.29 ± 0.03 |
| HflX$_{E29A}$ | 0.038 ± 0.002 | 0.14 ± 0.01 |
| HflX$_{R114A}$ | 0.058 ± 0.002 | 0.20 ± 0.02 |
| HflX$_{\Delta L372}$ | 0.065 ± 0.006 | 0.25 ± 0.02 |

To ascertain whether this slight decrease in activity was a result of the HflX variants altered affinity for the 70S ribosome, microfiltration assays were performed. HflX$_{E29A,}$ HflX$_{R114A}$ and HflX$_{\Delta L372}$ were all retained together with the 70S ribosome above the 100 kDA molecular weight cut-off membrane (Figure 3.3.2.3 and Figure 3.3.2.4), suggesting that the affinity for the 70S ribosome is not affected in these HflX variants.
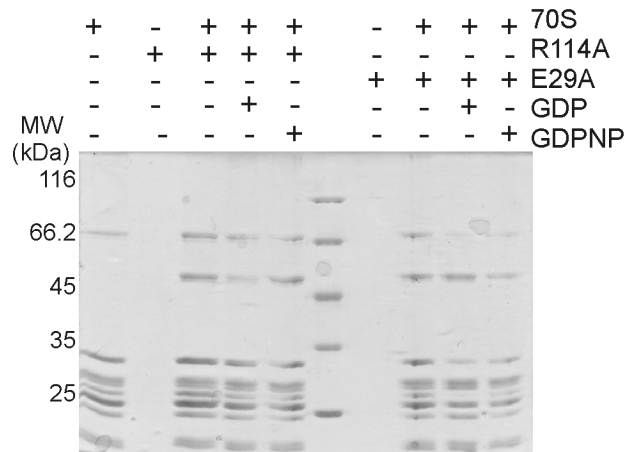
Figure 3.3.2.3 **HflX$_{E29A}$ and HflX$_{R114A}$ can bind 70S ribosomes.** In the presence of 70S, HflX (50.5 kDa) in its *apo,* GDP and GDPNP bound states, was retained above the 100 kDa molecular weight cut off filters following centrifugation.
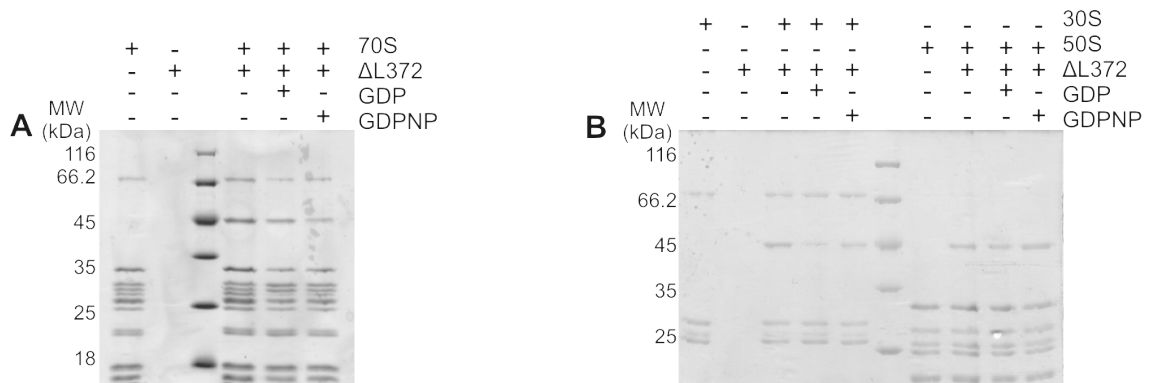


Figure 3.3.2.4 **HflX$_{\Delta L372}$ can bind 70S ribosomes and 30S and 50S ribosomal subunits in all nucleotide bound states.** (A) Truncated HflX (50.5kDa) was found in the retenate with 70S ribosomes upon filtration regardless of the absence or presence of guanine nucleotides. (B) Truncated HflX (50.5 kDa) was found in the retenate with 30S and 50S ribosomal subunits upon filtration regardless of the absence or presence of guanine nucleotides.

The intrinsic GTPase activity of the HflX variants was identical to wildtype HflX except for HflX$_{R114A,}$ which had previously been reported to not exhibit a faster rate of GTP hydrolysis by enzyme alone (46). HflX$_{R114A}$ had an intrinsic GTPase rate of 0.3 x 10$^{-4}$±3.0 x 10$^{-6}$ µMs$^{-1}$, which was approximately 5-fold quicker than HflX$_{E29A}$, HflX$_{\Delta L372}$ and even wildtype HflX (Figure 3.3.2.5 Panel A). Sequence

alignments have revealed that Arg 114 is 100% conserved compared to the 90% identity observed for Glu 29 and may provide some explanation as to the more pronounced effects of this HflX variant on intrinsic guanine nucleotide hydrolysis. Perhaps, the high level of conservation of this arginine amino acid among bacterial HflX proteins, hints at a critical role for this residue in ensuring efficient intrinsic hydrolysis of GTP by HflX.

HflX has been shown to be capable of hydrolyzing ATP and recently, a hypothesis was proposed that interruption of interdomain interactions stimulates the intrinsic ATPase activity of HflX (46,47). Thus, the hydrolysis of ATP both in the presence and absence of ribosomes was examined using nucleotide hydrolysis assays. $HflX_{E29A}$ alone was shown previously to hydrolyze ATP faster (46) but under conditions similar to those described in (47) the only HflX variant to exhibit any difference in the rate of ATP hydrolysis was $HflX_{R114A}$, which was about 3-fold slower at $3 \times 10^{-6} \pm 2 \times 10^{-6}$ µM s$^{-1}$ (Figure 3.3.2.5 Panel B) (46).
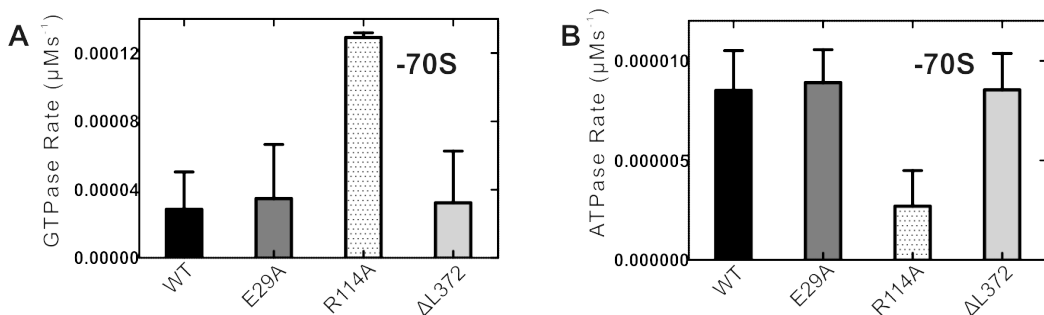
Figure 3.3.2.5 **HflX variants exhibit different rates of intrinsic ATPase and GTPase activity.** (A) Comparison of the rates of GTP hydrolysis by wildtype HflX alone (black), $HflX_{E29A}$ (dark grey), $HflX_{R114A}$ (white with polka dots) and $HflX_{\Delta L372}$ (light grey). (B) Comparison of the rates of ATP hydrolysis by wildtype HflX alone (black), $HflX_{E29A}$ (dark grey), $HflX_{R114A}$ (white with polka dots) and $HflX_{\Delta L372}$ (light grey).

Table 3.3.2.2 Specific intrinsic GTPase and ATPase activity of HflX variants.

| Variant | GTPase Rate ($\mu M\ s^{-1}$) | ATPase Rate ($\mu M\ s^{-1}$) |
|---|---|---|
| HflX$_{WT}$ | $2.9 \times 10^{-5} \pm 2.2 \times 10^{-5}$ | $9 \times 10^{-6} \pm 2 \times 10^{-6}$ |
| HflX$_{E29A}$ | $3.5 \times 10^{-5} \pm 3.2 \times 10^{-5}$ | $9 \times 10^{-6} \pm 2 \times 10^{-6}$ |
| HflX$_{R114A}$ | $1.3 \times 10^{-4} \pm 3.0 \times 10^{-6}$ | $3 \times 10^{-6} \pm 2 \times 10^{-6}$ |
| HflX$_{\Delta L372}$ | $3.2 \times 10^{-5} \pm 3.0 \times 10^{-5}$ | $9 \times 10^{-6} \pm 2 \times 10^{-6}$ |

Unpublished data from our laboratory suggests that HflX can dissociate 70S ribosomes in a nucleotide-dependent manner wherein the extent of light scattering observed in a stopped-flow measurement is the greatest when HflX is in the presence of GTP compared to its *apo* state (Jeffrey Fischer, Doctoral Dissertation 2011). All nucleotide hydrolysis assays are performed in buffer containing a concentration of 30 mM magnesium to prevent the splitting of 70S ribosomes. Unexpectedly, this high concentration of magnesium in solution only affected the 70S- and 50S- stimulated ATPase activity of wildtype HflX. A reduction in rate close to one order of magnitude for both wildtype HflX ATP hydrolysis in the presence of 70S ribosomes and 50S ribosomal subunits was observed in TAKM$_{30}$ (Figure 3.3.2.6). The ATPase activity of HflX$_{E29A,}$ HflX$_{R114A}$ and HflX$_{\Delta L372}$ in the presence of 50S contrasted with the ATPase rates of the variants stimulated by 70S ribosomes. No stimulation of HflX$_{\Delta L372}$ over intrinsic levels of ATP hydrolysis was observed, indicating that the C-terminus might play a role in regulating ATP hydrolysis (Figure 3.3.2.6 Panel B and Table 3.3.2.3). When stimulated by 50S ribosomal subunits, HflX$_{E29A}$ within error possessed a rate of ATP hydrolysis similar to HflX$_{WT}$ in TAKM$_7$ buffer (Figure 3.3.2.6 Panel B and Table 3.3.2.3).
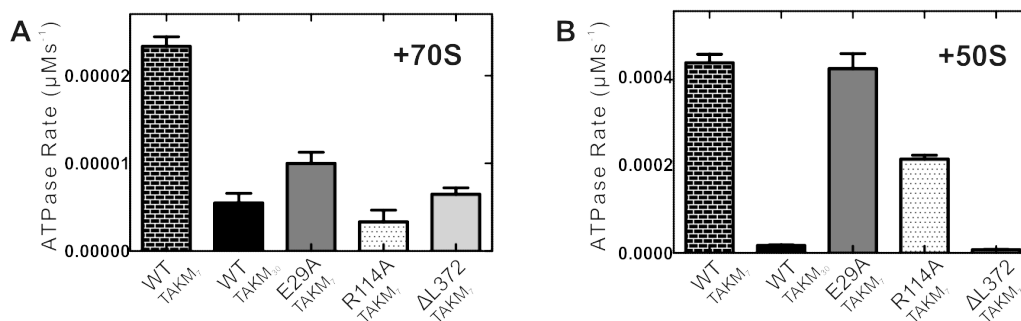
Figure 3.3.2.6. **The rates of 50S and 70S stimulated ATPase activity differ for HflX variants.** (A) Comparison of the rates of 70S ribosome stimulated ATP hydrolysis by wildtype HflX in $TAKM_7$ (black brick pattern), wild-type HflX in $TAKM_{30}$ (black), $HflX_{E29A}$ (dark grey), $HflX_{R114A}$ (white with polka dots) and $HflX_{\Delta L372}$ (light grey). (B) Comparison of the rates of 50S ribosomal subunit stimulated ATP hydrolysis by wildtype HflX in $TAKM_7$ (black brick pattern), wild-type HflX in $TAKM_{30}$ (black), $HflX_{E29A}$ (dark grey), $HflX_{R114A}$ (white with polka dots) and $HflX_{\Delta L372}$ (light grey).

Table 3.3.2.3 Specific ATPase of HflX variants stimulated by 70S ribosomes and 50S ribosomal subunits. It should be noted that assays in the presence of 50S ribosomal subunits were performed in $TAKM_7$ buffer.

| | 70S | 50S |
|---|---|---|
| **Variant** | **Rate ($\mu M\ s^{-1}$)** | **Rate ($\mu M\ s^{-1}$)** |
| $HflX_{WT}$ ($TAKM_7$) | $2 \times 10^{-5} \pm 1 \times 10^{-6}$ | $4.3 \times 10^{-4} \pm 1.9 \times 10^{-5}$ |
| $HflX_{WT}$ ($TAKM_{30}$) | $6 \times 10^{-6} \pm 1 \times 10^{-6}$ | $2 \times 10^{-5} \pm 1 \times 10^{-6}$ |
| $HflX_{E29A}$ ($TAKM_{30}$) | $1 \times 10^{-5} \pm 1 \times 10^{-6}$ | $4.2 \times 10^{-4} \pm 3.3 \times 10^{-5}$ |
| $HflX_{R114A}$ ($TAKM_{30}$) | $3 \times 10^{-6} \pm 1 \times 10^{-6}$ | $2.1 \times 10^{-4} \pm 8.3 \times 10^{-6}$ |
| $HflX_{\Delta L372}$ ($TAKM_{30}$) | $6 \times 10^{-6} \pm 1 \times 10^{-6}$ | $7 \times 10^{-6} \pm 7 \times 10^{-7}$ |

As previously mentioned, wildtype HflX has a propensity to split 70S ribosomes into 30S and 50S ribosomal subunits as has been witnessed by light scattering stopped-flow experiments. Consistent with this, rapidly mixing 1 µM of $HflX_{E29A,}$ $HflX_{R114A}$ and $HflX_{\Delta L372}$ in the presence of 125 µM GTP with 0.15 µM of 70S ribosomes resulted in decreases in Rayleigh light scattering when the samples were subjected to light at a wavelength of 436 nm. Complete dissociation of 70S ribosomes in a low magnesium concentration buffer has been reported to result in an approximate 29% decrease in Rayleigh light scattering (88). HflX in its

GTP bound form can catalyze ribosome dissociation to the same extent as has been observed by magnesium depletion and by known ribosome dissociation factors such as RRF and EF-G (88). HflX$_{E29A,}$ HflX$_{R114A}$ and HflX$_{ΔL372}$ were impaired both in the rate and extent of their catalysis of 70S ribosome dissociation (Figure 3.3.2.7). HflX$_{E29A}$ and HflX$_{R114A}$ reached the maximum decrease in light scattering (~30%) but at a slower rate than wildtype HflX (Figure 3.3.2.7). HflX$_{ΔL372}$ exhibited drastically reduced 70S ribosome dissociation reaching the maximal extent of light scattering at a much slower rate. For the first time, a role in regulating the dissociation of 70S ribosomes can be attributed to the C-terminal extension of HflX.
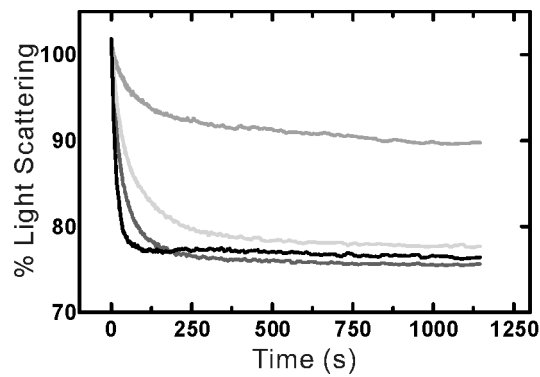


Figure 3.3.2.7 **HflX$_{E29A}$, HflX$_{R114A}$ and HflX$_{ΔL372}$ dissociate 70S ribosomes.** All variants of HflX assessed were found to split 70S into 50S and 30S ribosomal subunits slower and to lesser extents than wildtype. HflX$_{E29A}$ (dark grey) was most similar to wild-type (black) with HflX$_{R114A}$ (lightest grey) exhibiting a slower rate of 70S ribosome dissociation but was not as significantly impaired as HflX$_{ΔL372}$ (light grey).

## 3.4 Discussion and Future Directions

Through sequence alignments, several conserved stretches of residues or single amino acids within HflX have been discovered and their involvement in modulating one of its key cellular functions in *E. coli*, nucleotide hydrolysis has been studied. Previously, HflX was deemed to not be dependent on potassium ions for its intrinsic GTP hydrolysis activity (49). As an accurate procedure to study the intrinsic GTPase activity of HflX to obtain such kinetic parameters as Michaelis Menten constants or catalytic efficiencies has yet to be found, our focus remains on studying ribosome-stimulated nucleotide hydrolysis activity. This approach resulted in the discovery that the 70S stimulated GTPase activity of HflX is indeed regulated by potassium ions. Potassium dependence has been reported to act as a GTPase-Activating Element (GAE) (89). For the bacterial GTPase MnmE, the monovalent cation promotes dimerization that stabilizes the transition state that exists during the GTP hydrolysis process (68). For EngA, potassium allows for the nucleotide or catalytic machinery to be optimally positioned for efficient hydrolysis of GTP (89). As the ribosome has been shown to act as GAP for HflX, it is most likely that at lower concentrations, potassium ions act to optimally coordinate the nucleotide within the binding pocket of the factor for fast GTPase activity (47).

Having established that HflX possesses sequence elements that do indeed allow potassium ion concentration to fine-tune its ribosome-stimulated GTPase activity, several interesting conclusions can be drawn from the effects alterations to the domain contacts and deletion of the C-terminus has on HflX. The fact that

disrupting salt bridges connecting the HflX-domain to the G-domain can have opposing effects on intrinsic and ribosome stimulated purine nucleotide hydrolysis suggests that the mechanisms in which ATP and GTP hydrolysis are fine-tuned could indeed be different.  As the catalytic machinery contributed by HflX and the ribosome to nucleotide hydrolysis have not yet been elucidated, the link between overall domain or terminus movement to catalysis cannot be definitively determined. For ATP hydrolysis specifically, no unique binding site or P-loop/Walker A-like feature for recognizing only adenine nucleotides has been discovered for HflX (46). Mutation of P-loop residues has been shown to impair the GTP hydrolysis activity of GTPases such as dynamin, thus a similar methodology could be used to decipher the ATP hydrolysis machinery of HflX and whether it is also executed by residues within the G-domain (90).  Figuring out the catalytic machinery of HflX responsible for both ATP and GTP hydrolysis will serve as a basis for building bridges to the effects brought upon by residues found in other regions of the protein.

Of particular interest within this thesis, were the effects magnesium ion concentration had on the 70S ribosome and 50S ribosomal subunit stimulated ATPase activity of wild-type HflX and HflX variants. The important role of magnesium in the nucleotide hydrolysis reaction of phosphatases in general has been shown by quantum mechanics/molecular mechanics simulations (91). Cleavage of the phosphodiester bond is driven forward due to the fact that magnesium coordinating the nucleotide triphosphates elongates the bond between the beta and gamma phosphates mimicking the transition state of the

molecule (91). Beyond an influence in the nucleotide hydrolysis reaction, magnesium ions, through an interaction with the phosphate backbone of RNA, can stabilize the entire ribosome (92). As a result, a concentration of magnesium *in vivo* of 3 to 5 mM is also necessary for protein synthesis machinery to come together for effective translation (92). A concentration of magnesium ten fold over *in vivo* levels may hinder the natural motion of the macromolecular complex due to the excessive amounts of divalent cation interacting with rRNA. This movement could be required to stimulate the ATP hydrolysis capacity of HflX. Similarly, established preventers of ribosome dissociation, the polyamines, spermine and spermidine, slow the rates of ribosome-stimulated GTP hydrolysis by HflX (93). The reduced rates for both types of nucleotide hydrolysis are most likely both originating from extensive stabilization of the ribosome to the point that its natural dynamics are encumbered. Thus, large-scale movements of the ribosome, prevented by stabilizing factors such as metal ion concentration or naturally occurring compounds like polyamines, can critically affect the activity of associated factors.

To note as well, is that a more concrete role for the C-terminal extension of HflX from *E. coli* has been resolved. The absence of the C-terminus resulted in intrinsic levels of ATP hydrolysis in the presence of 50S ribosomal subunits. Together with the decrease in the maximum extent of light scattering observed for HflX$_{\Delta L372}$ variant, these results could suggest that the contacts wildtype HflX makes with 70S compared to the 50S alone are critical for both its ATP hydrolysis activity and ribosome dissociation activitycatalyzed by HflX in the

presence of GTP. Structures of HflX bound to the empty ribosome, ribosomal subunits or functional ribosome complexes containing tRNA in the P and E-sites especially, would allow for the determination of any changes in the contacts between the subunits constituting the 70S to be discovered as has been found for other translational factors such as RRF (94). In this way, a hypothesis as to the manner in which 70S ribosome splitting is severely affected when the C-terminus of HflX is removed could be formulated. The structural insight garnered from a structure of HflX on the ribosome would also allow for the impact of the $HflX_{E29A}$ and $HflX_{R114A}$ variants on ribosome dissociation to be confirmed. One assumption would be that coordinated movements of both of the domains comprising HflX would be necessary to orchestrate the separation of such a large macromolecular complex as the ribosome. With the guanine nucleotide-binding pocket positioned within the cleft formed by the HflX and G-domain, conformational changes required for catalyzing the splitting of ribosomes may also be altered when R114A-D251 and E29A-R257 are broken. In the future, variants consisting of several mutations disrupting salt-bridges all along the interface between the HflX and G domain will be tested to establish if there will be cumulative effects on nucleotide hydrolysis. This work will be of upmost importance to better understand communication networks between the protein domains.

Table 3.4.1 Summary of the Characterization of HflX Variants with Disrupted
Domain Interactions or Lacking the C-terminal Extension

| Variant | HflX$_{E29A}$ | HflX$_{R114A}$ | HflX$_{\Delta L372}$ |
|---|---|---|---|
| Amino Acid Conservation of Mutated Residue | 90% | 99% | <60% |
| Expression | At 37°C with 1 M IPTG | At 37°C with 1 M IPTG | At 37°C with 1 M IPTG |
| Purification | Non-Denaturing Conditions | Non-Denaturing Conditions | Non-Denaturing Conditions |
| Ribosome Binding | 1:1 Binding of Variant to 70S | 1:1 Binding of Variant to 70S | 1:1 Binding of Variant to 30S, 50S & 70S |
| ATP Hydrolysis | Intrinsic: Similar to WT 70S: Slower than WT 50S: Similar to WT | Intrinsic: Slower than WT 70S: Slower than WT 50S: Slower than WT | Intrinsic: Similar to WT 70S: Slower than WT 50S: Intrinsic Levels |
| GTP Hydrolysis | Intrinsic: Similar to WT 70S/50S: Slower than WT | Intrinsic: Faster than WT 70S/50S: Slower than WT | Intrinsic: Similar to WT 70S/50S: Slower than WT |

## 3.5 Conclusion

Previous publications from our laboratory have revealed that HflX can interact

with 30 and 50S ribosomal subunits and 70S ribosomes. Thus a better

understanding of the protein domain dynamics of HflX and its catalytic activity in

the context of it in complex with ribosomes was the main goal of this chapter of

the thesis. Regulation of HflX GTP hydrolysis by potassium ions, a contested

theory only proposed based on conserved structural elements, was for the first

time observed for the factor in the presence of 70S ribosomes. Additionally, the

elimination of highly conserved salt-bridge interactions and the less conserved C-

terminal domain of HflX were found to have effects on both 70S and 50S-stimulated nucleotide hydrolysis that was different from intrinsic activities determined for the variant factors. These results indicate that the movement of single amino acids or domains of HflX may differ depending on whether or not it is found bound to ribosomes and provides further evidence that the ribosome can modulate the activity of HflX by sending signals through its protein structure.

<u>**Chapter 4 –**</u>

***Insight into the NTPase-Activated States of HflX and YchF***

**4.1 Introduction**

    A plethora of clinical antibiotics target the bacterial ribosome, often altering different regions' conformations upon binding. Decoding centre antibiotics, paromomycin in particular, have been shown experimentally to alter the 30S ribosomal subunit by displacing nucleotides in relation to the minor groove of 16S rRNA (95,96). The peptidyl-transferase centre can support the binding of multiple antibiotics due to the fact that the rRNA can form hydrophobic, stacking and/or hydrogen bonding interactions with a variety of aromatic or non-polar small molecules (11,24,97). Invasion of these peptidyl-transferase centre drugs into the space occupied by the amino acid end of incoming tRNAs is considered to be their common mechanism of action. The evidence provided by the inhibitory function of these particular classes of antibiotics insinuates that base flips of rRNA, obstruction of interaction surfaces and perhaps even conformational changes to ribosomal proteins can disrupt vital communication networks between the ribosome and bound translation factors. This has been shown to be the case for the peptidyl transferase centre-targeting antibiotic, chloramphenicol which inhibits the ribosome-stimulated GTPase activity of HflX (47). This result contrasts with the fact that kanamycin, an antibiotic which binds to the decoding centre of the 70S does not slow the rate of GTP hydrolysis in the presence of ribosomes (47). It is unclear exactly what step in the GTPase cycle of HflX antibiotics can influence, resulting in overall slower rates of multiple

turnover GTP hydrolysis. The ribosome acts as GAP for HflX, stabilizing its GTPase activated state and stimulating hydrolysis (47,50), but it remains unclear as to whether the binding of antibiotics to the 70S can affect the affinity of HflX for ribosomes, guanine nucleotides or both. Antibiotics, such as chloramphenicol along with disrupting these interactions could also hinder the ribosome in its ability to contribute the catalytic machinery required for the catalysis of GTP hydrolysis or the release of inorganic phosphate necessary for the continuation of the cycle. Thus if different classes of antibiotics can affect the interaction between HflX and potentially YchF and the ribosome distinctly, this could potentially lead to the discovery of novel antibiotic targets. Perhaps, by assessing the effects of antibiotics on the NTP hydrolysis activities of HflX and YchF, which are critical to their functions as NTPases, the findings could provide insight into their cellular roles and maybe reveal some commonalities between the factors.

Before this could become a reality though, the connection between ribosome-targeting antibiotics and their influence on the ribosome-associated functions of HflX and YchF has to become evident. Here, a number of clinically relevant, bacteriostatic antibiotics were tested in order to observe their effects on the rates of HflX and YchF nucleotide hydrolysis in the presence of 70S ribosomes. Additionally, knowledge exists that chloramphenicol reduces the rate of ribosome-stimulated GTP hydrolysis yet the exact mode of how this is achieved is uncertain. Therefore, the rate constants describing guanine nucleotide association and dissociation from HflX in complex with ribosomes in the

90

presence of antibiotics were found using fluorescence based rapid kinetics. All of this work is a prerequisite to identifying states of the ribosome during protein synthesis that have remained hidden from researchers or new interactions with specialized stress factors such as HflX and YchF and utilizing this information as the inspiration for new antibiotic development.

## 4.2 Materials and Methods

### 4.2.1 Protein Expression and Purification

Refer to Section 2.2.3.

### 4.2.2 Preparation of Ribosomes

Refer to Section 2.2.4

### 4.2.3 Nucleotide Hydrolysis Assays

Assays were performed essentially as described in Section 2.2.7 but with the following changes: antibiotics to a final concentration of 500 µM were also included in the 60 µL reaction volume for screening purposes.  One way analysis of variance was performed to compare the rates of ribosome stimulated nucleotide hydrolysis obtained in the presence of antibiotics to the 70S-stimulated NTPase rate in the absence of antibiotics.

### 4.2.4 Pre-Steady State Fluorescence Stopped-Flow Experiments

*YchF* - All pre-steady-state kinetics of mant-nucleotide association and dissociation from YchF were determined using a KinTek SF-2004 Stopped-flow apparatus.  Through the radiationless mechanism, fluorescence resonance energy transfer (FRET), mant-nucleotides (Jena Bioscience) were excited by the tryptophan residues in the proteins.  The tryptophan in YchF was excited at 280

nm and the emission of the mant-nucleotides detected after passing through LG-400-F long-pass cutoff filters. Initially, complexes of YchF and 70S ribosomes or 30S ribosomal subunits were incubated at 20°C for 15 minutes. The association of the non-hydrolyzable analog of ATP, ADPNP, to YchF was determined by rapidly mixing 25 µL of preformed YchF complex (1.36 µM YchF and 2 or 8 µM 70S or 30S) with 25 µL of increasing concentrations of mant-nucleotides (5 to 40 µM for ADPNP) in TAKM$_7$ at 20°C. Fluorescence changes were best fit with a two exponential function, normalized and a minimum of ten traces averaged and refit with the appropriate equation. The concentration dependence of the rates obtained from fitting the fluorescence changes can be fit with a linear function to attain rate constants. The slope of the linear concentration dependence of $k_{app}$ is equal to the bimolecular association rate constant. To determine the dissociation rate of mant-nucleotides (30 µM) from the respective complexes, 25 µL of YchF•mant-nucleotide•ribosome complexes were rapidly mixed with 25 µL of an excess of unlabeled nucleotide (300 µM). Complexes were formed by incubating 1.36 µM YchF and 2 or 8 µM 70S ribosome or 2 µM 30S ribosomal subunit with 30 µM mant-nucleotide for 20 minutes at 20°C. The resulting fluorescence traces were best fit with the equation 4.2.4.1 where $k_{app}$ is the characteristic apparent rate constant, $A$ is the signal amplitude, $Fl$ is the fluorescence at time $t$, and $Fl_\infty$ is the final value of fluorescence.

$$Fl = Fl_\infty + A_1 \exp(-k_{app1}t) + A_2 \exp(-k_{app2}t) \qquad \text{(Equation 4.2.4.1)}$$

*HflX* - Stopped-flow experiments with HflX were performed and analyzed as in (50) but using TAKM$_{30}$ buffer (contents similar to TAKM$_7$ with the exception of 30

mM MgCl$_2$), which has been shown to prevent HflX catalyzed splitting of 70S ribosomes (Mackenzie Coatham and Tobias Schuemmer, unpublished data). The rate constants for the association and dissociation of mant-GDP and the non-hydrolyzable analog of GTP, GDPNP to and from the 70S ribosome respectively were monitored in the presence of 1 mM of the peptide exit tunnel binding antibiotic, erythromycin and clindamycin which targets the peptidyl-transferase centre, clindamycin.

*4.2.5 Microfiltration Binding Assays*

Microfiltration binding assays were performed similar to Section 2.2.9 with the only difference that antibiotics were present to a final concentration of 500 µM throughout the duration of the experiment.

**4.3 Results**

*4.3.1. The Effects of Antibiotics on YchF and HflX Nucleotide Hydrolysis Activity*

An assessment of the effect of currently used antibiotics (Table 4.3.1.1) on the ribosome-associated nucleotide hydrolysis activity of HflX and YchF was accomplished by performing antibiotic screens.  To this end, the amount of nucleotide hydrolyzed by 1 µM HflX or 5 µM YchF in the presence of 1 µM 70S and 500 µM antibiotics was quantified.

Table 4.3.1.1 Summary of Various Classes of Protein Synthesis Inhibitors

| Antibiotic | Class of Antibiotic | Mode of Action |
|---|---|---|
| Kanamycin (18) | Aminoglycoside | Decoding Centre Inhibitor |
| Paromomycin (12) | Aminoglycoside | Decoding Centre Inhibitor |
| Tobramycin (18) | Aminoglycoside | Decoding Centre Inhibitor |
| Viomycin (98) | Cyclic Peptide | Ribosome Translocation Inhibitor |
| Thiostrepton (27) | Thiopeptide | Translation Factor Inhibitor |
| Chloramphenicol (24) | N/A | PTC Inhibitor |
| Clindamycin (99) | Lincosamide | PTC Inhibitor |
| Lincomycin (99) | Lincosamide | PTC Inhibitor |
| Azithromycin (25) | Macrolide | PET Inhibitor |
| Erythromycin (99) | Macrolide | PET Inhibitor |

None of the classes of antibiotics tested had any significant effects on the ribosome-stimulated ATPase activity of YchF (Figure 4.3.1.1 and Table 4.3.1.2). No stimulatory or inhibitory effect was larger than 2-fold and therefore no correlation between the binding sites of the antibiotics and their influence on the rate of ribosome stimulated ATPase can be observed (Figure 4.3.1.1 and Table 4.3.1.2)
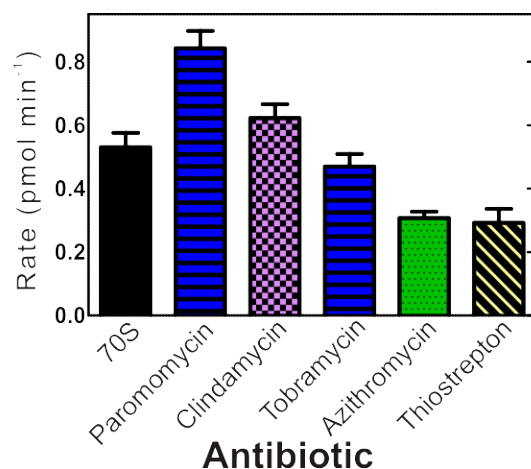
Figure 4.3.1.1 **Antibiotics affect ribosome stimulated YchF ATPase activity.** Comparison of the rates of 70S stimulated ATPase activity of YchF WT in the presence of representative antibiotics from the aminoglycoside (blue horizontal lines), translation factor inhibiting (yellow diagonal lines), lincosamide (light purple checkered pattern) and macrolide (green polka dot pattern) classes to the rate observed in the absence of antibiotics (solid black).

Table. 4.3.1.2 Specific ATPase activity of wild-type YchF stimulated by 70S ribosomes in the presence and absence of antibiotics. P values less than 0.05 were considered to be significant with the level of significance being denoted on tables by the number of  * markings.

| Condition | Rate (pmol min$^{-1}$) | Significance (P < 0.05) |
|---|---|---|
| No Antibiotic | 0.53 ± 0.04 | N/A |
| Paromomycin (Aminoglycoside) | 0.84 ± 0.05 | *** |
| Clindamycin (Lincosamide) | 0.62 ±0.04 | No |
| Tobramycin (Aminoglycoside) | 0.47 ± 0. 04 | No |
| Azithromycin (Macrolide) | 0.31 ± 0.02 | * |
| Thiostrepton (Translation Factor Inhibitor) | 0.29 ± 0.04 | ** |

In contrast to the effects observed on YchF ATPase activity, antibiotics, especially those of the lincosamide and macrolide class, inhibited the 70S stimulated GTPase activity of HflX by up to a factor of 50-fold (Figure 4.3.1.2 Panel A and Table 4.3.1.3).  This contrasted with the less than 5-fold inhibition observed for the rate of GTP hydrolyzed in the presence of aminoglycoside

95

antibiotics (Figure 4.3.1.2 Panel A and Table 4.3.1.3). The rates associated with the GTPase activity of HflX stimulated by 50S ribosomal subunits were slowed in a similar manner. Antibiotics targeting the peptidyl transferase centre, chloramphenicol and lincomycin, and the peptide exit tunnel, erythromycin reduced the rates of GTP hydrolysis by HflX by 10- to 15-fold (Figure 4.3.1.2 Panel B and Table 4.3.1.3).
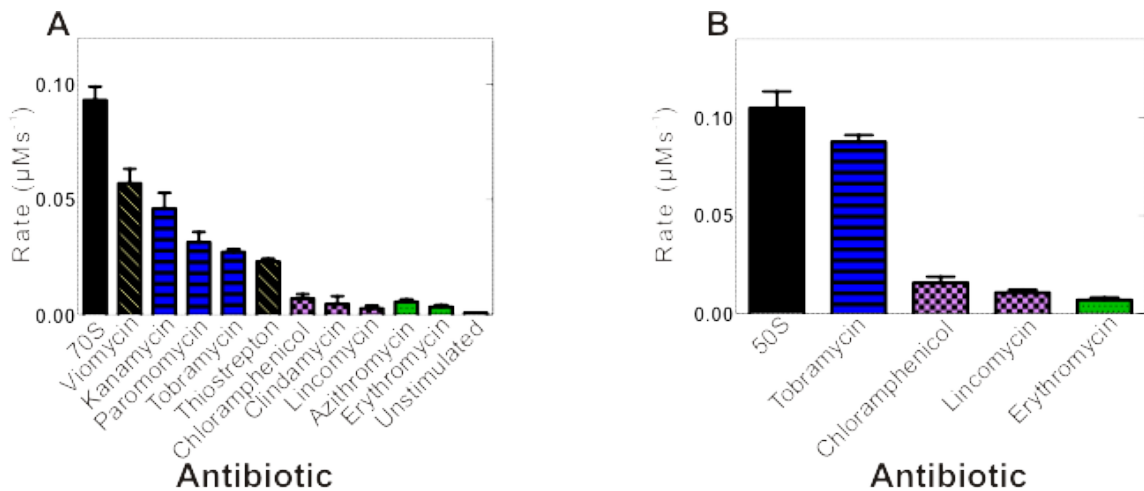


Figure 4.3.1.2 **Peptidyl-transferase centre and peptide exit tunnel targeting antibiotics significantly slow the rate 70S and 50S stimulated GTPase activity of HflX.** (A) The rate of 70S stimulated GTPase activity of HflX WT in the presence aminoglycosides (blue horizontal lines), translation factor inhibitors (yellow diagonal lines), PTC targeting antibiotics (light purple checkered pattern) and macrolides (green polka dot pattern) were compared to the absence of antibiotic (solid black). (B) Rates of HflX GTPase activity stimulated by the 50S ribosomal subunit in the presence of antibiotics obtained in a similar manner as in (A).

Table 4.3.1.3 Specific GTPase activity of wildtype HflX stimulated by 70S ribosomes and 50S ribosomal subunits in the presence and absence of antibiotics.  P values less than 0.05 were considered to be significant with the level of significance being denoted on tables by the number of  * markings.

| Condition | 70S Rate ($\mu M\ s^{-1}$) | 50S Rate ($\mu M\ s^{-1}$) | Significance (P < 0.05) |
|---|---|---|---|
| No Antibiotic | 0.093 ± 0.006 | 0.105 ± 0.008 | N/A |
| Viomycin (Translation Factor Inhibitor) | 0.057 ± 0.006 | N.D. | *** |
| Kanamycin (Aminoglycoside) | 0.046 ± 0.007 | N.D. | *** |
| Paromomycin (Aminoglycoside) | 0.031 ± 0.004 | N.D. | *** |
| Tobramycin (Aminoglycoside) | 0.027 ± 0.001 | 0.088 ± 0.003 | *** |
| Thiostrepton (Translation Factor Inhibitor) | 0.023 ± 0.001 | N.D. | *** |
| Chloramphenicol (PTC Inhibitor) | 0.007 ± 0.001 | 0.016 ± 0.002 | **** |
| Clindamycin (Lincosamide) | 0.004 ± 0.003 | N.D. | **** |
| Lincomycin (Lincosamide) | 0.003 ± 0.001 | 0.010 ± 0.001 | **** |
| Azithromycin (Macrolide) | 0.006 ± 0.001 | N.D. | **** |
| Erythromycin (Macrolide) | 0.003 ± 0.001 | 0.007 ± 0.001 | **** |
| No Antibiotic & No Stimulation by 70S or 50S | 0.00084 ± 0.00001 | 0.00084 ± 0.00001 | **** |

To elucidate whether the salt-bridges between the HflX and G-domain or the presence of the C-terminus of HflX were required for the inhibition of ribosome-stimulated GTP hydrolysis by antibiotics, the GTPase activity of HflX variants in the presence of the antibiotics, erythromycin and clindamycin was determined. Intriguingly, the rates of HflX variants' GTPase activity in the presence of 70S and in the presence of representative PTC and PET targeting antibiotics were similar within error, regardless of the difference in rates observed for the variants

in the absence of antibiotics (Figure 4.3.1.3 and Table 4.3.1.4). These results suggest that the salt-bridges connecting the HflX domain to the G-domain as well as the C-terminal extension are not required for the inhibition of ribosome-stimulated GTPase activity by antibiotics binding to the peptidyl-transferase centre and peptide-exit tunnel regions of the ribosome.
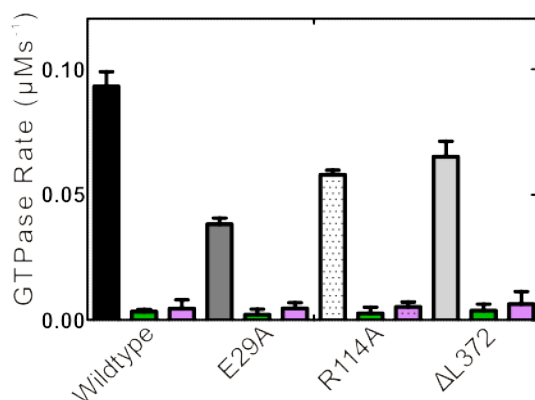


Figure 4.3.1.3 **The rates of 70S ribosome stimulated GTPase activity of HflX variants are similar to wildtype HflX in the presence of peptidyl-transferase centre and peptide-exit tunnel targeting antibiotics.** In the presence of erythromycin (green) or clindamycin (pink), $HflX_{E29A}$, $HflX_{R114A}$ and $HflX_{\Delta L372}$ hydrolyze GTP in the presence of ribosomes as slow as wildtype HflX under the same conditions.

Table 4.3.1.4 Specific GTPase activity of wildtype HflX and HflX variants stimulated by 70S ribosomes in the presence and absence of antibiotics.

| Rates ($\mu M\ s^{-1}$) | Wildtype | E29A | R114A | ΔL372 |
|---|---|---|---|---|
| No Antibiotic | 0.099±0.006 | 0.038±0.002 | 0.057±0.002 | 0.065±0.006 |
| Erythromycin | 0.004±0.001 | 0.002±0.002 | 0.003±0.002 | 0.004±0.003 |
| Clindamycin | 0.005±0.003 | 0.005±0.002 | 0.005±0.002 | 0.006±0.005 |

To ensure that the effects on GTP hydrolysis in the presence of ribosomes were not due to an inability of HflX to bind to the 70S ribosome, microfiltration assays were performed. SDS-PAGE analysis of the retenates revealed that antibiotics did not interfere with binding of HflX to the ribosome as HflX was found to remain

above the filter with the large ribosomal particles regardless of the antibiotic and the guanine nucleotide present in the experiment (Figure 4.3.1.4).
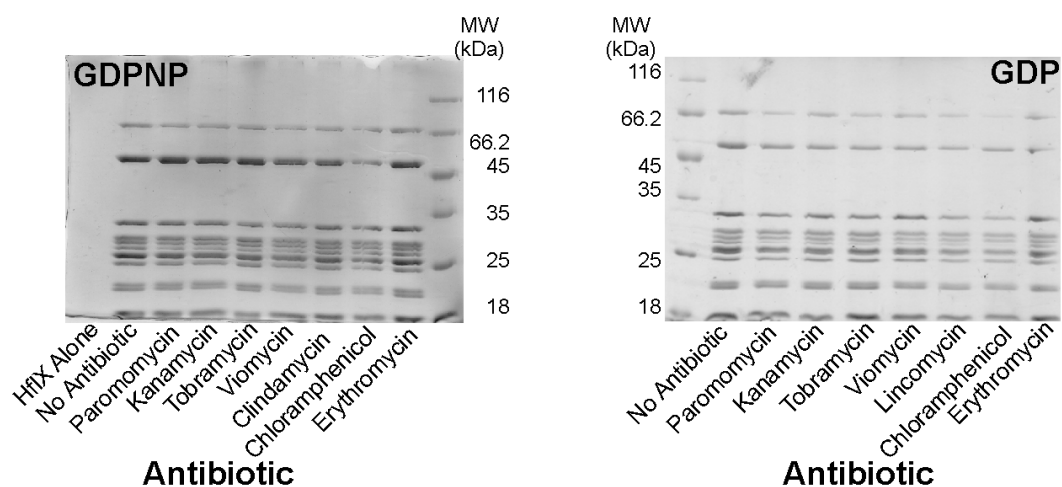


Figure. 4.3.1.4 **Antibiotics targeting various functional centers on the ribosome do not affect binding of HflX to 70S ribosomes.** HflX in its GDPNP- and GDP- bound form was retained above a 100 kDa MWCO filter with 70S ribosomes in the presence of aminoglycoside antibiotics (paromomycin, kanamycin and tobramycin), the translation factor inhibitor, viomycin and PTC/PET antibiotics (clindamycin or lincomycin, chloramphenicol and erythromycin).

*4.3.2 Pre-Steady State Kinetics of Guanine Nucleotide Binding to HflX in the Presence of Antibiotics*

To pinpoint the exact step in the GTPase cycle of HflX that is affected by antibiotics and resulting in slower rates of GTP hydrolysis, pre-steady state rapid kinetic measurements were carried out to assess whether the binding or dissociation of guanine nucleotides from HflX are contributing to the observed antibiotic inhibition. Previously, the rates of association and dissociation of mant-labeled GDP and GDPNP have been reported for HflX when in complex with 70S ribosomes and 50S and 30S ribosomal subunits. The 70S ribosome and 50S ribosomal subunit stabilize the binding of GTP by at least 250-fold up to a factor of 70000, most likely assisting HflX in adopting a 'GTPase-activated state' (50).

Previously, these experiments were performed in buffer conditions where HflX is capable of dissociating ribosomes, thus a buffer containing a high concentration of magnesium ions (30 mM) was utilized.  Under these experimental conditions, in the presence of HflX, stable 70S ribosomes should be found, resulting in the determination of kinetic constants that truly reflect guanine nucleotide association dissociation from HflX in complex with 70S (not a mixture of 50S or 30S ribosomal subunits).   Association experiments with mant-GDP were carried out by rapidly mixing 1 μM HflX-70S complex with increasing concentrations of mant-GDP (10 to 50 μM) in a stopped-flow apparatus. Monophasic fluorescence changes were observed, supporting a one-step binding process (Scheme 4.3.2.1) and accordingly fit with a single exponential function (Figure 4.3.2.1 Panel A).   The apparent rates obtained for this step increased with the concentration of mant-GDP allowing for the calculation of $k_1$ values from the slope of this concentration dependence. In the presence of 30 mM $Mg^{2+}$ (0.37 ± 0.10 $μMs^{-1}$) or 1 mM of clindamycin (0.49 ± 0.04 $μMs^{-1}$) and erythromycin (0.61 ± 0.11 $μMs^{-1}$) the $k_1$ values determined were within error of the rate constant of 0.49 ± 0.10 $μMs^{-1}$ reported in (50) in $TAKM_7$ (Figure 4.3.2.1 Panel B and Table 4.3.2.1).    Chase experiments, in which preformed HflX-70S-mant-GDP complexes were rapidly mixed with an excess of unlabeled GDP, led to the observance of a decrease in fluorescence over time indicative of guanine nucleotide dissociation (Figure 4.3.2.1 Panel C). The decays in fluorescence could be best described as monophasic in nature and best fit with a single-exponential function. A value for $k_{-1}$ of 2.5 ± 0.1 $s^{-1}$ which was determined in (50)

under low $Mg^{2+}$ conditions was consistent with the $2.8 \pm 0.3$ $s^{-1}$, $2.4 \pm 0.3$ $s^{-1}$, and

$2.2 \pm 0.3$ $s^{-1}$ reported here in the presence of 30 mM $Mg^{2+}$, 1 mM of clindamycin

or 1 mM of erythromycin, respectively (Table 4.3.2.1). From the experimentally

determined rate constants, equilibrium dissociation constants ($K_D$) governing the

interaction of mant-GDP to HflX-70S complexes under high $Mg^{2+}$ conditions or in

the presence of PTC or PET targeting antibiotics were calculated. Whether under

30 mM $Mg^{2+}$ conditions ($K_D = 7.6 \pm 2.2$ µM), or in the presence of clindamycin

($K_D = 4.9 \pm 0.7$ µM) or erythromycin ($K_D = 3.6 \pm 0.8$ µM), the determined

equilibrium dissociation constants were close to the $3.1 \pm 0.8$ µM affinity of HflX-

70S for GDP reported previously (50) (Table 4.3.2.1). Thus, antibiotics that

inhibit the ribosome-stimulated GTPase activity of HflX do not affect either the

binding or dissociation of mant-GDP from the HflX-70S complex. These results

prompted an examination of the pre-steady state kinetics with regards to the

association and dissociation of mant-GDPNP to and from HflX in complex with

70S ribosomes.

$$HflX \bullet 70S + mant - GDP \underset{k_{-1}}{\overset{k_1}{\rightleftharpoons}} HflX \bullet mant - GDP \bullet 70S \qquad \text{(Scheme 4.3.2.1)}$$
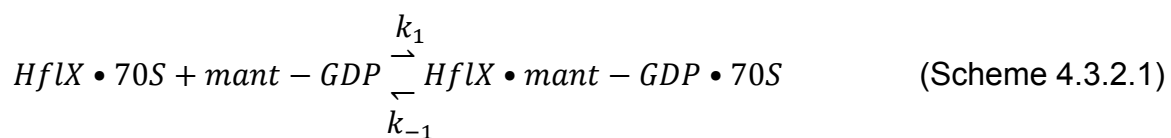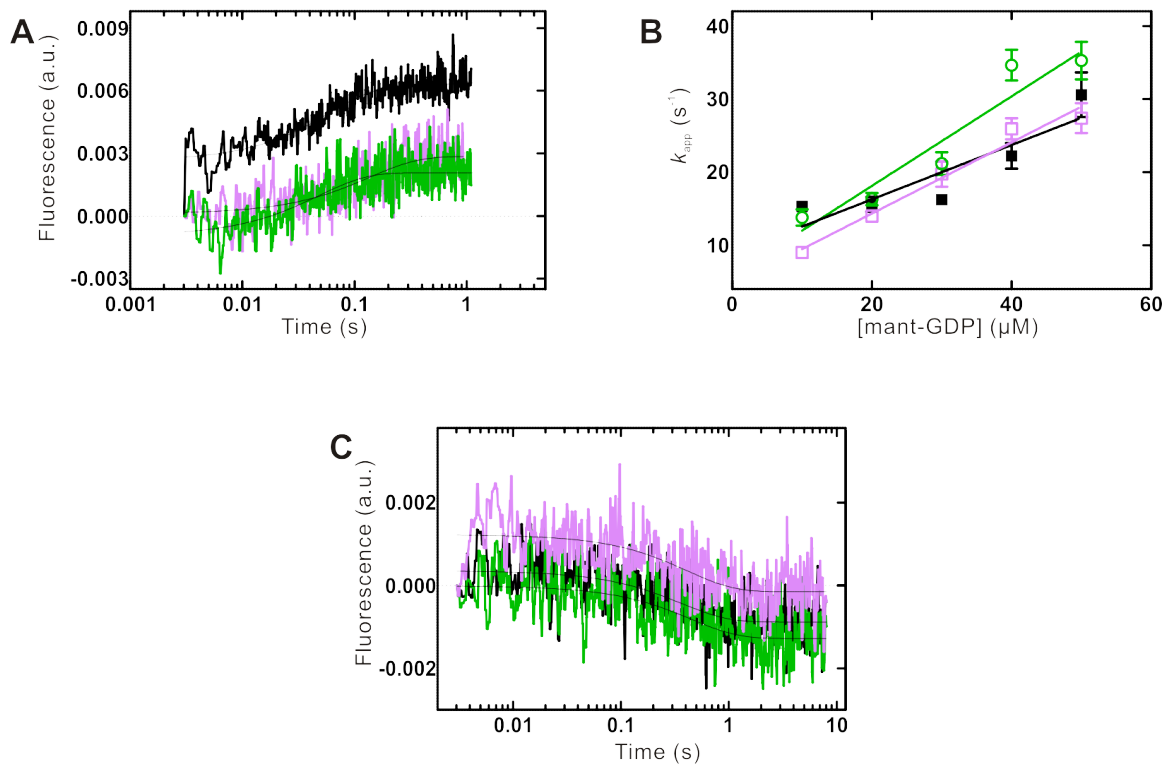
Figure 4.3.2.1 **Pre-steady state kinetics of mant-GDP binding and dissociation for HflX WT in complex with 70S in the presence or absence of inhibitors of ribosome-stimulated GTPase activity.** (A) Representative fluorescent traces observed upon rapidly mixing HflX-70S complexes with 30 μM mant-GDP. The normalized, average trace obtained in the absence of antibiotic is shown in black, while the traces obtained in the presence of clindamycin and erythromycin are represented in light purple and green, respectively. (B) Concentration dependence of the $k_{app}$ values for mant-GDP association to HflX-70S complexes in the absence of antibiotics (black), or in the presence of the antibiotics, clindamycin (light purple) and erythromycin (green). (C) Representative time courses of the dissociation of mant-GDP from HflX-70S upon being rapidly mixed with an excess of unlabeled nucleotide. The normalized, average trace obtained in the absence of antibiotic is shown in black, while the traces obtained in the presence of clindamycin and erythromycin are represented in light purple and green, respectively.

Table 4.3.2.1  Summary of experimentally determined rates and constants for the binding of mant-GDP to HflX under buffer conditions in which ribosome dissociation is inhibited and the presence or absence of antibiotics.

| | High Mg$^{2+}$ Conditions | High Mg$^{2+}$ Conditions & Clindamycin | High Mg$^{2+}$ Conditions & Erythromycin |
|---|---|---|---|
| $k_1$ ($\mu$Ms$^{-1}$) | 0.37 ± 0.10 | 0.49 ± 0.04 | 0.61 ± 0.11 |
| $k_{-1}$ (s$^{-1}$) | 2.8 ± 0.3 | 2.4 ± 0.3 | 2.2 ± 0.3 |
| $k_{-1}$ (s$^{-1}$) from $k_1$ plot | 8.8 ± 3.5 | 4.6 ± 1.5 | 5.9 ± 3.6 |
| $K_D$ ($\mu$M) | 7.6 ± 2.2 | 4.9 ± 0.7 | 3.6 ± 0.8 |

In a similar fashion as the studies of mant-GDP association to HflX in complex with the ribosome, the binding of 5 to 25 $\mu$M of mant-GDPNP to HflX-70S was monitored in a stopped-flow apparatus in TAKM$_{30}$ buffer, where the resulting fluorescent changes upon excitation at 280 nm exhibited biphasic behavior (Figure 4.3.2.2 Panel A).  The obtained time courses were best fit with a two-exponential function (Figure 4.3.2.2 Panel A).  Consistent with a two-step binding model (Scheme 4.3.2.2), the apparent rate constants determined for the first fast change in fluorescence were concentration dependent, whereas the second slower phase appeared to be concentration independent (Figure 4.3.2.2 Panel B).  This suggests that the binding of mant-GDPNP to HflX-70S complexes in high Mg$^{2+}$ buffer conditions, and either in the presence or absence of the PTC inhibitor, clindamycin or the PET antibiotic, erythromycin is similar to that observed for the same reaction in TAKM$_7$.  However, one consequence of increasing the concentration of magnesium to 30 mM was a 10-fold reduction in the $k_2$ value or rate of conformational change from 0.019 ± 0.005 s$^{-1}$ under 7 mM Mg$^{2+}$ conditions to 0.0017±0.0006 s$^{-1}$ under 30 mM Mg$^{2+}$ conditions (Table 4.3.2.2).  To determine the rate of dissociation of mant-GDPNP from HflX-70S,

an identical nucleotide chase experiment that was previously used to monitor mant-GDP dissociation was utilized. The time courses obtained from these experiments, featuring fluorescence decays characteristic of nucleotide dissociation, were best fit with a two exponential function (Figure 4.3.2.2 Panel C). Strikingly, both the faster dissociation rate constant $k_{-1}$ and the slower $k_{-2}$ value are at least 10-fold faster under 30 mM $Mg^{2+}$ conditions or the presence of clindamycin or erythromycin at a concentration of 1 mM in solution (Figure 4.3.2.2 Panel C and Table 4.3.2.2). Repetition of the same experiment performed in (50), monitoring mant-GDPNP dissociation from wildtype HflX in 7 mM $Mg^{2+}$ resulted in a $k_{-2}$ of a similar order of magnitude ($0.0041\pm0.0003$ $s^{-1}$ in $TAKM_7$ compared to $0.0012 \pm 0.0001$ $s^{-1}$ in (50)). On the other hand, values for $k_{-1}$ ($1.36 \pm 0.60$ $s^{-1}$ in $TAKM_7$ compared to $0.012 \pm 0.004$ $s^{-1}$ in (50)) were in agreement with the faster dissociation rate constants observed in $TAKM_{30}$ and the presence of clindamycin and erythromycin, inhibitors of the ribosome-stimulated GTPase activity of HflX (Figure 4.3.2.2 Panel C and Table 4.3.2.2). Comparison of the affinities of HflX-70S for mant-GDPNP calculated from the rate constants determined experimentally did not reveal a 250-fold stabilization of mant-GDPNP binding observed under low $Mg^{2+}$ conditions (50) rather only 3-fold (Table 4.3.2.2). The presence of a 30 mM $Mg^{2+}$ ($K_D$ = 227 $\pm$ 118 µM) along with the antibiotics clindamycin ($K_D$ = 215 $\pm$ 124 µM) or erythromycin ($K_D$ = 49 $\pm$ 17 µM) led to $K_D$ values either increased by a factor of two or within error of the dissociation constant ($K_D$ = 49 $\pm$ 13 µM) governing the interaction of mant-GDPNP to HflX alone (47,50) (Table 4.3.2.2).

Rate and equilibrium dissociation constants determined for HflX in complex with ribosomes in TAKM$_7$ that indicate that the 70S can stabilize a GTPase-activated state of the ribosome are not observed under 30 mM Mg$^{2+}$, which inhibits HflX-catalyzed ribosome dissociation. Furthermore, it appears as though the kinetic parameters obtained in the presence of PTC or PET targeting antibiotics do not significantly differ from those determined in the 30 mM Mg$^{2+}$ conditions.

$$HflX \bullet 70S + mant-GDPNP \underset{k_{-1}}{\overset{k_1}{\rightleftharpoons}} HflX \bullet mant-GDPNP \bullet 70S \underset{k_{-2}}{\overset{k_2}{\rightleftharpoons}} HflX \bullet mant-GDPNP \bullet 70S^* \quad \text{(Scheme 4.3.2.2)}$$
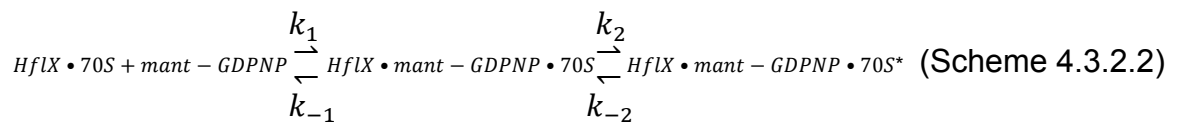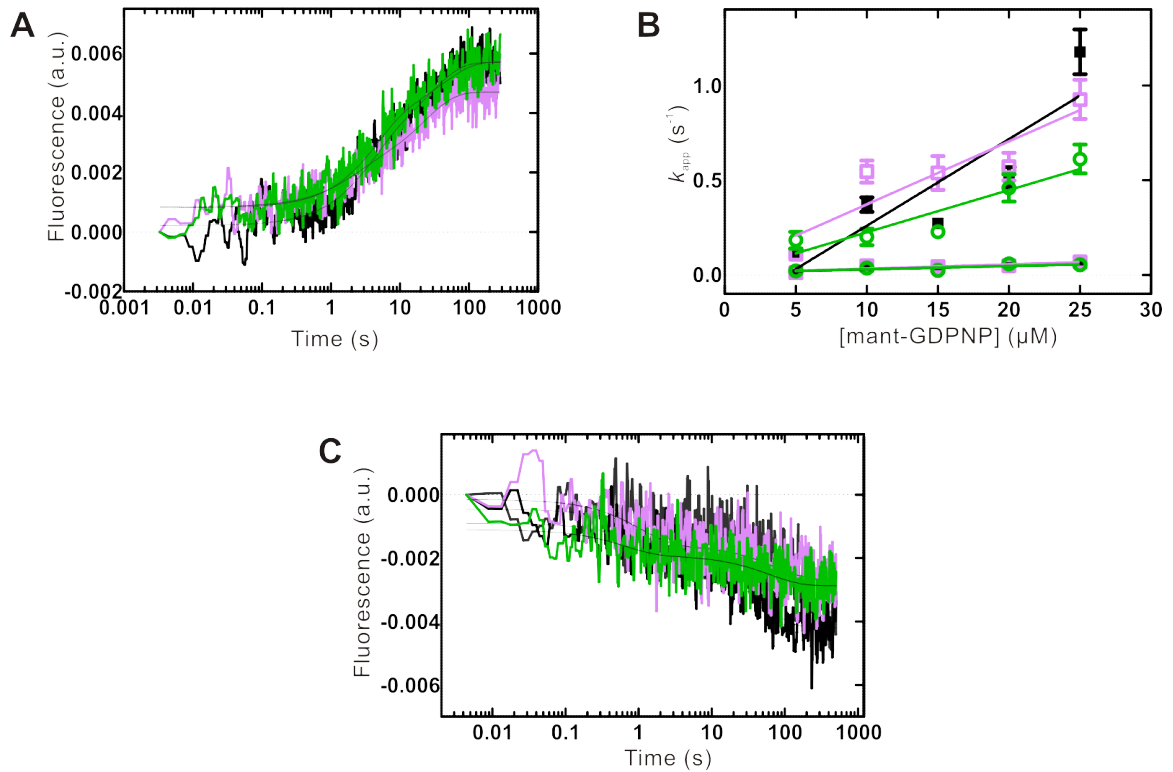
Figure 4.3.2.2 **Pre-steady state kinetics of mant-GDPNP binding and dissociation for HflX WT in complex with 70S in the presence or absence of inhibitors of ribosome-stimulated GTPase activity.** (A) Representative fluorescent traces observed upon rapidly mixing HflX-70S complexes with 15 $\mu$M mant-GDP. The normalized, average trace obtained in the absence of antibiotic is shown in black, while the traces obtained in the presence of clindamycin and erythromycin are represented in light purple and green, respectively. (B) Concentration dependence of the $k_{app}$ values for mant-GDPNP association to HflX-70S complexes in the absence of antibiotics (black), or in the presence of the antibiotics, clindamycin (light purple) and erythromycin (green). (C) Representative time courses of the dissociation of mant-GDPNP from HflX-70S upon being rapidly mixed with an excess of unlabeled nucleotide. The normalized, average trace obtained in the absence of antibiotic is shown in black, while the traces obtained in the presence of clindamycin and erythromycin are represented in light purple and green, respectively.

106

Table 4.3.2.2 Summary of experimentally determined rate and constants for the binding of mant-GDPNP to HflX under buffer conditions in which ribosome dissociation is inhibited and the presence or absence of antibiotics.  Highlighted in grey are rates determined from (50).

| | 7 mM $Mg^{2+}$ Conditions | 30 mM $Mg^{2+}$ Conditions | 30 mM $Mg^{2+}$ Conditions & Clindamycin | 30 mM $Mg^{2+}$ Conditions & Erythromycin |
|---|---|---|---|---|
| $k_1$ ($\mu$M $s^{-1}$) | 0.017 ± 0.002 | 0.045 ± 0.014 | 0.033 ± 0.009 | 0.022 ± 0.002 |
| $k_2$ ($s^{-1}$) | 0.019 ± 0.005 | 0.0017±0.0006 | 0.0017±0.0007 | 0.0022±0.0007 |
| $k_{-1}$ ($s^{-1}$) | 1.36 ± 0.60 | 0.79 ± 0.17 | 0.93 ± 0.18 | 1.49 ± 0.42 |
| $k_{-2}$ ($s^{-1}$) | 0.0041±0.0003 | 0.022 ± 0.001 | 0.013 ± 0.003 | 0.016 ± 0.003 |
| $k_{-1}$ ($s^{-1}$) from $k_1$ plot | N/A | 0.041 ± 0.148 | 0.041 ± 0.148 | 0.002 ± 0.086 |
| $K_D$ ($\mu$M) | 17 ± 9 | 227 ± 118 | 215 ± 124 | 49 ± 17 |

### 4.3.3.  Pre-Steady State Kinetics of Adenine Nucletide Binding to YchF in Complex with Ribosomes

YchF has been found to interact with 70S ribosomes or 50S and 30S ribosomal subunits, with the 70S ribosome stimulating the ATPase activity of YchF by a factor of 10 fold (66). Although, YchF has been reported to only bind to approximately 30% of the ribosomes in the respective ribosome preparation, it has been shown by *in vitro* reconstitution assays, that differential binding of YchF to ribosomal particles can be observed as a function of the nucleotide bound state of the protein (66).  To screen for potential alterations in the interaction between nucleotides and YchF in complex with 70S or 30S or 50S, preliminary pre-steady state stopped-flow experiments were carried out.  Initially, equimolar amounts of YchF (1 µM) and 30S or 70S (1 µM) were incubated and subsequently mixed with an increasing concentration of mant-ADPNP, ranging from 5 µM to 40 µM.  The resulting increases in fluorescence displayed biphasic behavior and were best fit with a two-exponential function (Scheme 4.3.3.1 and

Figure 4.3.3.1 Panel A). The rate constant, $k_1$ was calculated from the slope of the concentration dependence and directly compared to the kinetics of mant-ADPNP binding to YchF alone, although no significant differences could be found (Figure 4.3.3.1 Panel B an Table 4.3.3.1). It is important to note that under these experimental conditions, most YchF will be free in solution and therefore, most of the fluorescence changes detected by the stopped-flow for mant-ADPNP association to YchF will be due to this population of YchF, providing a simple explanation for the similarity between the rates obtained. The formation of YchF-ribosome complexes was accomplished by incubating 1 μM YchF with a 4-fold excess of 70S ribosomes. As a result of the high concentration of ribosomes in solution, inner filter effects were observed within the stopped-flow. Fluorescence emission from mant-ADPNP as a result of FRET from the tryptophan residues in YchF became difficult to detect due to the fact that intensity of excitation wavelength reaching the tryptophan residues in YchF was lessened (Figure 4.3.3.1 Panel A). YchF alone or in complex with 30S or 70S, as confirmed by microfiltration binding assays, all exhibited biphasic fluorescence signal decays and a fast rate of dissociation of 30 μM mant-ADPNP following mixing with 300 μM unlabeled ADPNP (Figure 4.3.3.1 Panel C and Table 4.3.3.1). Dissimilar between YchF in complex with 30S or 70S to YchF alone, were ten-fold slower $k_{-2}$ values at $0.012 \pm 0.0003$ s$^{-1}$ and $0.079 \pm 0.017$ s$^{-1}$ for the former compared to $0.87 \pm 0.14$ s$^{-1}$ for the latter (Table 4.3.3.1). The dissociation rate constant for the release of mant-ATP from YchF alone, also a biphasic fluorescence event, at $0.33 \pm 0.05$ s$^{-1}$ is close to the slow rate determined for mant-ADPNP dissociation

from YchF in the absence of ribosomal particles (Kirsten Rosler, Masters Thesis 2013). The fact that 30S ribosomal subunits and 70S ribosomes may have an effect on the slower step of mant-ADPNP dissociation hints at a role for the 70S ribosome and 30S ribosomal subunit in regulating the adenine nucleotide binding properties of YchF.

$$YchF \bullet 70S/30S + mant - ADPNP \underset{k_{-1}}{\overset{k_1}{\rightleftharpoons}} YchF \bullet mant - ADPNP \bullet 70S/30S \underset{k_{-2}}{\overset{k_2}{\rightleftharpoons}} YchF \bullet mant - ADPNP \bullet 70S/30S* \text{ (Scheme 4.3.3.1)}$$
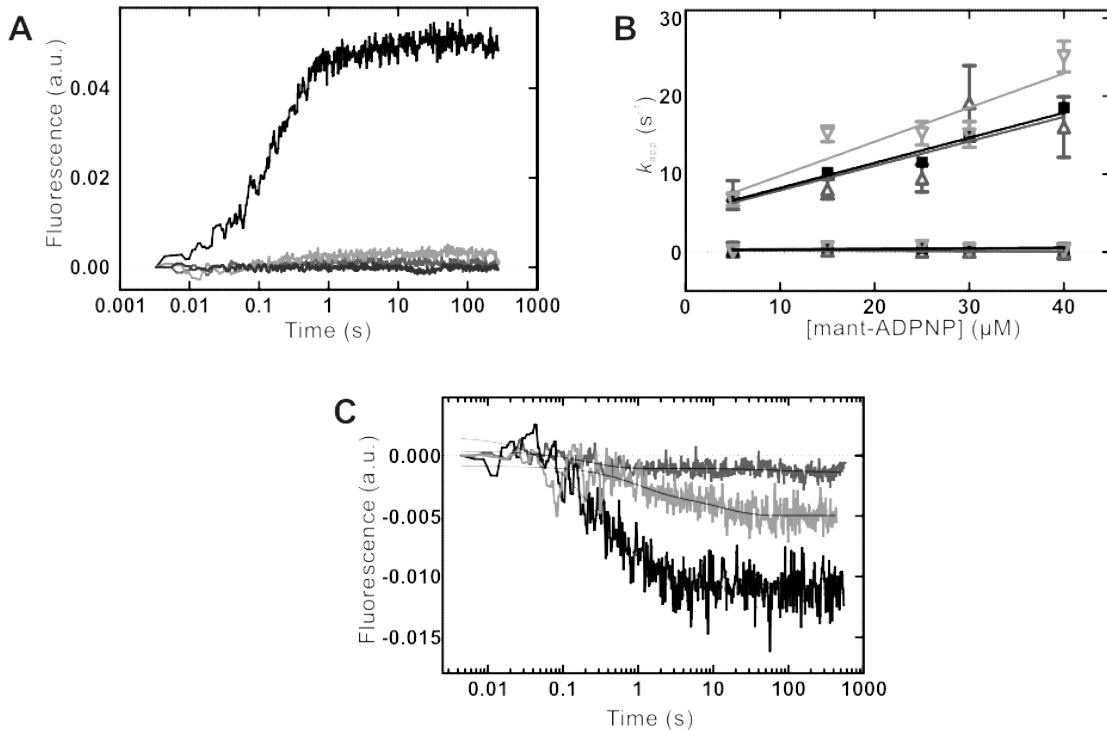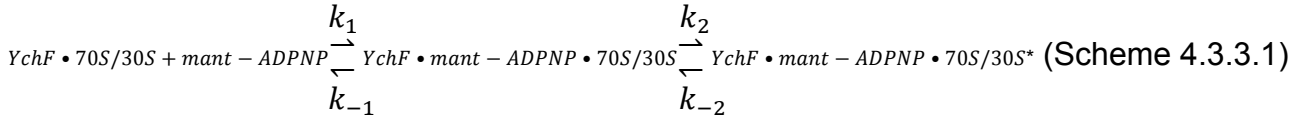


Figure 4.3.3.1 **Pre-steady state kinetics of mant-ADPNP binding and dissociation for wild-type YchF alone or in complex with 30S or 70S.** (A) Representative normalized and averaged fluorescent traces observed upon rapidly mixing 15 µM mant-ADPNP with 1 µM YchF alone (black), 1 µM YchF in the presence of 4 µM 70S ribosomes (dark grey), or 1 µM YchF in complex with 1 µM 70S (light grey) or 1 µM 30S (lightest grey). (B) Concentration dependence of the $k_{app}$ values for mant-ADPNP association to YchF alone (black) or YchF in complex with 70S (light grey) or 30S (lightest grey). (C) Representative normalized and averaged time courses of the dissociation of mant-ADPNP from YchF alone (black), or in complex with 70S (dark grey) or 30S (light grey) upon being rapidly mixed with an excess of unlabeled nucleotide.

109

Table 4.3.3.1 Summary of experimentally determined rate and constants for the binding of mant-ADPNP to YchF-30S or YchF-70S complexes in different stoichiometric ratios.

| | YchF alone | YchF-30S (1:1) | YchF-70S (1:1) |
|---|---|---|---|
| $k_1$ ($\mu M\ s^{-1}$) | 0.32 ± 0.04 | 0.43 ± 0.11 | 0.31 ± 0.13 |
| $k_2$ ($s^{-1}$) | 0.0082 ± 0.0081 | 0.0016 ± 0.0118 | 0.0058 ± 0.0022 |
| $k_{-1}$ ($s^{-1}$) | 5.2 ± 1.1 | 1.0 ± 0.2 | 4.7 ± 0.7 |
| $k_{-2}$ ($s^{-1}$) | 0.87 ± 0.14 | 0.012 ± 0.0003 | 0.079 ± 0.017 |
| $k_{-1}$ ($s^{-1}$) from $k_1$ plot | 5.0 ± 1.0 | 5.4 ± 3.0 | 4.7 ± 3.5 |

## 4.4 Discussion and Future Directions

Both HflX and YchF act as GTPases, associating with both the diphosphate and triphosphate forms of purine nucleotides during their functional cycle. Based on current knowledge, each of these proteins is regulated to some extent by the ribosome. A better understanding of how the 70S ribosome modulates their NTPase activity will allow for the assessment if these interactions are viable targets for novel or even already existing antibiotics. The peptidyl-transferase centre of the 70S ribosome is a flexible environment that can be easily influenced by a plethora of factors ranging from tRNA to proteins to small molecules like antibiotics (100). Communication between the PTC in the large ribosomal subunit and the small subunit's decoding centre has been reported, but signaling from the PTC in the form of conformational changes to other sites of the ribosome such as the E-site remains elusive (101-104). HflX crosslinks to proteins near the ribosomal E-site of the ribosome, L2, L5 and S18 in particular (Jeffrey Fischer, Doctoral Dissertation 2011), so the observation that chloramphenicol along with other PTC-targeting antibiotics such as the

lincosamides, clindamycin and lincomycin can inhibit the ribosome-stimulated GTPase activity of HflX hints at a new mode of communication from the central active site of the macromolecular complex to extraneous factors. Further evidence that supports such an arrangement is the fact that antibiotics acting on the peptide-exit tunnel, adjacent to the PTC, also exhibit a similar inhibition on the activity of HflX. Evidence also suggests that peptidyl-tRNA in the P-site can modulate the activity of A-site interacting translation factors such as IF2, EF-Tu, EF-G and RF3 (102), making studying HflX in a similar manner imperative to indeed establish if a new communication network originating from the P-site and acting on the E-site exists. Not surprisingly, none of the antibiotics tested had an effect on the ribosome-stimulated ATPase activity of YchF pointing at different modes of NTPase activation for both HAS-GTPases upon interaction with the ribosome.

To gain knowledge on enzymatic interactions and reactions in order to better understand the evolution of proteins, detailed kinetic information related to the NTPase cycles of ribosome-regulated factors such as HflX and YchF can be elucidated. The 50S ribosomal subunit stabilizes the binding of mant-GDPNP to HflX by 70000-fold (50). As the ribosome can modulate guanine nucleotide binding to the GTPase HflX, I proposed a hypothesis in this thesis that in a similar fashion the ribosome could serve as of regulator of adenine nucleotide binding and dissociation from YchF. To perform pre-steady state stopped-flow experiments where the majority of YchF is bound to ribosomes required that over 3 μM of ribosomes compared to less than 1 μM of YchF be in solution. As no

fluorescence change was observed utilizing the intrinsic tryptophan residues of YchF as a FRET donor to the mant-nucleotide acceptor, this was not the experimental set-up in which to study the adenine nucleotide binding dynamics of YchF in the presence of ribosomes.  Direct excitation of the mant group on adenine nucleotides avoids the use of the FRET phenomenon in the presence of a large concentration of ribosomes in solution. Using this methodology instead of FRET might allow for the monitoring of dissociation events as has been used to study the nucleotide exchange mechanism of EF-Tu (105,106).  50S ribosomal subunits lowered the $K_D$ and thus increased the affinity of mant-GDPNP for HflX by slowing the rate of dissociation of the labeled nucleotide triphosphate (50). Although a method to precisely study the association of mant-adenine nucleotides to YchF in complex with 30S, 50S and 70S in real time has yet to be determined, evidence for a similar slowing of the nucleotide dissociation rate by ribosomal particles might suggest that the ribosome is capable of triggering tight binding of ATP by YchF.

The main goal of repeating the pre-steady state stopped-flow analysis of HflX in complex with 70S under non-70S splitting buffer conditions (30 mM $Mg^{2+}$) was to elucidate if ribosome-targeting inhibitors exhibited any effect on the GTPase cycle of HflX. The binding or dissociation of guanine nucleotides from HflX in complex with 70S was not the consequence of the mode of action of antibiotics such as clindamycin and erythromycin which target the peptidyl-transferase centre and peptide exit tunnel of the ribosome. This leads to the hypothesis that the actual hydrolysis event or catalytic machinery contribution to hydrolysis

offered by the ribosome is the point of inhibition by antibiotics. Even though, the exact contribution of the ribosome to nucleotide hydrolysis by HflX is unknown, the presence of the C-terminal region of HflX or the movement of the HflX domain in relation to the G-domain are not responsible for the reduction in the rates of GTP hydrolysis determined in the presence of antibiotics. Two intriguing discoveries were made upon altering the buffer conditions of pre-steady state kinetic experiments monitoring guanine nucleotide binding to HflX in complex with 70S ribosomes. Not only was $k_{-1}$ an order of magnitude larger from what has been reported previously which could be a result of different HflX and ribosome preparations, but of more interest was that the very small $k_{-2}$ value responsible for the 250-fold stabilization of mant-GDPNP on HflX as reported in (50) being an order of magnitude faster under the conditions tested here and resulting in only a 2-fold higher affinity for mant-GDPNP to HflX in the presence of 70S. Taken together with data presented in Chapter 2 and 3, a dominant interaction between HflX and the 50S ribosomal subunit is emerging. The 50S ribosomal subunit displayed the most significant fluorescence changes when reacted with fluorescently labeled HflX and variants of HflX where domain interactions were disrupted or the C-terminus removed were most severely affected in their 50S-stimulated ATPase activity. Perhaps a role for HflX in ribosome biogenesis under specific cellular conditions such as heat shock is a possibility based on the increasing evidence pointing to a more specific interaction between HflX and 50S ribosomal subunits. Der, a ribosome biogenesis factor in *E. coli* associates specifically with 50S, a feature

characteristic of many prokaryotic factors involved in that stage of the ribosome functional cycle, but it is dispensable for growth at high temperatures, an environment during which HflX levels are thought to be increased (107). Nucleotide hydrolysis assays and pre-steady state kinetic analysis with functional ribosome complexes containing tRNA and mRNA will allow for the final classification of HflX as either a translational or biogenesis factor.

## 4.5 Conclusions

It had been reported earlier by our laboratory that 70S ribosomes and 50S ribosomal subunits could stabilize the GTPase-activated state of HflX. The aim of this chapter of the thesis was to understand how the ribosome regulates the GTP hydrolysis cycle of HflX. To this end, additional antibiotics other than chloramphenicol, but also binding to the peptidyl-transferase centre or adjacent peptide exit tunnel region, were discovered to inhibit the GTPase activity of HflX. Antibiotics do not affect the affinity of HflX for 70S ribosomes or influence guanine nucleotide binding or dissociation to any degree. These results suggest that the actual hydrolysis of GTP by HflX in conjunction with the 70S must be the steps afflicted in the presence of antibiotics. Also for the first time, an investigation into whether 70S ribosomes or 50S and 30S ribosomal subunits could influence the adenine nucleotide binding properties of YchF was undertaken using the stopped-flow apparatus. Preliminary data presented in this chapter has led to an initial proposal that indeed the presence of ribosomes or ribosomal subunits can stabilize an ATPase-activated state of YchF, but further experiments will be necessary to confirm such an effect.

**Chapter 5 -**

**Conclusion**

**5.1 The role of intrinsic cysteines in HflX and YchF**

In **Chapter 2** of this thesis, I have demonstrated that the cysteine residues naturally occurring within HflX and YchF can be labeled with cysteine-specific fluorescent dye, 5-IAF. Pre-steady state experiments revealed that increases in fluorescence could be observed for fluorescently labeled HflX in all its nucleotide-bound states when rapidly mixed with 30S, 50S or 70S. The three cysteines in HflX, 96, 98 and 415 are 88, 99 and less than 60% conserved among prokaryotic organisms, respectively. Substitution of the two highly conserved residues resulted in HflX variants that were insoluble, suggesting these amino acids might play a structural role in HflX. Fluorescent labeling of wild-type YchF with its six intrinsic cysteines led to protein that was inactive with regard to ATP hydrolysis in the presence of 70S ribosomes. A YchF variant with alanines substituted for cysteines in positions 5, 35 and 106, was also impaired in ribosome-stimulated ATP hydrolysis. With amino acid identities of 98%, 100% and 100% for cysteines 5, 35 and 106, respectively, these residues likely indirectly participate in ATP hydrolysis by playing critical structural roles within the YchF. Whether fluorescently labeled or cysteines substituted, modified YchF was either incapable of distinguishing between the different phosphorylated states of adenosine nucleotides or possessed a lower affinity for 70S ribosomes.

## 5.2 Requirements for ribosome stimulated nucleotide hydrolysis by HflX

**Chapter 3** of this work focused on the effect of $K^+$ on the nucleotide hydrolysis activity of HflX. Structurally, HflX contains all the elements of a GTPase that utilizes the monovalent cation to speed up its intrinsic rate of GTP hydrolysis, but this phenomenon has yet to be observed experimentally. Nucleotide hydrolysis assays presented here demonstrate that the rates of ribosome-stimulated GTPase activity of HflX are influenced by potassium ions. Additionally, within **Chapter 3** the nucleotide hydrolysis activity of variants lacking salt-bridge interactions between the HflX domain and the G-domain or lacking the C-terminus was further examined. Interestingly, the 50S stimulated ATP hydrolysis activity of *E. coli* HflX without a C-terminus was found to be near unstimulated wild-type levels while HflX variants with alanines replacing residues involved in interdomain salt-bridges exhibited dissimilar rates of purine nucleotide hydrolysis when alone or in the presence of ribosomal particles. These results suggest that the modes of GTP and ATP hydrolysis by HflX could indeed differ, a finding published recently (46). Furthermore, the contributions 70S ribosomes or 50S ribosomal subunits make to the catalysis of these different purine nucleotides could also have evolved to be differentiated. Perhaps HflX can tap into both stores of purine nucleotides for different cellular roles and therefore requires different mechanisms of regulation in each case.

## 5.3 Modulation of purine nucleotide binding to YchF and HflX by the ribosome

Results presented in **Chapter 4** revealed that perturbations to the peptidyl-transferase centre and peptide exit tunnel regions of the 70S ribosome as

caused by the binding of antibiotics to these areas can reduce the rate of GTP hydrolysis by HflX. Therefore, a communication network between the P-site and the E-site of the ribosome where HflX is proposed to bind must exist. Additionally, the presence of antibiotics in these regions of the ribosome appears to hinder the contribution of the ribosome to the actual nucleotide hydrolysis event as pre-steady state kinetic experiments revealed no effects on nucleotide association and dissociation rate constants in the presence or absence of antibiotics. Also presented in **Chapter 4** are preliminary pre-steady state kinetic experiments performed to elucidate whether the ribosome or ribosomal subunits could influence the binding of adenine nucleotides to YchF and stabilize an activated state of the enzyme upon binding of ADPNP. Within this work, I have demonstrated that under our experimental conditions, YchF in complex with 30S and 70S exhibits a slower rate of conformational change not observed with YchF alone. This data could indicate tighter binding of ADPNP to YchF when bound to 30S or 70S, results already published for the binding of GDPNP to HflX in the presence of 50S and 70S (50).

# References

1.      Chopra, I., Hesse, L., and O'Neill, A. J. (2002) Exploiting current understanding of antibiotic action for discovery of new drugs. *Symp Ser Soc Appl Microbiol*, 4S-15S

2.      Ogle, J. M., and Ramakrishnan, V. (2005) Structural insights into translational fidelity. *Annu Rev Biochem* **74**, 129-177

3.      Kaczanowska, M., and Ryden-Aulin, M. (2007) Ribosome biogenesis and the translation process in *Escherichia coli*. *Microbiol Mol Biol Rev* **71**, 477-494

4.      Aitchison, J. D., and Rout, M. P. (2000) The road to ribosomes. Filling potholes in the export pathway. *J Cell Biol* **151**, F23-26

5.      Williamson, J. R. (2003) After the ribosome structures: how are the subunits assembled? *RNA* **9**, 165-167

6.      McCutcheon, J. P., Agrawal, R. K., Philips, S. M., Grassucci, R. A., Gerchman, S. E., Clemons, W. M., Jr., Ramakrishnan, V., and Frank, J. (1999) Location of translational initiation factor IF3 on the small ribosomal subunit. *Proc Natl Acad Sci U S A* **96**, 4301-4306

7.      Ramakrishnan, V. (2002) Ribosome structure and the mechanism of translation. *Cell* **108**, 557-572

8.      Mohr, D., Wintermeyer, W., and Rodnina, M. V. (2002) GTPase activation of elongation factors Tu and G on the ribosome. *Biochemistry* **41**, 12520-12528

9.      Peske, F., Rodnina, M. V., and Wintermeyer, W. (2005) Sequence of steps in ribosome recycling as defined by kinetic analysis. *Mol Cell* **18**, 403-412

10.     Savelsbergh, A., Rodnina, M. V., and Wintermeyer, W. (2009) Distinct functions of elongation factor G in ribosome recycling and translocation. *RNA* **15**, 772-780

11.     Schlunzen, F., Zarivach, R., Harms, J., Bashan, A., Tocilj, A., Albrecht, R., Yonath, A., and Franceschi, F. (2001) Structural basis for the interaction of antibiotics with the peptidyl transferase centre in eubacteria. *Nature* **413**, 814-821

12.     Brodersen, D. E., Carter, A. P., Clemons, W. M., Jr., Morgan-Warren, R. J., Murphy, F. V. t., Ogle, J. M., Tarry, M. J., Wimberly, B. T., and Ramakrishnan, V. (2001) Atomic structures of the 30S subunit and its complexes with ligands and antibiotics. *Cold Spring Harb Symp Quant Biol* **66**, 17-32

13.     Wilson, D. N. (2009) The A-Z of bacterial translation inhibitors. *Crit Rev Biochem Mol Biol* **44**, 393-433

14.     Kohanski, M. A., Dwyer, D. J., Hayete, B., Lawrence, C. A., and Collins, J. J. (2007) A common mechanism of cellular death induced by bactericidal antibiotics. *Cell* **130**, 797-810

15.     Gromadski, K. B., and Rodnina, M. V. (2004) Streptomycin interferes with conformational coupling between codon recognition and GTPase activation on the ribosome. *Nat Struct Mol Biol* **11**, 316-322

16.     Pape, T., Wintermeyer, W., and Rodnina, M. V. (2000) Conformational switch in the decoding region of 16S rRNA during aminoacyl-tRNA selection on the ribosome. *Nat Struct Biol* **7**, 104-107

17.     Karimi, R., and Ehrenberg, M. (1994) Dissociation rate of cognate peptidyl-tRNA from the A-site of hyper-accurate and error-prone ribosomes. *Eur J Biochem* **226**, 355-360

18.     Ogle, J. M., Carter, A. P., and Ramakrishnan, V. (2003) Insights into the decoding mechanism from recent ribosome structures. *Trends Biochem Sci* **28**, 259-266

19.     Zaher, H. S., and Green, R. (2009) Fidelity at the molecular level: lessons from protein synthesis. *Cell* **136**, 746-762

20.     Zaher, H. S., and Green, R. (2009) Quality control by the ribosome following peptide bond formation. *Nature* **457**, 161-166

21.     Voss, N. R., Gerstein, M., Steitz, T. A., and Moore, P. B. (2006) The geometry of the ribosomal polypeptide exit tunnel. *J Mol Biol* **360**, 893-906

22.     Lu, J., and Deutsch, C. (2008) Electrostatics in the ribosomal tunnel modulate chain elongation rates. *J Mol Biol* **384**, 73-86

23.     Rheinberger, H. J., and Nierhaus, K. H. (1990) Partial release of AcPhe-Phe-tRNA from ribosomes during poly(U)-dependent poly(Phe) synthesis and the effects of chloramphenicol. *Eur J Biochem* **193**, 643-650

24.     Hansen, J. L., Moore, P. B., and Steitz, T. A. (2003) Structures of five antibiotics bound at the peptidyl transferase center of the large ribosomal subunit. *J Mol Biol* **330**, 1061-1075

25.     Hansen, J. L., Ippolito, J. A., Ban, N., Nissen, P., Moore, P. B., and Steitz, T. A. (2002) The structures of four macrolide antibiotics bound to the large ribosomal subunit. *Mol Cell* **10**, 117-128

26.    Tenson, T., Lovmar, M., and Ehrenberg, M. (2003) The mechanism of action of macrolides, lincosamides and streptogramin B reveals the nascent peptide exit path in the ribosome. *J Mol Biol* **330**, 1005-1014

27.    Harms, J. M., Wilson, D. N., Schluenzen, F., Connell, S. R., Stachelhaus, T., Zaborowska, Z., Spahn, C. M., and Fucini, P. (2008) Translational regulation via L11: molecular switches on the ribosome turned on and off by thiostrepton and micrococcin. *Mol Cell* **30**, 26-38

28.    Bourne, H. R., Sanders, D. A., and McCormick, F. (1991) The GTPase superfamily: conserved structure and molecular mechanism. *Nature* **349**, 117-127

29.    Caldon, C. E., Yoong, P., and March, P. E. (2001) Evolution of a molecular switch: universal bacterial GTPases regulate ribosome function. *Mol Microbiol* **41**, 289-297

30.    Lemichez, E., and Aktories, K. (2013) Hijacking of Rho GTPases during bacterial infection. *Exp Cell Res* **319**, 2329-2336

31.    Jurnak, F., Heffron, S., and Bergmann, E. (1990) Conformational changes involved in the activation of ras p21: implications for related proteins. *Cell* **60**, 525-528

32.    Sprang, S. R. (1997) G protein mechanisms: insights from structural analysis. *Annu Rev Biochem* **66**, 639-678

33.    Verstraeten, N., Fauvart, M., Versees, W., and Michiels, J. (2011) The universally conserved prokaryotic GTPases. *Microbiol Mol Biol Rev* **75**, 507-542

34.    Leipe, D. D., Wolf, Y. I., Koonin, E. V., and Aravind, L. (2002) Classification and evolution of P-loop GTPases and related ATPases. *J Mol Biol* **317**, 41-72

35.    Pai, E. F., Krengel, U., Petsko, G. A., Goody, R. S., Kabsch, W., and Wittinghofer, A. (1990) Refined crystal structure of the triphosphate conformation of H-ras p21 at 1.35 A resolution: implications for the mechanism of GTP hydrolysis. *EMBO J* **9**, 2351-2359

36.    Exton, J. H. (1998) Small GTPases minireview series. *J Biol Chem* **273**, 19923

37.    Cooper, E. L., Garcia-Lara, J., and Foster, S. J. (2009) YsxC, an essential protein in *Staphylococcus aureus* crucial for ribosome assembly/stability. *BMC Microbiol* **9**, 266

38.    Savelsbergh, A., Mohr, D., Wilden, B., Wintermeyer, W., and Rodnina, M. V. (2000) Stimulation of the GTPase activity of translation elongation factor G by ribosomal protein L7/12. *J Biol Chem* **275**, 890-894

39.    Mishra, R., Gara, S. K., Mishra, S., and Prakash, B. (2005) Analysis of GTPases carrying hydrophobic amino acid substitutions in lieu of the catalytic glutamine: implications for GTP hydrolysis. *Proteins* **59**, 332-338

40.    Banuett, F., and Herskowitz, I. (1987) Identification of polypeptides encoded by an *Escherichia coli* locus (hflA) that governs the lysis-lysogeny decision of bacteriophage lambda. *J Bacteriol* **169**, 4076-4085

41.    Noble, J. A., Innis, M. A., Koonin, E. V., Rudd, K. E., Banuett, F., and Herskowitz, I. (1993) The *Escherichia coli* hflA locus encodes a putative GTP-binding protein and two membrane proteins, one of which contains a protease-like domain. *Proc Natl Acad Sci U S A* **90**, 10866-10870

42.    Dutta, D., Bandyopadhyay, K., Datta, A. B., Sardesai, A. A., and Parrack, P. (2009) Properties of HflX, an enigmatic protein from *Escherichia coli*. *J Bacteriol* **191**, 2307-2314

43.    Chuang, S. E., and Blattner, F. R. (1993) Characterization of twenty-six new heat shock genes of *Escherichia coli. J Bacteriol* **175**, 5242-5252

44.    Blombach, F., Launay, H., Zorraquino, V., Swarts, D. C., Cabrita, L. D., Benelli, D., Christodoulou, J., Londei, P., and van der Oost, J. (2011) An HflX-type GTPase from *Sulfolobus solfataricus* binds to the 50S ribosomal subunit in all nucleotide-bound states. *J Bacteriol* **193**, 2861-2867

45.    Wu, H., Sun, L., Blombach, F., Brouns, S. J., Snijders, A. P., Lorenzen, K., van den Heuvel, R. H., Heck, A. J., Fu, S., Li, X., Zhang, X. C., Rao, Z., and van der Oost, J. (2010) Structure of the ribosome associating GTPase HflX. *Proteins* **78**, 705-713

46.    Jain, N., Vithani, N., Rafay, A., and Prakash, B. (2013) Identification and characterization of a hitherto unknown nucleotide-binding domain and an intricate interdomain regulation in HflX-a ribosome binding GTPase. *Nucleic Acids Res* **41**, 9557-9569

47.    Shields, M. J., Fischer, J. J., and Wieden, H. J. (2009) Toward understanding the function of the universally conserved GTPase HflX from *Escherichia coli:* a kinetic approach. *Biochemistry* **48**, 10793-10802

48.    Rafay, A., Majumdar, S., and Prakash, B. (2012) Exploring potassium-dependent GTP hydrolysis in TEES family GTPases. *FEBS Open Bio* **2**, 173-177

49.     Ash, M. R., Maher, M. J., Mitchell Guss, J., and Jormakka, M. (2012) The cation-dependent G-proteins: in a class of their own. *FEBS Lett* **586**, 2218-2224

50.     Fischer, J. J., Coatham, M. L., Bear, S. E., Brandon, H. E., De Laurentiis, E. I., Shields, M. J., and Wieden, H. J. (2012) The ribosome modulates the structural dynamics of the conserved GTPase HflX and triggers tight nucleotide binding. *Biochimie* **94**, 1647-1659

51.     Jain, N., Dhimole, N., Khan, A. R., De, D., Tomar, S. K., Sajish, M., Dutta, D., Parrack, P., and Prakash, B. (2009) *E. coli* HflX interacts with 50S ribosomal subunits in presence of nucleotides. *Biochem Biophys Res Commun* **379**, 201-205

52.     Polkinghorne, A., Ziegler, U., Gonzalez-Hernandez, Y., Pospischil, A., Timms, P., and Vaughan, L. (2008) *Chlamydophila pneumoniae* HflX belongs to an uncharacterized family of conserved GTPases and associates with the Escherichia coli 50S large ribosomal subunit. *Microbiology* **154**, 3537-3546

53.     Huang, B., Wu, H., Hao, N., Blombach, F., van der Oost, J., Li, X., Zhang, X. C., and Rao, Z. (2010) Functional study on GTP hydrolysis by the GTP-binding protein from *Sulfolobus solfataricus*, a member of the HflX family. *J Biochem* **148**, 103-113

54.     Cruz-Vera, L. R., Galindo, J. M., and Guarneros, G. (2002) Transcriptional analysis of the gene encoding peptidyl-tRNA hydrolase in *Escherichia coli*. *Microbiology* **148**, 3457-3466

55.     Das, G., and Varshney, U. (2006) Peptidyl-tRNA hydrolase and its critical role in protein biosynthesis. *Microbiology* **152**, 2191-2195

56.     Khil, P. P., and Camerini-Otero, R. D. (2002) Over 1000 genes are involved in the DNA damage response of *Escherichia coli*. *Mol Microbiol* **44**, 89-105

57.     Galperin, M. Y., and Koonin, E. V. (2004) 'Conserved hypothetical' proteins: prioritization of targets for experimental study. *Nucleic Acids Res* **32**, 5452-5463

58.     Dassain, M., Leroy, A., Colosetti, L., Carole, S., and Bouche, J. P. (1999) A new essential gene of the 'minimal genome' affecting cell division. *Biochimie* **81**, 889-895

59.     Koller-Eichhorn, R., Marquardt, T., Gail, R., Wittinghofer, A., Kostrewa, D., Kutay, U., and Kambach, C. (2007) Human OLA1 defines an ATPase subfamily in the Obg family of GTP-binding proteins. *J Biol Chem* **282**, 19928-19937

60.     Matsuzawa, A., Kanno, S., Nakayama, M., Mochiduki, H., Wei, L., Shimaoka, T., Furukawa, Y., Kato, K., Shibata, S., Yasui, A., Ishioka, C., and Chiba, N. (2014) The BRCA1/BARD1-interacting protein OLA1 functions in centrosome regulation. *Mol Cell* **53**, 101-114

61.     Wenk, M., Ba, Q., Erichsen, V., MacInnes, K., Wiese, H., Warscheid, B., and Koch, H. G. (2012) A universally conserved ATPase regulates the oxidative stress response in *Escherichia coli. J Biol Chem* **287**, 43585-43598

62.     Zhang, J., Rubio, V., Lieberman, M. W., and Shi, Z. Z. (2009) OLA1, an Obg-like ATPase, suppresses antioxidant response via nontranscriptional mechanisms. *Proc Natl Acad Sci U S A* **106**, 15356-15361

63.     Teplyakov, A., Obmolova, G., Chu, S. Y., Toedt, J., Eisenstein, E., Howard, A. J., and Gilliland, G. L. (2003) Crystal structure of the YchF protein reveals binding sites for GTP and nucleic acid. *J Bacteriol* **185**, 4031-4037

64.     Tomar, S. K., Kumar, P., and Prakash, B. (2011) Deciphering the catalytic machinery in a universally conserved ribosome binding ATPase YchF. *Biochem Biophys Res Commun* **408**, 459-464

65.     Gradia, D. F., Rau, K., Umaki, A. C., de Souza, F. S., Probst, C. M., Correa, A., Holetz, F. B., Avila, A. R., Krieger, M. A., Goldenberg, S., and Fragoso, S. P. (2009) Characterization of a novel Obg-like ATPase in the protozoan *Trypanosoma cruzi. Int J Parasitol* **39**, 49-58

66.     Becker, M., Gzyl, K. E., Altamirano, A. M., Vuong, A., Urban, K., and Wieden, H. J. (2012) The 70S ribosome modulates the ATPase activity of *Escherichia coli* YchF. *RNA Biol* **9**

67.     Anand, B., Surana, P., and Prakash, B. (2010) Deciphering the catalytic machinery in 30S ribosome assembly GTPase YqeH. *PLoS One* **5**, e9944

68.     Scrima, A., and Wittinghofer, A. (2006) Dimerisation-dependent GTPase reaction of MnmE: how potassium acts as GTPase-activating element. *EMBO J* **25**, 2940-2951

69.     Epstein, W., and Schultz, S. G. (1966) Cation transport in *Escherichia coli*. VI. K exchange. *J Gen Physiol* **49**, 469-481

70.     Shabala, L., Bowman, J., Brown, J., Ross, T., McMeekin, T., and Shabala, S. (2009) Ion transport and osmotic adjustment in *Escherichia coli* in response to ionic and non-ionic osmotica. *Environ Microbiol* **11**, 137-148

71.     Gavin, A. C., Bosche, M., Krause, R., Grandi, P., Marzioch, M., Bauer, A., Schultz, J., Rick, J. M., Michon, A. M., Cruciat, C. M., Remor, M., Hofert, C.,

Schelder, M., Brajenovic, M., Ruffner, H., Merino, A., Klein, K., Hudak, M., Dickson, D., Rudi, T., Gnau, V., Bauch, A., Bastuck, S., Huhse, B., Leutwein, C., Heurtier, M. A., Copley, R. R., Edelmann, A., Querfurth, E., Rybin, V., Drewes, G., Raida, M., Bouwmeester, T., Bork, P., Seraphin, B., Kuster, B., Neubauer, G., and Superti-Furga, G. (2002) Functional organization of the yeast proteome by systematic analysis of protein complexes. *Nature* **415**, 141-147

72.    Berggard, T., Linse, S., and James, P. (2007) Methods for the detection and analysis of protein-protein interactions. *Proteomics* **7**, 2833-2842

73.    Brinkley, M. (1992) A brief survey of methods for preparing protein conjugates with dyes, haptens, and cross-linking reagents. *Bioconjug Chem* **3**, 2-13

74.    De Laurentiis, E. I., Mo, F., and Wieden, H. J. (2011) Construction of a fully active Cys-less elongation factor Tu: functional role of conserved cysteine 81. *Biochim Biophys Acta* **1814**, 684-692

75.    Nicholas K.B., N. H. B. J. (1997) GeneDoc: a tool for editing and annotating multiple sequence alignments.

76.    Girish, V., and Vijayalakshmi, A. (2004) Affordable image analysis using NIH Image/ImageJ. *Indian J Cancer* **41**, 47

77.    Rodnina, M. V., and Wintermeyer, W. (1995) GTP consumption of elongation factor Tu during translation of heteropolymeric mRNAs. *Proc Natl Acad Sci U S A* **92**, 1945-1949

78.    Sreerama, N., Venyaminov, S. Y., and Woody, R. W. (1999) Estimation of the number of alpha-helical and beta-strand segments in proteins using circular dichroism spectroscopy. *Protein Sci* **8**, 370-380

79.    Kane, J. F., and Hartley, D. L. (1991) Properties of recombinant protein-containing inclusion bodies in *Escherichia coli. Bioprocess Technol* **12**, 121-145

80.    Baneyx, F., and Mujacic, M. (2004) Recombinant protein folding and misfolding in *Escherichia coli. Nat Biotechnol* **22**, 1399-1408

81.    Bhattacharyya, R., Pal, D., and Chakrabarti, P. (2004) Disulfide bonds, their stereospecific environment and conservation in protein structures. *Protein Eng Des Sel* **17**, 795-808

82.    Miseta, A., and Csutora, P. (2000) Relationship between the occurrence of cysteine in proteins and the complexity of organisms. *Mol Biol Evol* **17**, 1232-1239

83.    Zhou, P., and Wagner, G. (2010) Overcoming the solubility limit with solubility-enhancement tags: successful applications in biomolecular NMR studies. *J Biomol NMR* **46**, 23-31

84.    Daviter, T., Wieden, H. J., and Rodnina, M. V. (2003) Essential role of histidine 84 in elongation factor Tu for the chemical step of GTP hydrolysis on the ribosome. *J Mol Biol* **332**, 689-699

85.    Cunha C.E., B. R., Peske F., Holtkamp W., Wintermeyer W. and Rodnina M.V. (2013) Dual Use of GTP hydrolysis by elongation factor G on the ribosome. *Translation* **1**

86.    Bharat, A., Jiang, M., Sullivan, S. M., Maddock, J. R., and Brown, E. D. (2006) Cooperative and critical roles for both G domains in the GTPase activity and cellular function of ribosome-associated *Escherichia coli* EngA. *J Bacteriol* **188**, 7992-7996

87.    Nissen, P., Kjeldgaard, M., Thirup, S., Polekhina, G., Reshetnikova, L., Clark, B. F., and Nyborg, J. (1995) Crystal structure of the ternary complex of Phe-tRNAPhe, EF-Tu, and a GTP analog. *Science* **270**, 1464-1472

88.    Hirokawa, G., Nijman, R. M., Raj, V. S., Kaji, H., Igarashi, K., and Kaji, A. (2005) The role of ribosome recycling factor in dissociation of 70S ribosomes into subunits. *RNA* **11**, 1317-1328

89.    Foucher, A. E., Reiser, J. B., Ebel, C., Housset, D., and Jault, J. M. (2012) Potassium acts as a GTPase-activating element on each nucleotide-binding domain of the essential *Bacillus subtilis* EngA. *PLoS One* **7**, e46795

90.    Chappie, J. S., Acharya, S., Leonard, M., Schmid, S. L., and Dyda, F. (2010) G domain dimerization controls dynamin's assembly-stimulated GTPase activity. *Nature* **465**, 435-440

91.    Rudack, T., Xia, F., Schlitter, J., Kotting, C., and Gerwert, K. (2012) The role of magnesium for geometry and charge in GTP hydrolysis, revealed by quantum mechanics/molecular mechanics simulations. *Biophys J* **103**, 293-302

92.    Hurwitz, C., and Rosano, C. L. (1967) The intracellular concentration of bound and unbound magnesium ions in *Escherichia coli. J Biol Chem* **242**, 3719-3722

93.    Umekage, S., and Ueda, T. (2006) Spermidine inhibits transient and stable ribosome subunit dissociation. *FEBS Lett* **580**, 1222-1226

94.   Weixlbaumer, A., Petry, S., Dunham, C. M., Selmer, M., Kelley, A. C., and Ramakrishnan, V. (2007) Crystal structure of the ribosome recycling factor bound to the ribosome. *Nat Struct Mol Biol* **14**, 733-737

95.   Fourmy, D., Yoshizawa, S., and Puglisi, J. D. (1998) Paromomycin binding induces a local conformational change in the A-site of 16 S rRNA. *J Mol Biol* **277**, 333-345

96.   Yoshizawa, S., Fourmy, D., and Puglisi, J. D. (1999) Recognition of the codon-anticodon helix by ribosomal RNA. *Science* **285**, 1722-1725

97.   Schlunzen, F., Harms, J. M., Franceschi, F., Hansen, H. A., Bartels, H., Zarivach, R., and Yonath, A. (2003) Structural basis for the antibiotic activity of ketolides and azalides. *Structure* **11**, 329-338

98.   Misumi, M., Tanaka, N., and Shiba, T. (1978) Binding of [14C]tuberactinomycin O, an antibiotic closely related to viomycin, to the bacterial ribosome. *Biochem Biophys Res Commun* **82**, 971-976

99.   Tu, D., Blaha, G., Moore, P. B., and Steitz, T. A. (2005) Structures of MLSBK antibiotics bound to mutated large ribosomal subunits provide a structural explanation for resistance. *Cell* **121**, 257-270

100.   Polacek, N., and Mankin, A. S. (2005) The ribosomal peptidyl transferase center: structure, function, evolution, inhibition. *Crit Rev Biochem Mol Biol* **40**, 285-311

101.   Thompson, J., Kim, D. F., O'Connor, M., Lieberman, K. R., Bayfield, M. A., Gregory, S. T., Green, R., Noller, H. F., and Dahlberg, A. E. (2001) Analysis of mutations at residues A2451 and G2447 of 23S rRNA in the peptidyltransferase active site of the 50S ribosomal subunit. *Proc Natl Acad Sci U S A* **98**, 9002-9007

102.   Thompson, J., O'Connor, M., Mills, J. A., and Dahlberg, A. E. (2002) The protein synthesis inhibitors, oxazolidinones and chloramphenicol, cause extensive translational inaccuracy in vivo. *J Mol Biol* **322**, 273-279

103.   O'Connor, M., Brunelli, C. A., Firpo, M. A., Gregory, S. T., Lieberman, K. R., Lodmell, J. S., Moine, H., Van Ryk, D. I., and Dahlberg, A. E. (1995) Genetic probes of ribosomal RNA function. *Biochem Cell Biol* **73**, 859-868

104.   Weiss-Brummer, B., Zollner, A., Haid, A., and Thompson, S. (1995) Mutation of a highly conserved base in the yeast mitochondrial 21S rRNA restricts ribosomal frameshifting. *Mol Gen Genet* **248**, 207-216

105. Wieden, H. J., Gromadski, K., Rodnin, D., and Rodnina, M. V. (2002) Mechanism of elongation factor (EF)-Ts-catalyzed nucleotide exchange in EF-Tu. Contribution of contacts at the guanine base. *J Biol Chem* **277**, 6032-6036

106. Gromadski, K. B., Wieden, H. J., and Rodnina, M. V. (2002) Kinetic mechanism of elongation factor Ts-catalyzed nucleotide exchange in elongation factor Tu. *Biochemistry* **41**, 162-169

107. Hwang, J., and Inouye, M. (2006) The tandem GTPase, Der, is essential for the biogenesis of 50S ribosomal subunits in *Escherichia coli*. *Mol Microbiol* **61**, 1660-1672